THE ASTROPHYSICAL JOURNAL SUPPLEMENT SERIES, 44:319–381, 1980 November

ON THE STELLAR CONTENT AND STRUCTURE OF THE SPIRAL GALAXY M33

ROBERTA M. HUMPHREYS[1,2,3]
Department of Astronomy, University of Minnesota

AND

ALLAN SANDAGE[3]
Mount Wilson and Las Campanas Observatories,[4]
Received 1980 March 20; accepted 1980 April 24

ABSTRACT

A blink survey for blue and red stars over the face of M33 has isolated candidates for the brightest member stars. These stars provide further data for the luminosity calibration of the brightest resolved stars as extragalactic distance indicators. Photographic photometry in the magnitude range $14 \lesssim V \lesssim 20$, $14 \lesssim B \lesssim 22$ is given for ~ 1000 of the brightest blue and red stars. The color-magnitude (CM) diagrams show a strong main sequence and a weaker, but definite, system of red supergiants.

Spectroscopy has isolated the brightest members from the foreground stars. The brightest blue supergiant has $M_V(1) = -9.4$, and the mean luminosity of the three brightest blue stars is $\langle M_V(3) \rangle = -9.3$. For the red supergiants, $M_V(1) = -8.15$, and $\langle M_V(3) \rangle = -7.95$, which is further evidence in favor of constant $M_V(\sim -8)$ for the brightest red supergiants in galaxies of very different absolute magnitudes. We have assumed an apparent distance modulus of $(m-M)_{AV} = 24.65$ for M33.

The CM diagrams are displayed for stars inside and outside the 143 associations that have been identified. The brightest red and blue stars occur inside the association boundaries; however, young blue stars as bright as $M_V = -6.5$ do occur in the spiral features outside the association boundaries. Foreground contamination for the red stars over the face of M33 is severe and has been estimated from a CM diagram to $V = 22$ of the nearby control field, Selected Area 45.

The spiral pattern of M33 is outlined using the associations, H II regions, dust, and the surface brightness of young unresolved stars. Ten arms have been found, five on each side of the center. The dust pattern is chaotic and does not by itself outline the spiral arms.

Individual CM diagrams are presented for six associations at various distances from the center. Interpretation of the diagrams in terms of stellar models gives nearly the same age ($\sim 5 \times 10^6$ years) for all six. The age estimate for 42 additional associations shows a near equality of ages for all, with a range of only 4×10^6 years to 6×10^6 years. There is no significant difference in age *along* the two bright inner arms, nor is there a lack of associations as young as 5×10^6 years in the outermost arms.

The data on the structure of the spiral arms in M33 may provide evidence in support of both density-wave arms (the two innermost arms) and material arms in the outer parts. The two broad, massive innermost arms are well defined by all of the classical spiral tracers and can be traced for about 180°. The morphology of the southern arm especially appears to fit the predictions of density-wave models while its northern counterpart is quite difficult to interpret with present data. The eight outer spiral features cannot be explained by a straightforward interpretation based on the density-wave. These pieces of spiral arms are not well defined and can only be mapped by combining the distribution of a few large, young associations with the surface brightness distribution from a fainter underlying stellar population.

[1]Alfred P. Sloan Foundation Fellow.
[2]Guest Investigator, Mount Wilson and Las Campanas Observatories.
[3]Visiting Astronomer, Kitt Peak National Observatory, which is operated by AURA under contract with the National Science Foundation.
[4]Operated by the Carnegie Institution of Washington.

Finally, the time for M33 to lock its present supply of $2\times10^9\ \mathfrak{M}_\odot$ of H I permanently into stars is calculated from estimates of the present birth rate of stars of all mass. This evolutionary time depends critically on whether low mass stars are presently being born in the OB associations or if the *formation luminosity function* has a cutoff below a certain mass. The calculated M33 evolution time varies between 4×10^{10} years and 10^9 years, depending on where the cutoff lies.

Subject headings: clusters: associations — galaxies: individual — galaxies: stellar content — galaxies: structure — stars: luminosities — stars: supergiants

I. INTRODUCTION

M33, a member of the Local Group, is the nearest Sc spiral galaxy and as such has played a decisive role in delineating the properties of galaxies as stellar systems. M33 was first resolved into stars probably as early as 1895 by Isaac Roberts (1899), by Keeler (1908) in 1900, and then certainly by Ritchey (1910), and later by others, although neither Roberts, Ritchey, nor Shapley (1919) believed they had done so. These authors called their resolved objects "nebulous stars." The conclusion that the condensations are true stellar images was made by Lundmark (1921, 1925) and was later proved beyond doubt by Hubble (1926) in his famous paper, *A Spiral Nebula As A Stellar System M33*.

We became interested in the stellar content of M33 because of its importance for the absolute magnitude calibration of the brightest resolved stars. Evidence available from other nearby galaxies suggests that their brightest *red* supergiants have a stable upper luminosity of $M_V=-8.0\pm0.2\ (\sigma)$ (Sandage and Tammann 1974*b*, hereafter, ST2; Humphreys 1978, 1979*a*, 1980*a*, hereafter Paper V). Clearly the potential of such stars for rather accurate measurement of distances to resolved local galaxies is enormous, providing one can establish that the upper luminosity is, in fact, so stable in all galaxies. Evidence exists that blue supergiants are also useful distance indicators; however, their absolute magnitude depends on the luminosity of the parent galaxy (Hubble 1936; Holmberg 1950; ST2; Paper V, and earlier papers of this series), and hence the precision associated with their use is degraded.

M33 provides one of the few galaxies in which a calibration of the absolute magnitudes of the brightest stars can be made. Clearly, galaxies whose distances are known *a priori* are the only ones that can be used for this purpose. Hence, if we adopt this precept, only galaxies whose distances are determined from Cepheids are available for the brightest star calibration. The number of such galaxies has not yet increased beyond those used by Sandage and Tammann (1974*a* [hereafter ST1], Table 2), although additional distances based on Cepheids can soon be expected for members of the NGC 300 group (J. Graham, from work in progress at Cerro Tololo), for IC 5152 (G. Tammann, in progress at ESO), and for Sextans A, Sextans B, NGC 3109, and WLM, from work in progress by A. Sandage at Mount Wilson and Las Campanas.

The calibration of the brightest stars in M33 presents abnormal difficulties because the galaxy has such a large angular extent. The contamination by galactic foreground dwarfs is severe, a circumstance that has previously prevented a convincing identification of the brightest individual stars in M33. To overcome this problem it was clear from the beginning that a combined photometric and spectroscopic study was needed.

As the work progressed, other aspects of the stellar content became so interesting that we expanded the initial plan beyond the brightest stars to include the stellar associations, the dust content, the spiral pattern, the age of the associations and of the arms, and the rate of star formation in M33 and its evolutionary history. Evidence for warping of the optical plane of M33 is discussed elsewhere (Sandage and Humphreys 1980, hereafter SH).

In the following sections we discuss the search for the brightest red and blue stars and the identification of the associations (§ II); the photometry and the photographic catalogs (§ III); the identification of the brightest stars and their absolute magnitude calibration (§ IV); the spiral pattern from the associations, H II regions, and dust (§ V); the ages of the associations and the blue to red supergiant ratio (§ VI); and the nature of the arm system and the evolutionary fate of M33 as an Sc galaxy (§ VII).

II. THE BLINK SURVEY

a) Photographic Centers and Plates

A photographic survey of M33 was begun in 1955 using plates obtained on the Hale 5 meter reflector. The good photometric field of such plates is 16′ diameter, and the scale is $11\farcs06\ \mathrm{mm}^{-1}$ when the Ross f/3.67 corrector is used at the prime focus. Because of the small field, a number of plate centers were needed to cover the main body of M33, $\gtrsim1°$ in diameter. The seven principal centers studied here are shown in Figure 1 (Plate 3) and are labeled as fields 8, 9, 10, 15, 16, 17, and 25. Their 1950 coordinates are listed in Table 1. The centers were chosen so that the fields have considerable overlap to permit the photoelectric sequences on the east and west sides (Sandage and Johnson 1974, hereafter SJ) to be spread over the face of M33 by conventional photographic methods.

Blue (103aO+GG13), yellow (103aD+GG11), and red (103aE+RG2) plates were taken to study various components of the stellar content. Some of the earlier results from these plates have been (1) a survey of H II regions by one of us with J. L. Sersic, briefly discussed

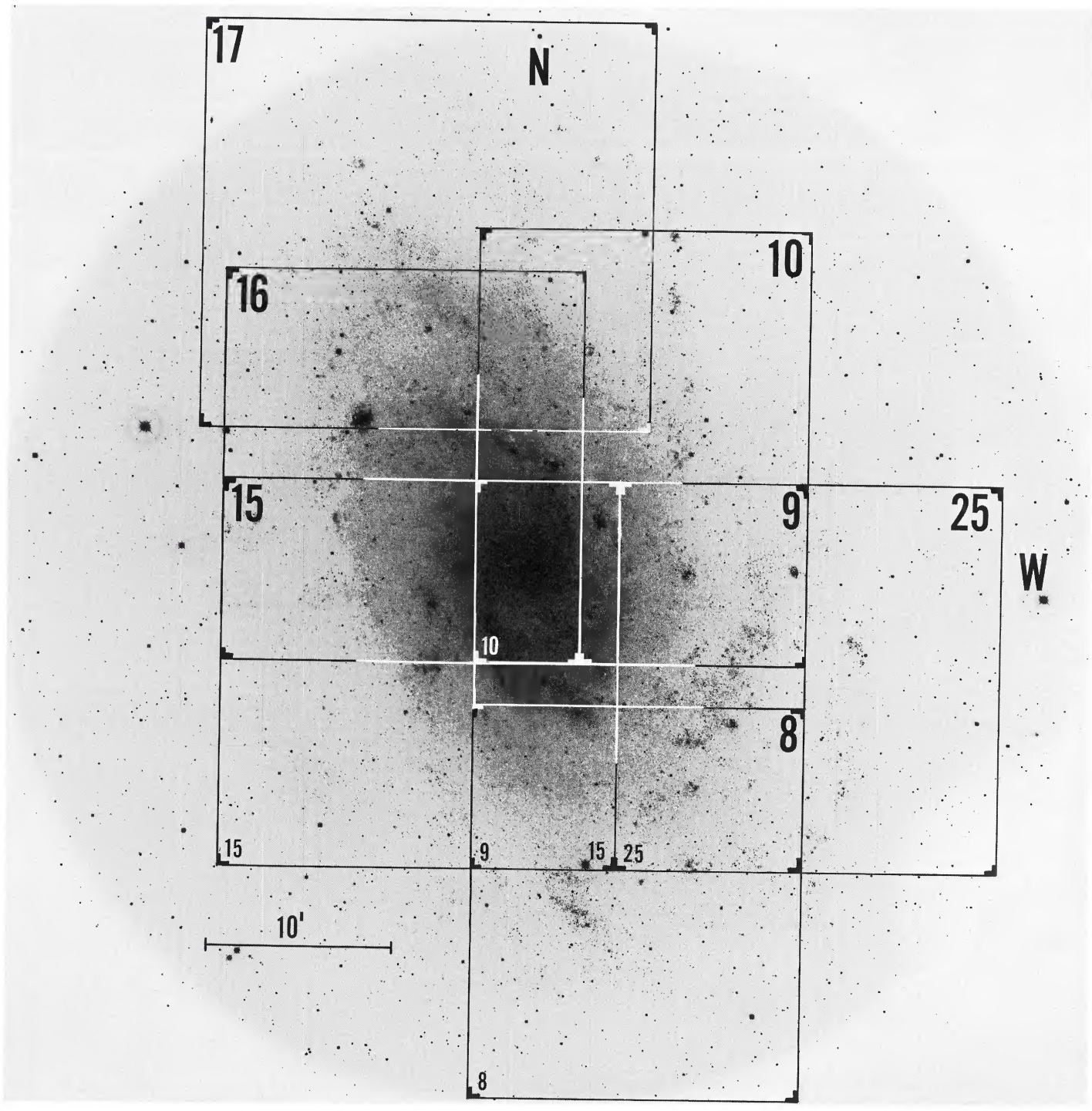

FIG. 1.—Identification of the separate centers of the Palomar 5 m reflector plates listed in Table 1, superposed on a 103aO + Scott 395 plate of the face of M33 taken with the Kitt Peak Mayall 4 m reflector. The approximate borders define the general region covered by the detailed Palomar 5 m charts in Figs. 3–16.

TABLE 1

CENTERS FOR THE PRINCIPAL AREAS OF THE 5 METER PHOTOGRAPHIC SURVEY

Area	α(1950)	δ(1950)
8	$1^h30^m32^s$	+30°06′17″
9	$1^h30^m32^s$	+30°18′17″
10	$1^h30^m32^s$	+30°30′17″
15	$1^h31^m30^s$	+30°18′17″
16	$1^h31^m30^s$	+30°42′17″
17	$1^h31^m28^s$	+30°42′17″
25	$1^h30^m04^s$	+30°18′03″

elsewhere (Sandage 1962), (2) a study of possible color gradients across the principal south-preceding arm by Dixon (1971), and (3) an unpublished study of the system of ~500 clusters by Sandage, with photometry by Hiltner (1960) for some of them.

b) Identification of the Associations

To locate the brightest stars, we blinked the blue and yellow plates in each field and marked the bluest and reddest stars found. Over 1700 blue stars and 800 red stars were eventually marked in the seven separate fields. Photographic magnitudes and colors were measured for 488 of the brightest blue stars and 360 of the brightest red stars.

As a method of organizing the very large amount of information, we found it useful to first identify the obvious associations over the face of M33. Following standard conventions, we have defined these as regions which have a significant blue star enhancement over their immediate adjacent neighborhood. The assignment of stars to associations was, surprisingly, quite straightforward, as the regions are well separated even by casual inspection of the plates. Evidently, the concept of stellar associations as originally introduced by Ambartsumian (1947, 1949, 1955) (see also Blaauw [1964] and Sharpless [1965] for reviews and references) describes the fact that discrete but *coherent* regions of star formation exist as separate cells of size of order $\sim 10^2$ pc. Hence, as with clusters, it is sensible to discuss the *age* of any particular association because the member stars formed at essentially the same time. As the work developed, one of the aims of the bright star study became the age determination of the *system* of associations in any given spiral arm because variations in the ages of the cells along the arms may reveal aspects of the formation of the arms themselves.

We have identified 143 associations in the area covered by the seven fields. They are marked in Figure 2 (Plate 4) on a print from a Mount Wilson 2.5 meter Hooker reflector plate taken on 103aO emulsion with no filter.

The spiral pattern of the two inner arms (I N and I S in the notation of SH 1980) is well defined by associations 1–27 on the south, and 61–99 on the north. These are the two arms of high surface brightness that appear with good contrast on the early photographs of M33 by Roberts (1899), Keeler (1908, Plate 3), and Ritchey (Hubble 1926, Plate IV).

The centers of the associations relative to the nucleus are listed in Table 2 in a coordinate system with positive X toward the east and Y toward the north. The coordinates were read from a grid over a print and are accurate to only $\sim \pm 20''$, considering that the centers of the association are defined only approximately.

Studies of associations in other galaxies include those in M31 (van den Bergh 1964), LMC (Lucke and Hodge 1970; Hodge and Lucke 1970), NGC 6822 (Hodge 1977), IC 1613 (Hodge 1978), and in our own galaxy by many astronomers starting with the classical work of Morgan, Whitford, and Code (1953). The associations marked here clearly are of the same type as regards stellar content and size. From the scale marked in Figure 2 and using the conversion factor of 10′ per 2 kpc for M33, one sees that the typical association in M33 has a diameter of order ~200 psc.

c) Identification of the Red and Blue Stars

The brighter blue candidates in the seven fields are identified on the large scale charts in Figures 3–9. The prints are reproductions of the Hale reflector 5 m yellow plates. Many fainter blue stars were also marked during the blink survey, and although they are marked on Figures 3–9, they are not numbered. The association boundaries from Figure 2 have also been put onto the charts as are certain special stars that were used in the photometric transfers discussed in § III.

The brighter red star candidates are identified on the large scale charts in Figures 10–16 which are reproductions of the same 103aD plates used for Figures 3–9. The bulk of the red stars were found by blinking the 5 m plates. However, a second blink survey was made using a pair of plates (103aO+GG385) and IVN+RGb95) taken at the prime focus of the 4 m Mayall telescope. These plates cover the field shown in Figure 1, which is nearly the entire face of M33. The effective wavelength of the Kitt Peak IVN plate is enough further to the red than the 103aD+GG11 Palomar plates so as to favor the very reddest stars. These are marked but not numbered in Figures 10–16 and are shown by crosses in Figure 22, discussed later (§ V*a*). Most of these red stars are expected to be members rather than foreground red dwarfs, as we expect their colors to be redder than $B-V=1.9$.

III. PHOTOMETRY

a) Methods

Photometry of individual objects in galaxies is always difficult due to the severe crowding by stars and

Plate 4

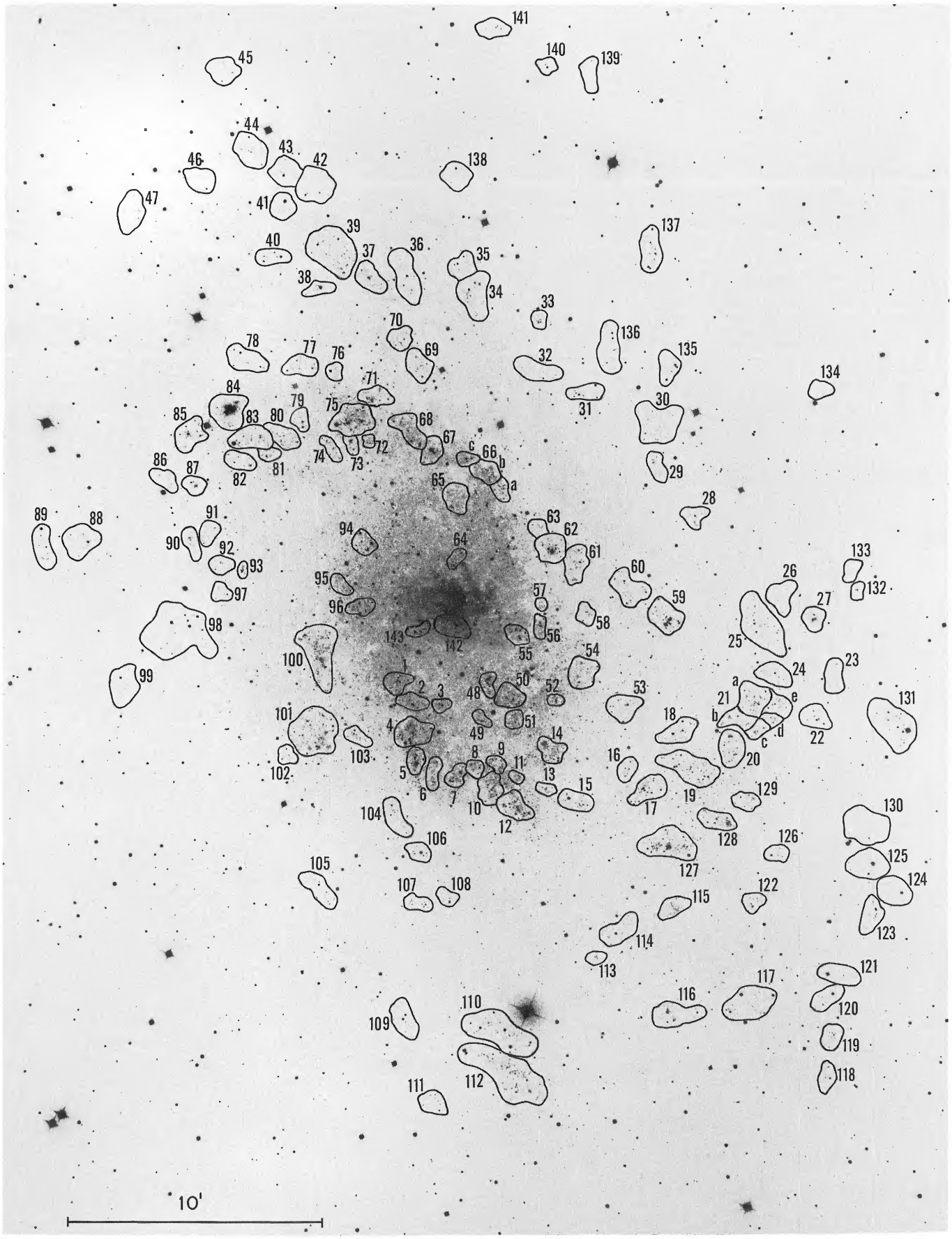

FIG. 2.—Identification of the 143 associations over the face of M33 superposed on a 103aO plate taken with the Mount Wilson 2.5 m Hooker reflector. The telescope was diaphragmed to 58 (1.5 m) inches to increase the coma-free field.

TABLE 2

COORDINATES OF THE ASSOCIATIONS REFERRED TO THE M33 CENTER

Number	X″	Y″	Number	X″	Y″	Number	X″	Y″	Number	X″	Y″
1	+131	-196	37	+202	+764	71	+183	+483	107	+91	-718
2	+98	-242	38	+320	+738	72	+196	+379	108	+20	-702
3	+33	-248	39	+287	+829	73	+242	+372	109	+124	-993
4	+98	-320	40	+431	+816	74	+287	+359	110	-104	-1025
5	+91	-379	41	+405	+934	75	+235	+431	111	+59	-1188
6	+52	-408	42	+326	+980	76	+281	+542	112	-118	-1123
7	-6	-411	43	+392	+1012	77	+359	+562	113	-326	-849
8	-52	-398	44	+477	+1064	78	+490	+575	114	-392	-784
9	-98	-385	45	+542	+1260	79	+359	+431	115	-509	-725
10	-85	-451	46	+601	+993	80	+405	+392	116	-509	-980
11	-137	-418	47	+764	+927	81	+438	+346	117	-692	-953
12	-137	-483	48	-78	-196	82	+470	+320	118	-868	-1123
13	-209	-444	49	-59	-281	83	+477	+392	119	-882	-1032
14	-222	-359	50	-131	-229	84	+529	+457	120	-868	-940
15	-281	-470	51	-144	-281	85	+627	+392	121	-901	-888
16	-398	-398	52	-235	-235	86	+686	+287	122	-699	-712
17	-457	-444	53	-398	-255	87	+614	+274	123	-973	-744
18	-522	-313	54	-300	-170	88	+882	+144	124	-1025	-686
19	-549	-392	55	-144	-78	89	+966	+131	125	-966	-627
20	-653	-346	56	-202	-65	90	+614	+144	126	-757	-594
21	-712	-268	57	-202	-13	91	+575	+157	127	-503	-575
22	-842	-274	58	-307	-65	92	+549	+85	128	-614	-522
23	-888	-176	59	-496	-46	93	+496	+72	129	-686	-346
24	-751	-176	60	-411	+26	94	+209	+137	130	-966	-529
25	-718	-59	61	-281	+85	95	+268	+39	131	-1032	-294
26	-764	+7	62	-229	+124	96	+215	-13	132	-947	+26
27	-842	-46	63	-196	+170	97	+549	+20	133	-934	+72
28	-562	+196	64	-7	+98	98	+653	-65	134	-855	+503
29	-477	+313	65	-7	+242	99	+784	-196	135	-503	+562
30	-477	+418	66a	-111	+261	100	+320	-131	136	-366	+601
31	-307	+496	66b	-72	+307	101	+333	-313	137	-457	+836
32	-189	+542	66c	-26	+333	102	+392	-366	138	0	+999
33	-196	+666	67	+52	+353	103	+229	-326	139	-313	+1241
34	-46	+725	68	+104	+405	104	+144	-509	140	-215	+1260
35	-20	+790	69	+85	+562	105	+320	-686	141	-85	+1352
36	+118	+771	70	+124	+620	106	+88	-594	142	0	-59
									143	+85	-72

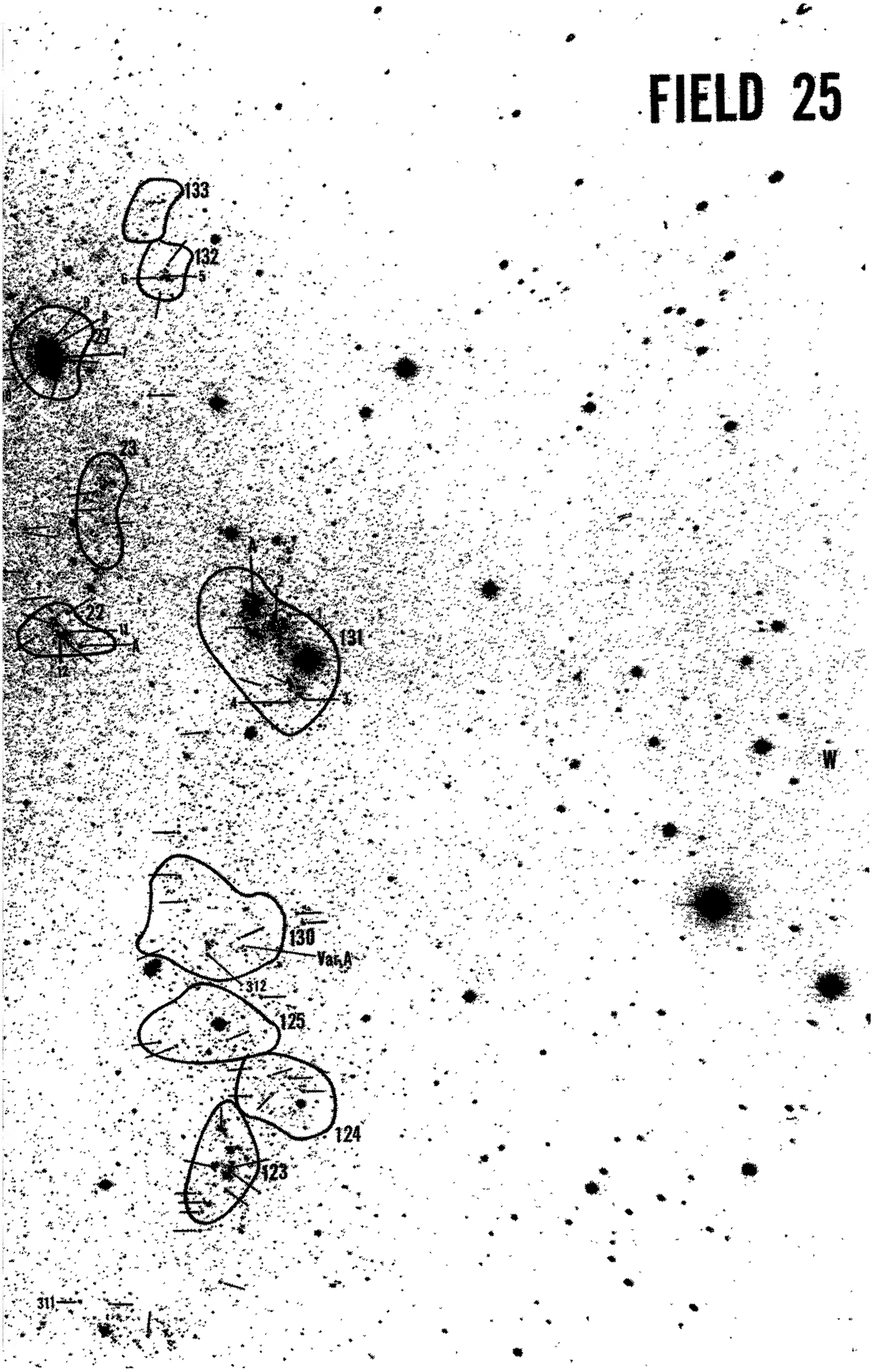

ighter stars are numbered and the photometry is given in Tables 5 and 7. The approximate boundaries of the egions are not generally identified again here.

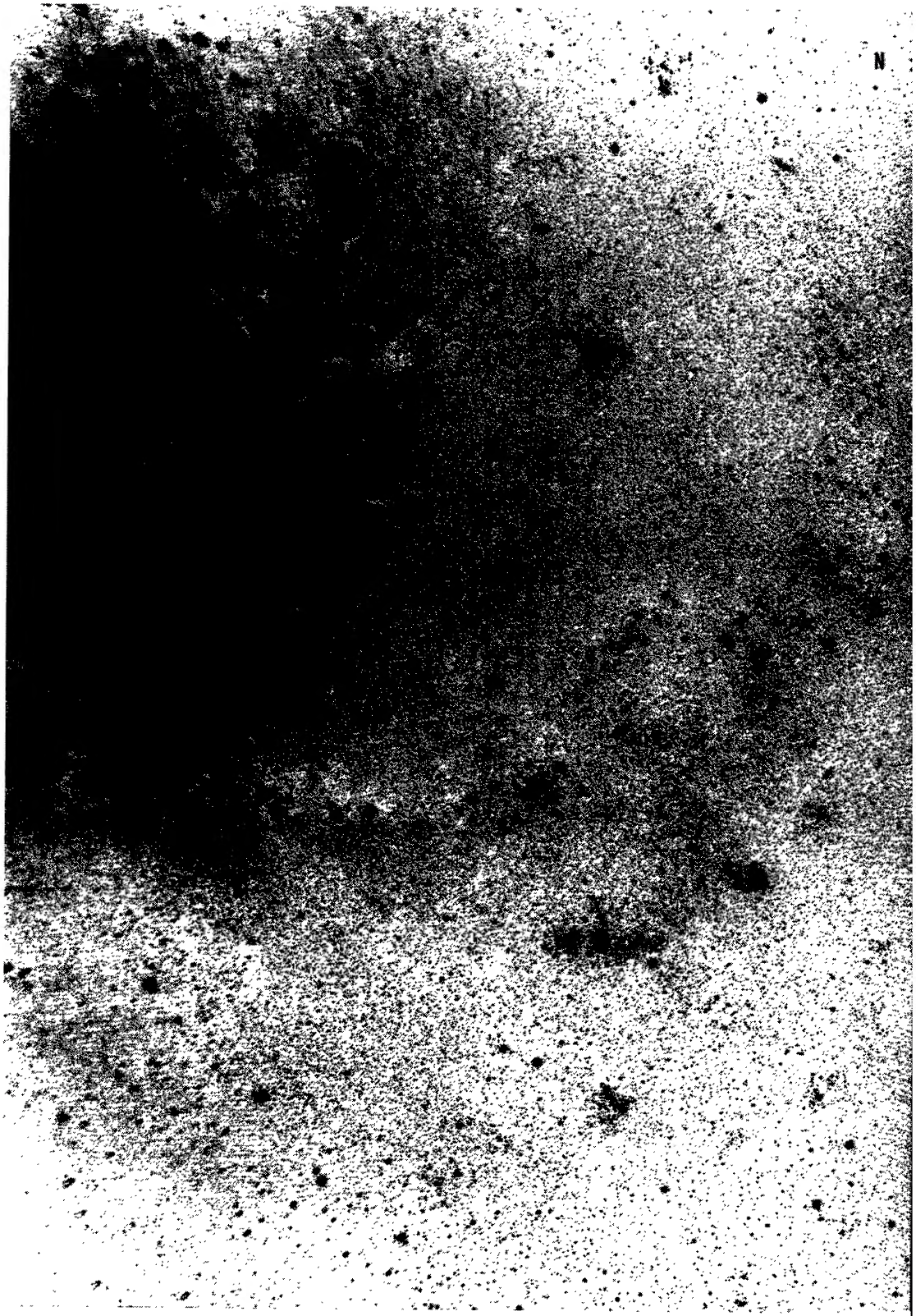

FIG. 3.—Finding chart for the blue stars in field 25 from a deep Palomar 5 m exposure on a 103aO+GG13 plate. The br
associations on the western edge of Fig. 2 are outlined. The overlap with field 9 in Fig. 4 is substantial, but the duplicated

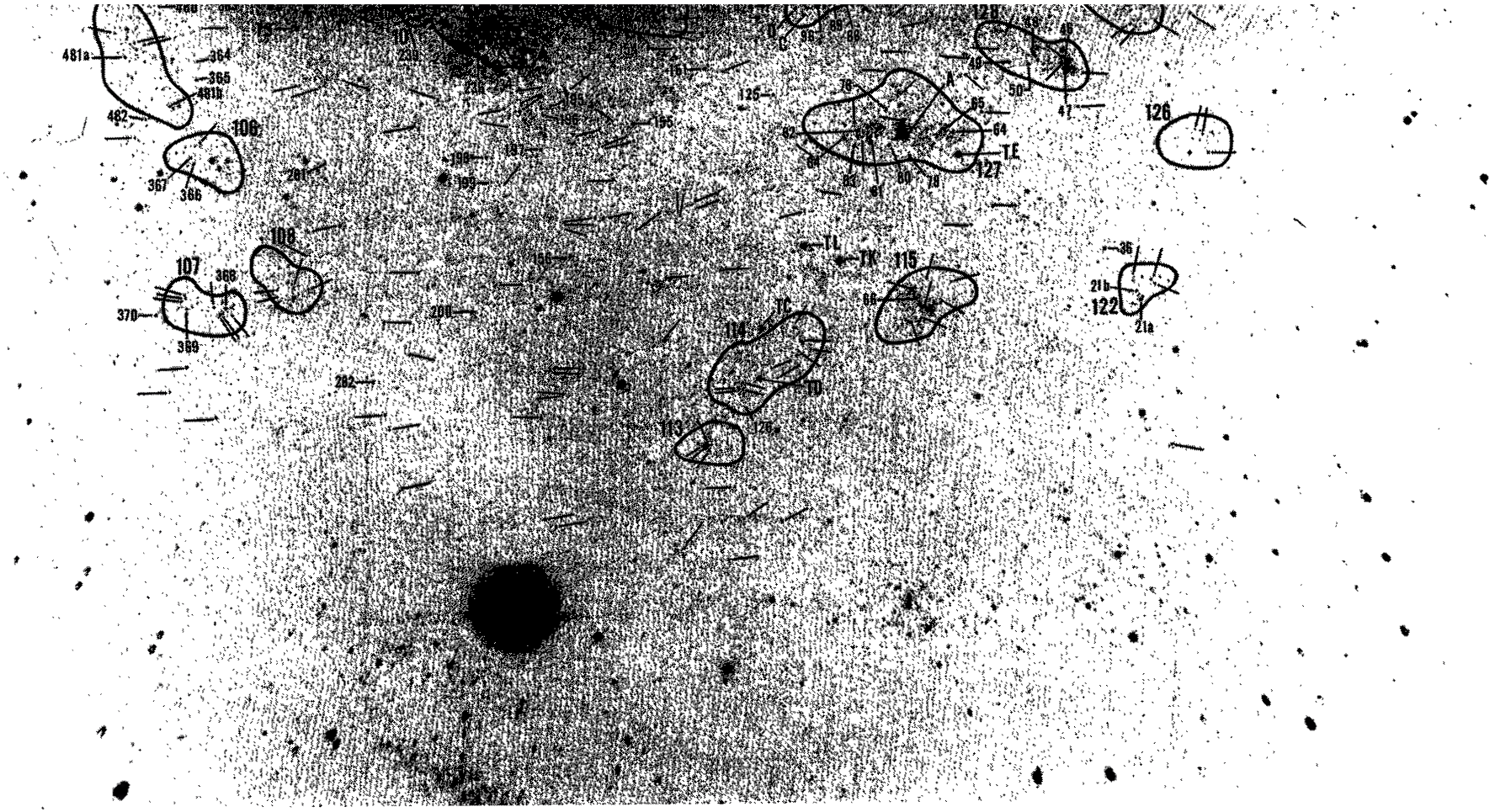

FIG. 4.—Finding chart for the blue stars in field 9 from a short exposure (10 min) 103aD+GG11 plate taken with the Palomar 5 m reflector. The approximate outlines of the associations from Fig. 2 are superposed on the field. Photometry of the numbered objects is listed in Tables 5 and 7.

1980ApJS...44..319H

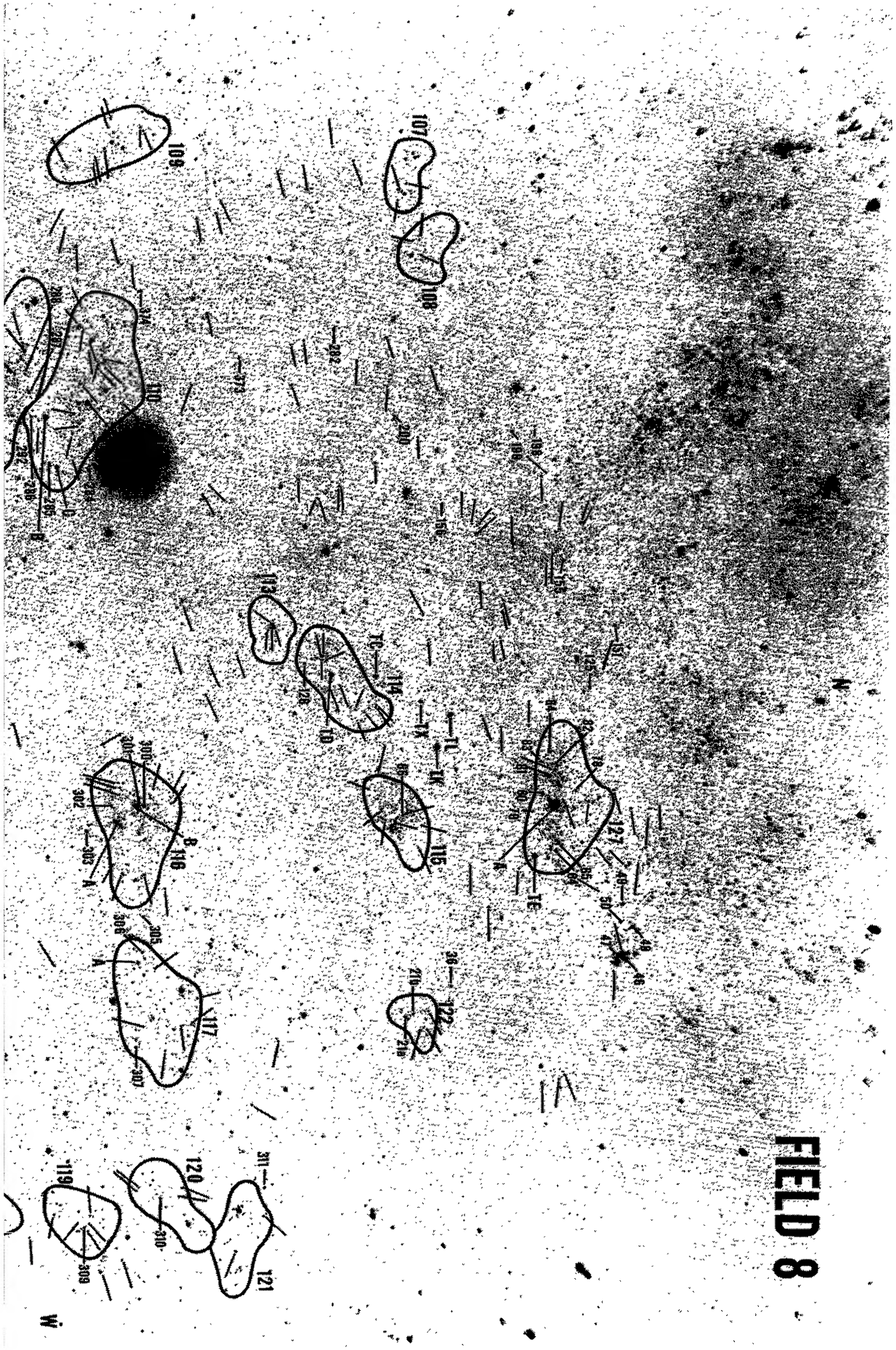

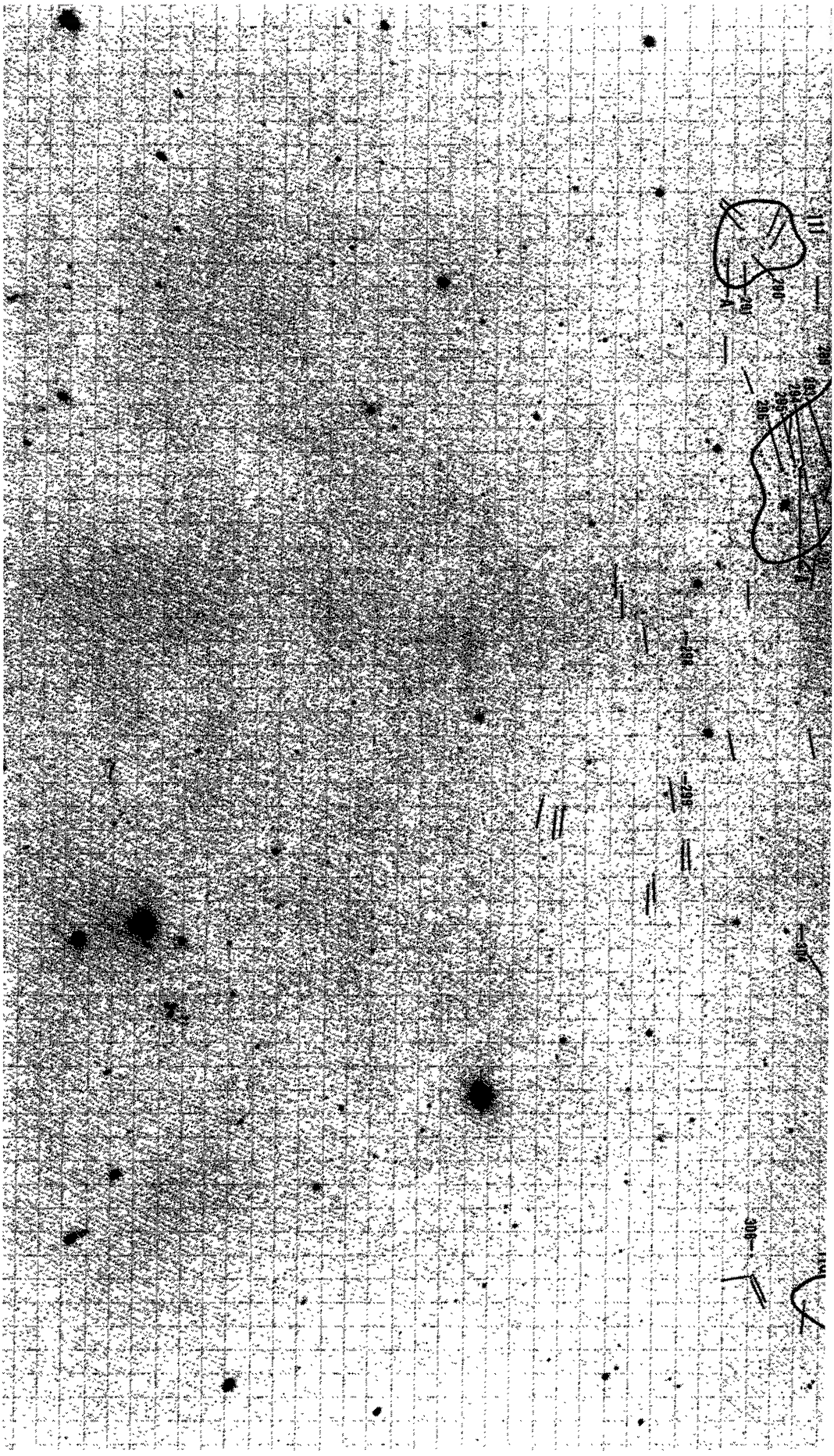

FIG. 5.—Finding chart for the blue stars in field 8 from a Palomar 5 m 103aD+GG11 plate

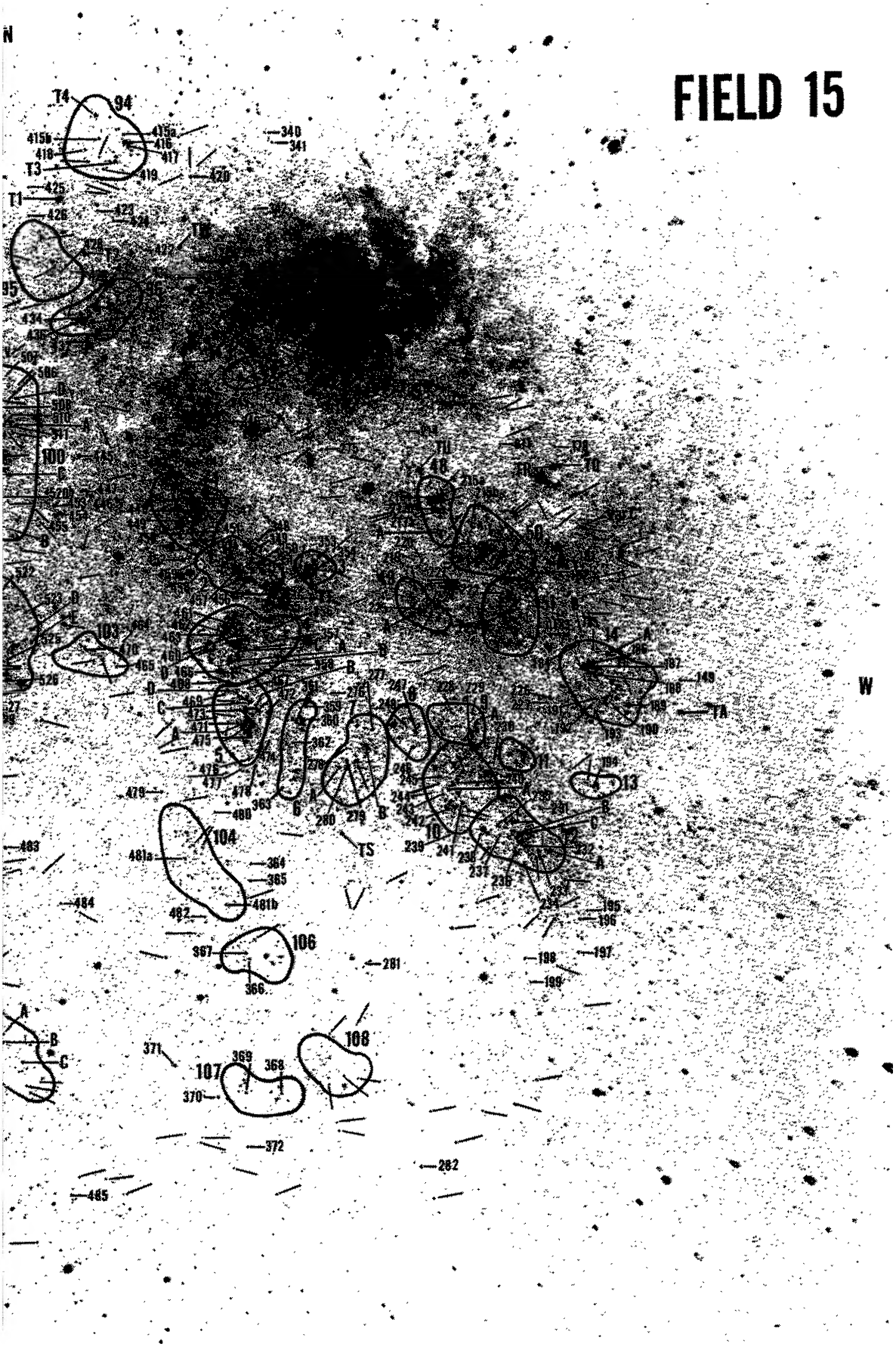

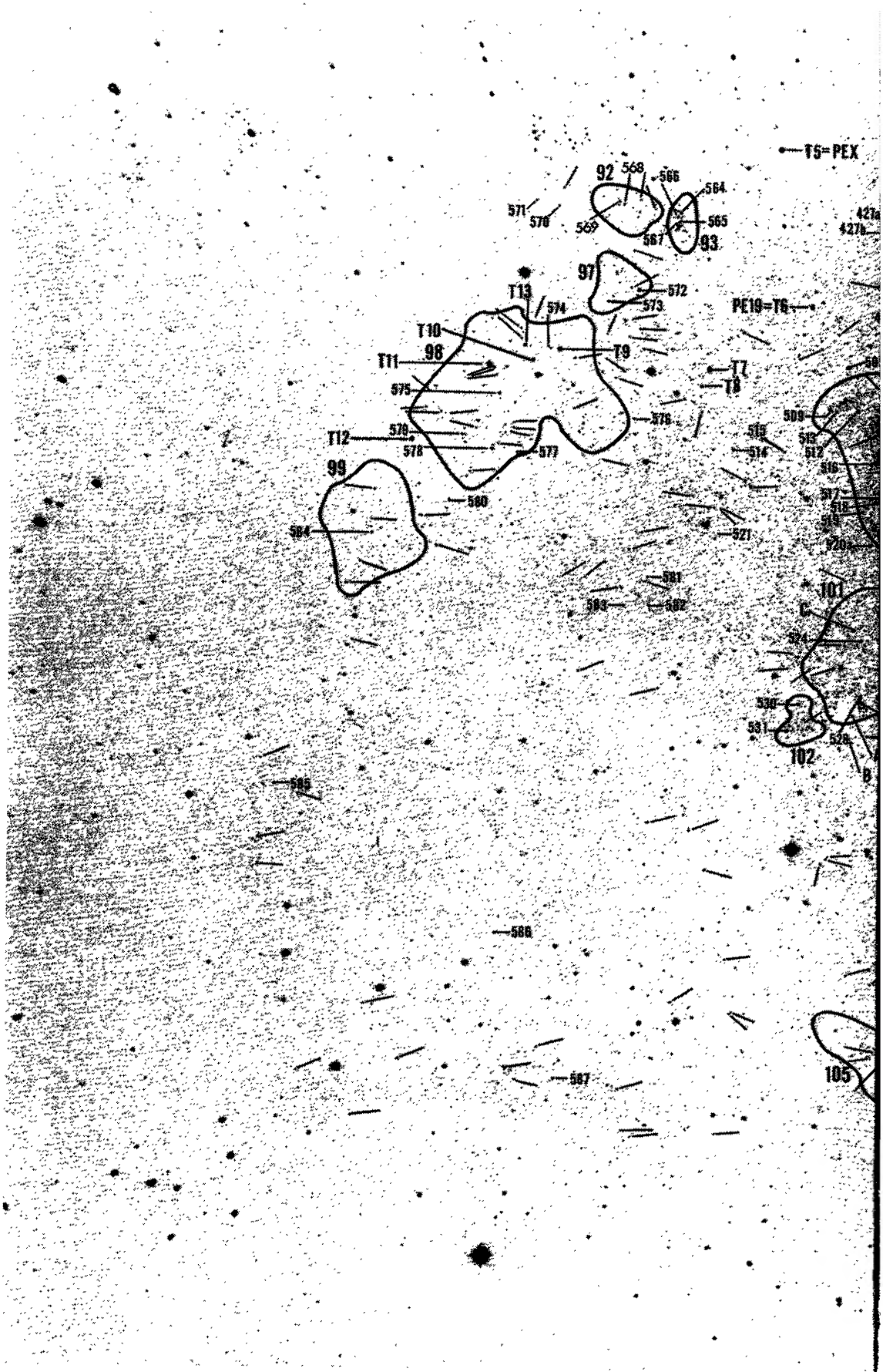

FIG. 6.—Finding chart for the blue stars in field 15 from a Palomar 5 m 103aD+GG11 plate

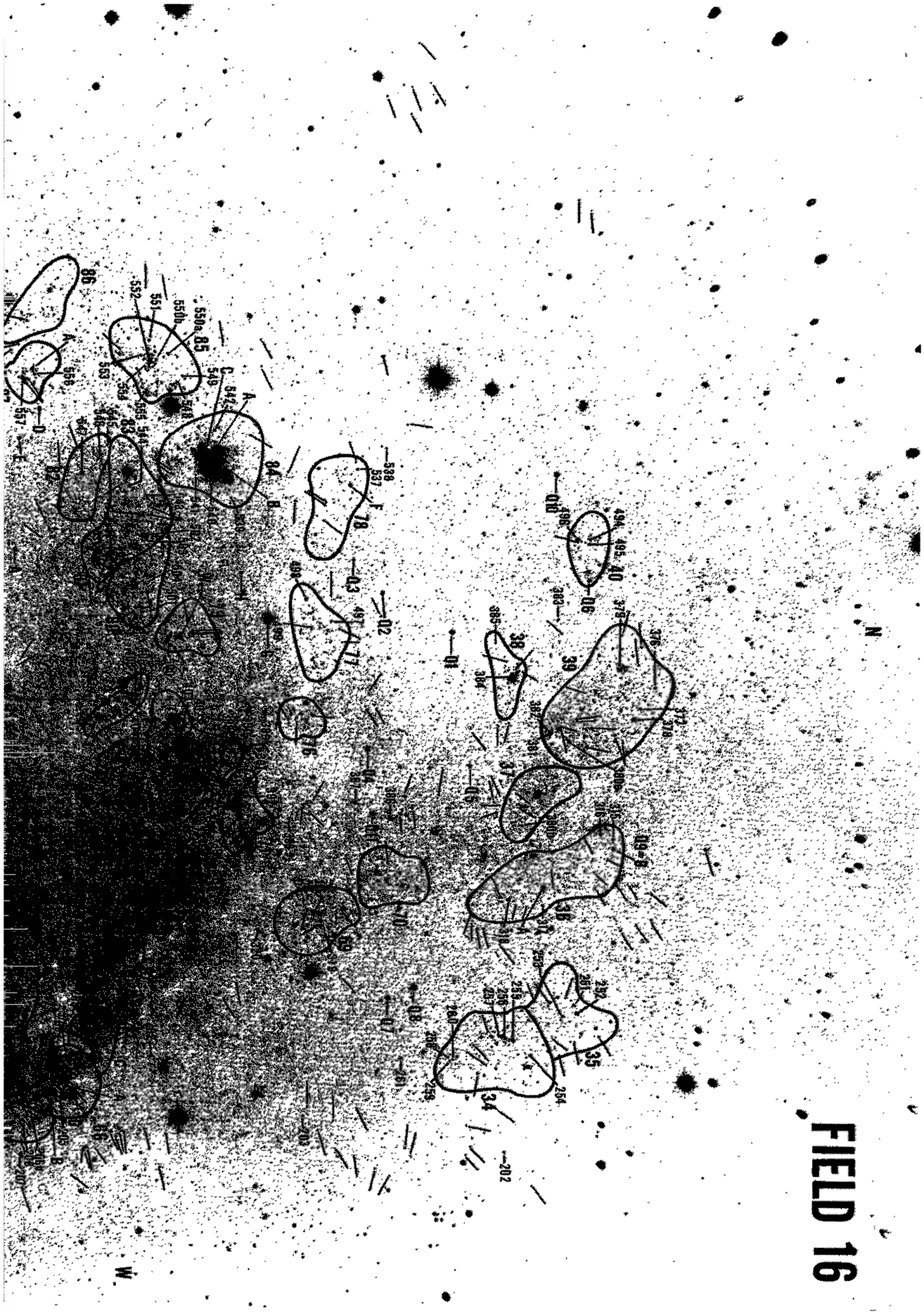

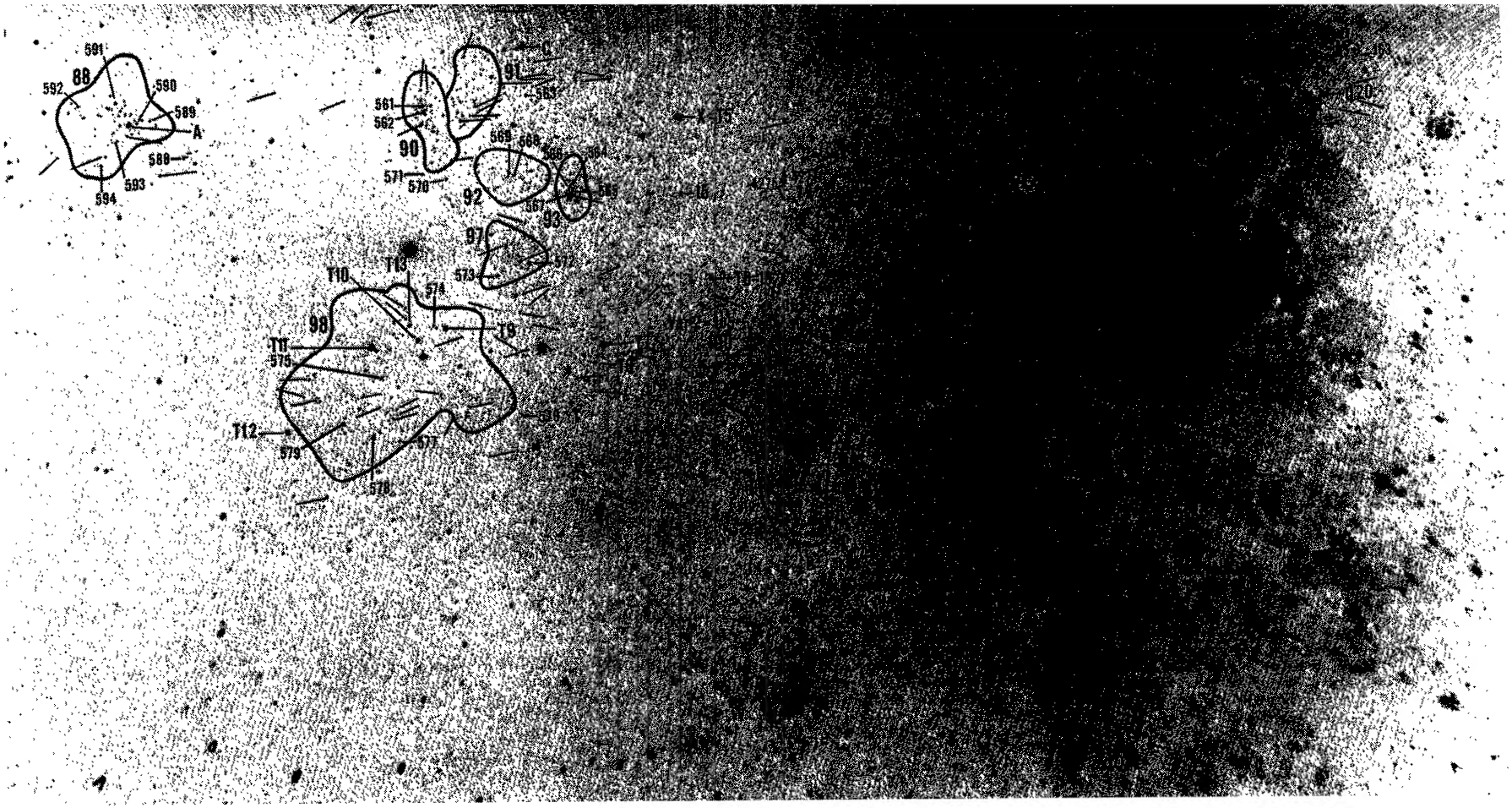

FIG. 7.—Finding chart for the blue stars in field 16 from a Palomar 5 m 103aD+GG11 plate

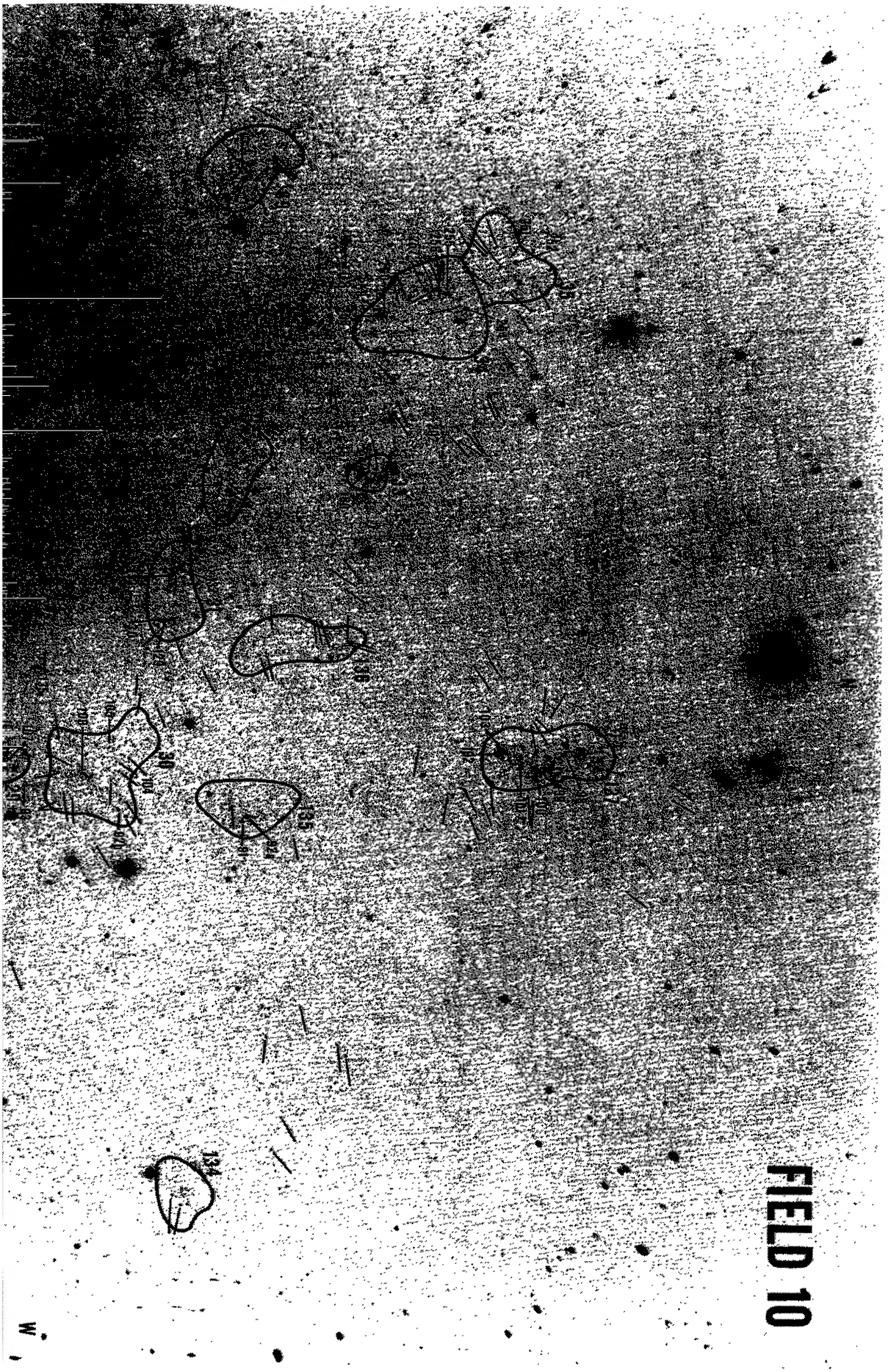

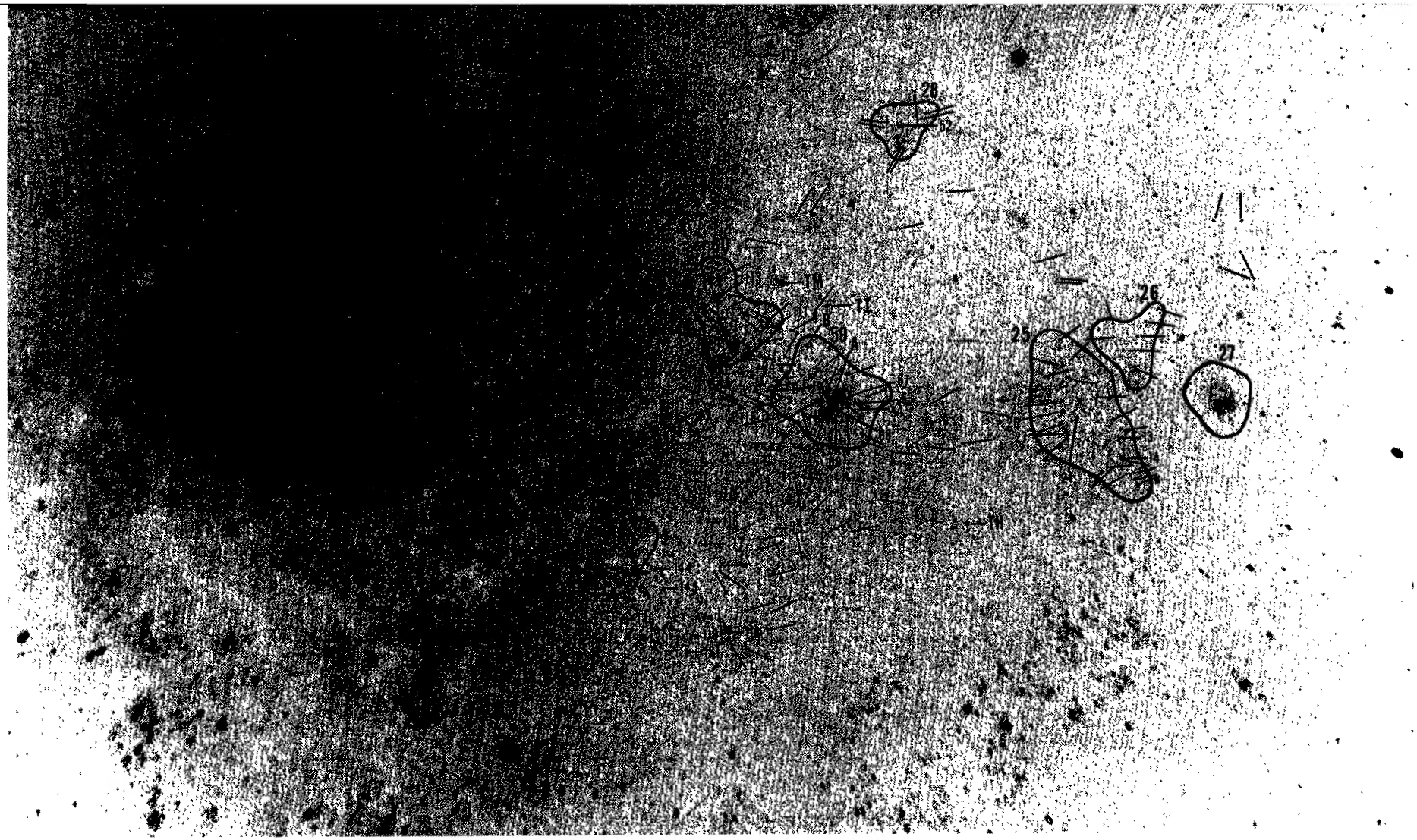

FIG. 8.—Finding chart for the blue stars in field 10 from a Palomar 5 m 103aD+GG11 plate

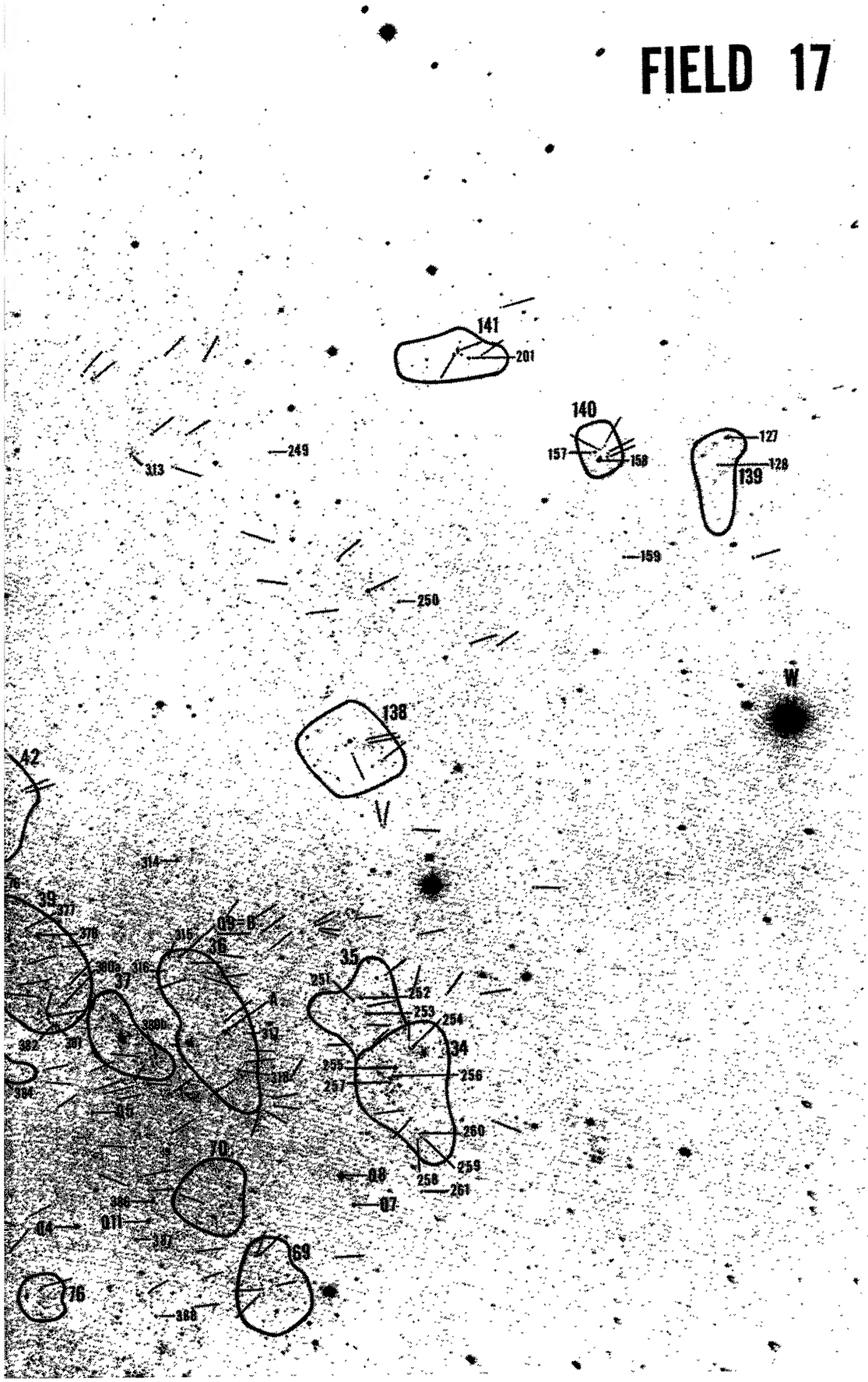

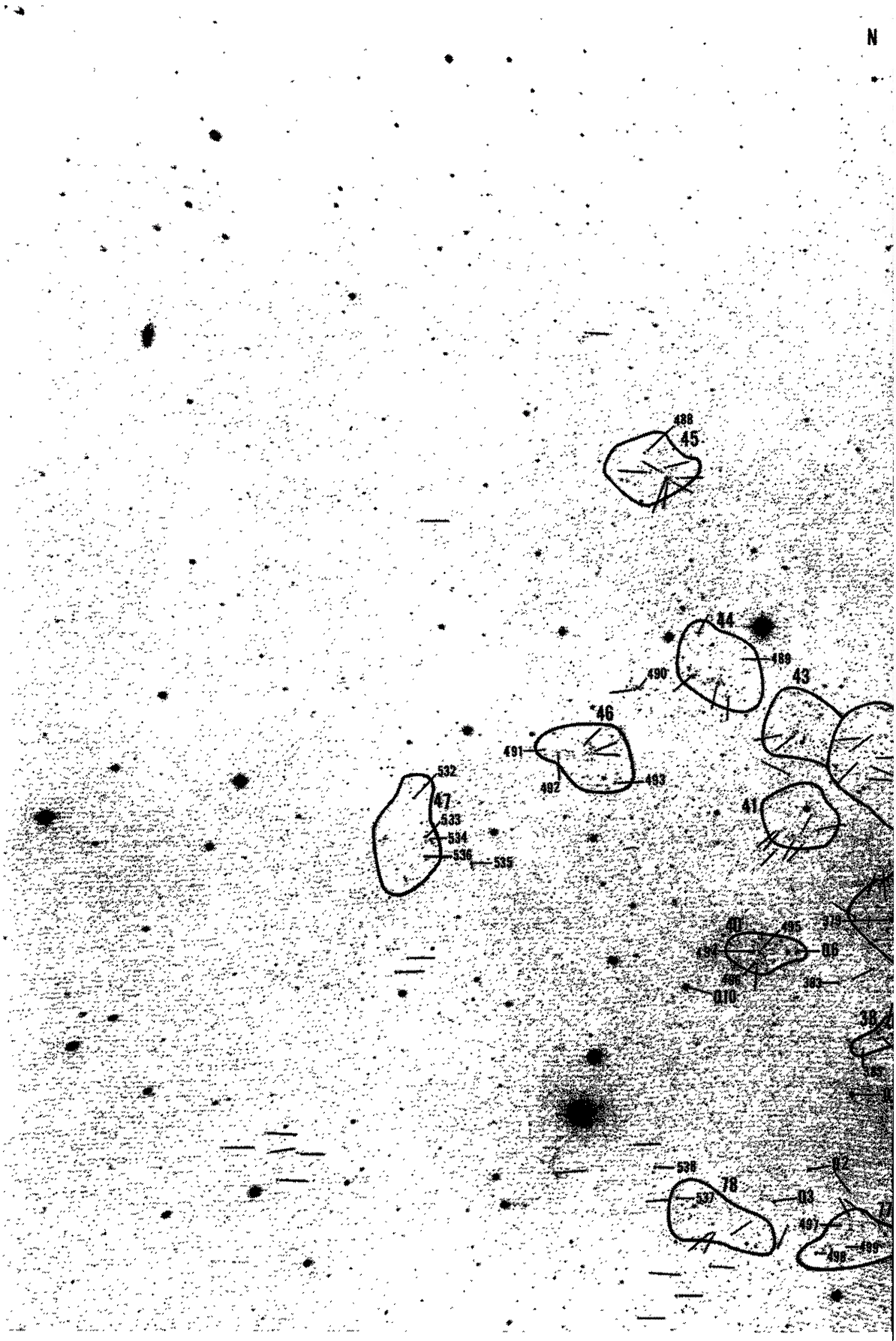

FIG. 9.—Finding chart for the blue stars in field 17 from a Palomar 5 m 103aD+GG11 plate

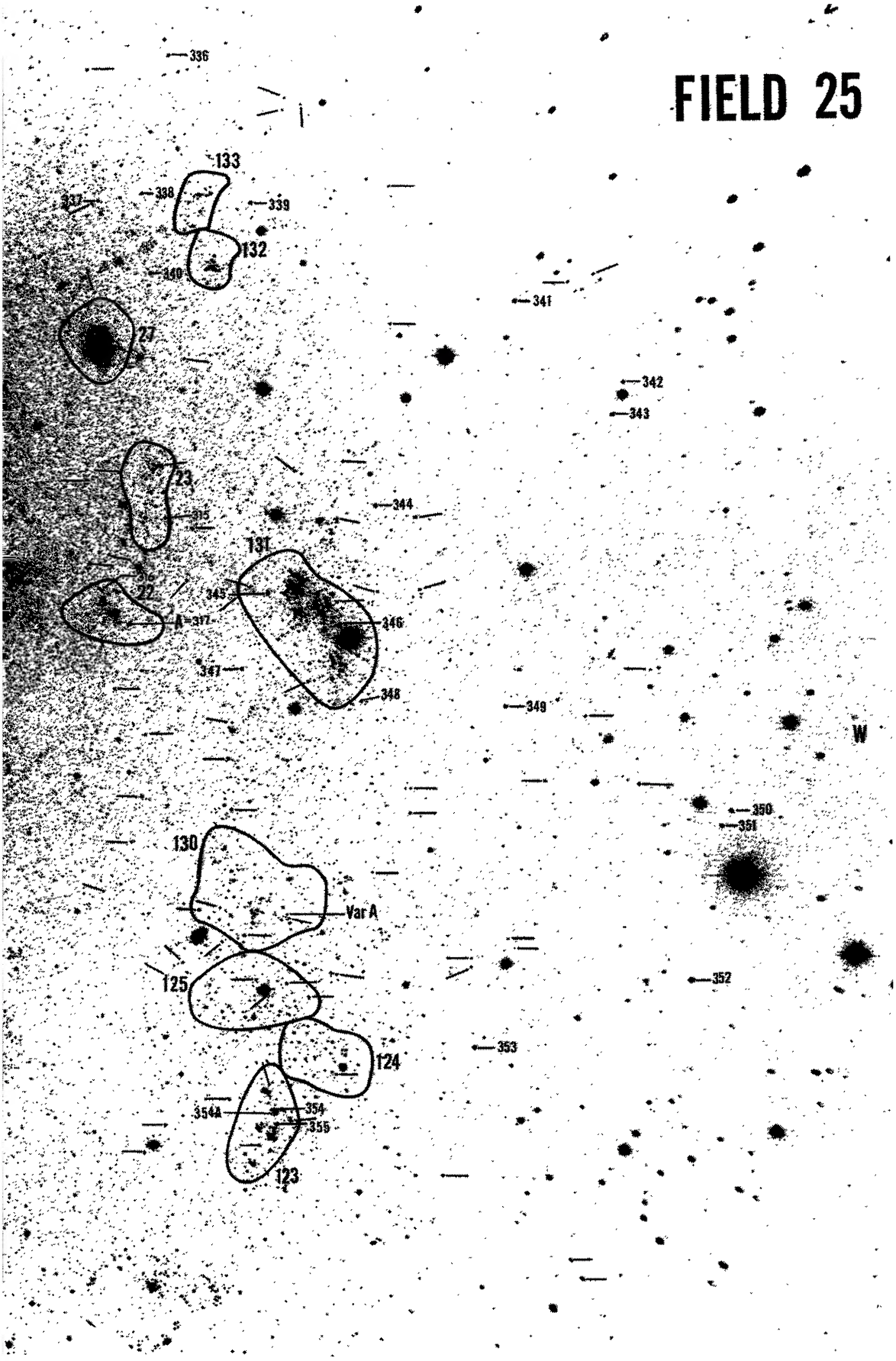

nbered objects is listed in Table 6.

FIG. 10.—Finding chart for the red stars in field 25 from a Palomar 5 m 103aD+GG11 plate. Photometry for the nu

FIELD 9

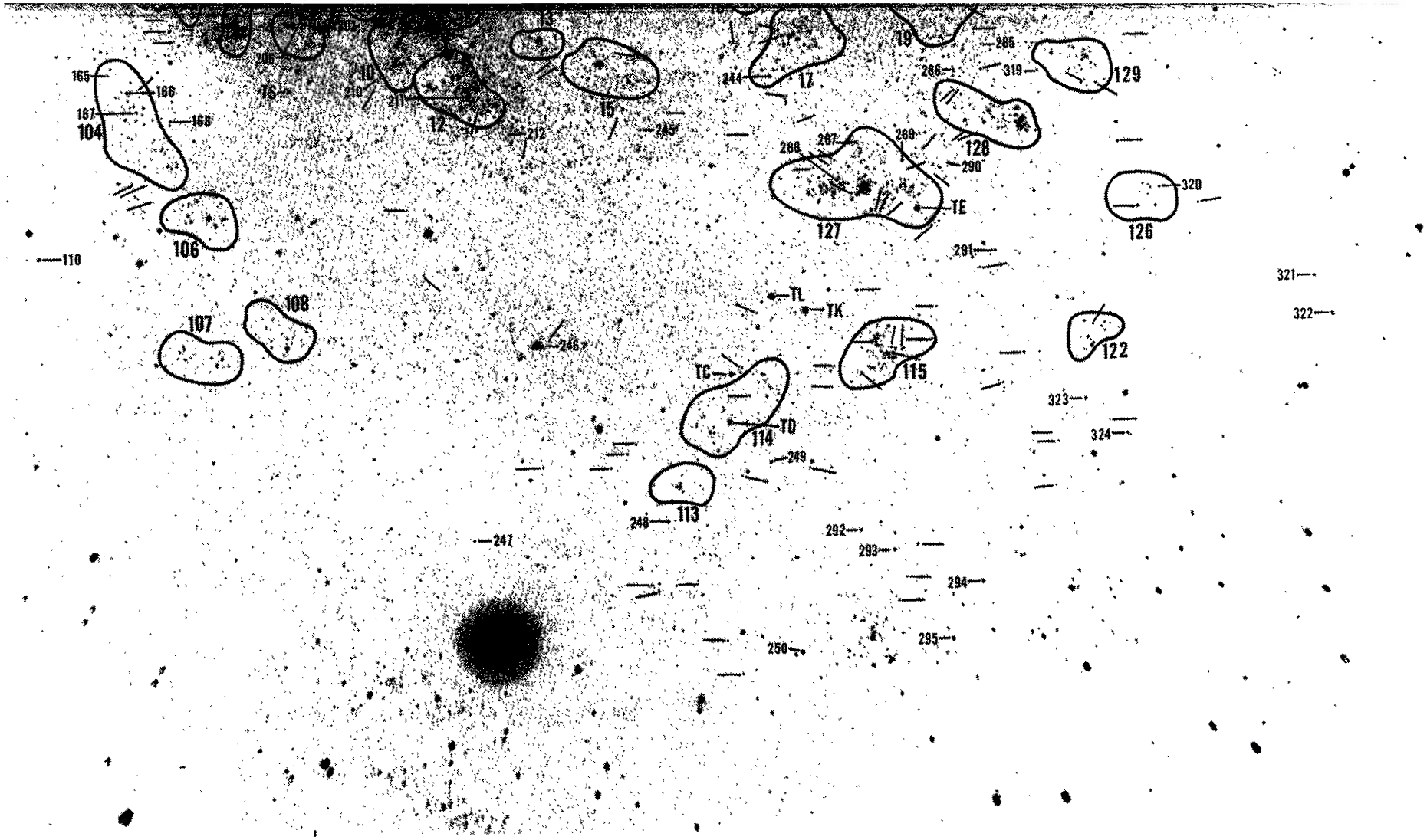

FIG. 11.—Finding chart for the red stars in field 9 from a Palomar 5 m 103aD+GG11 plate

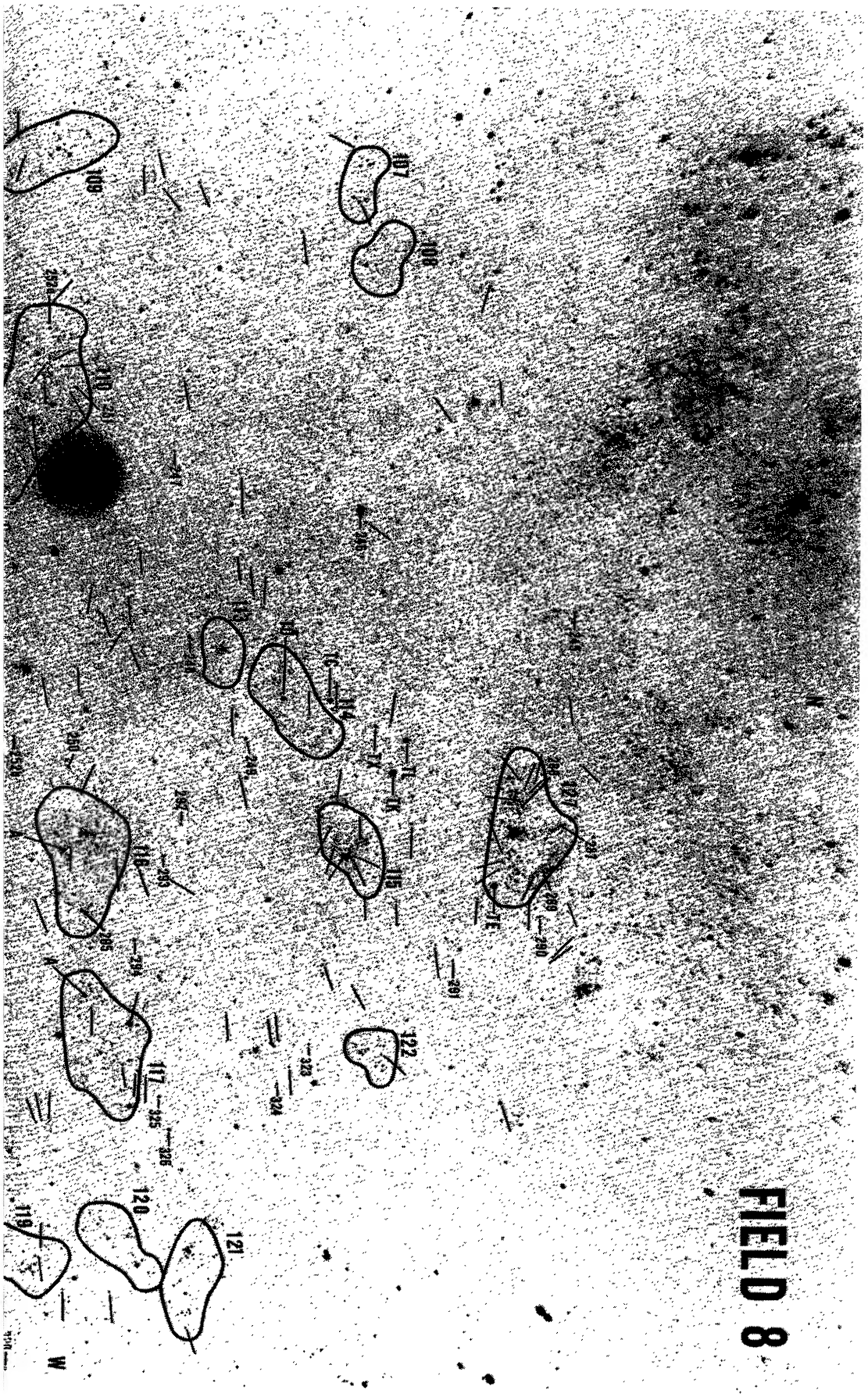

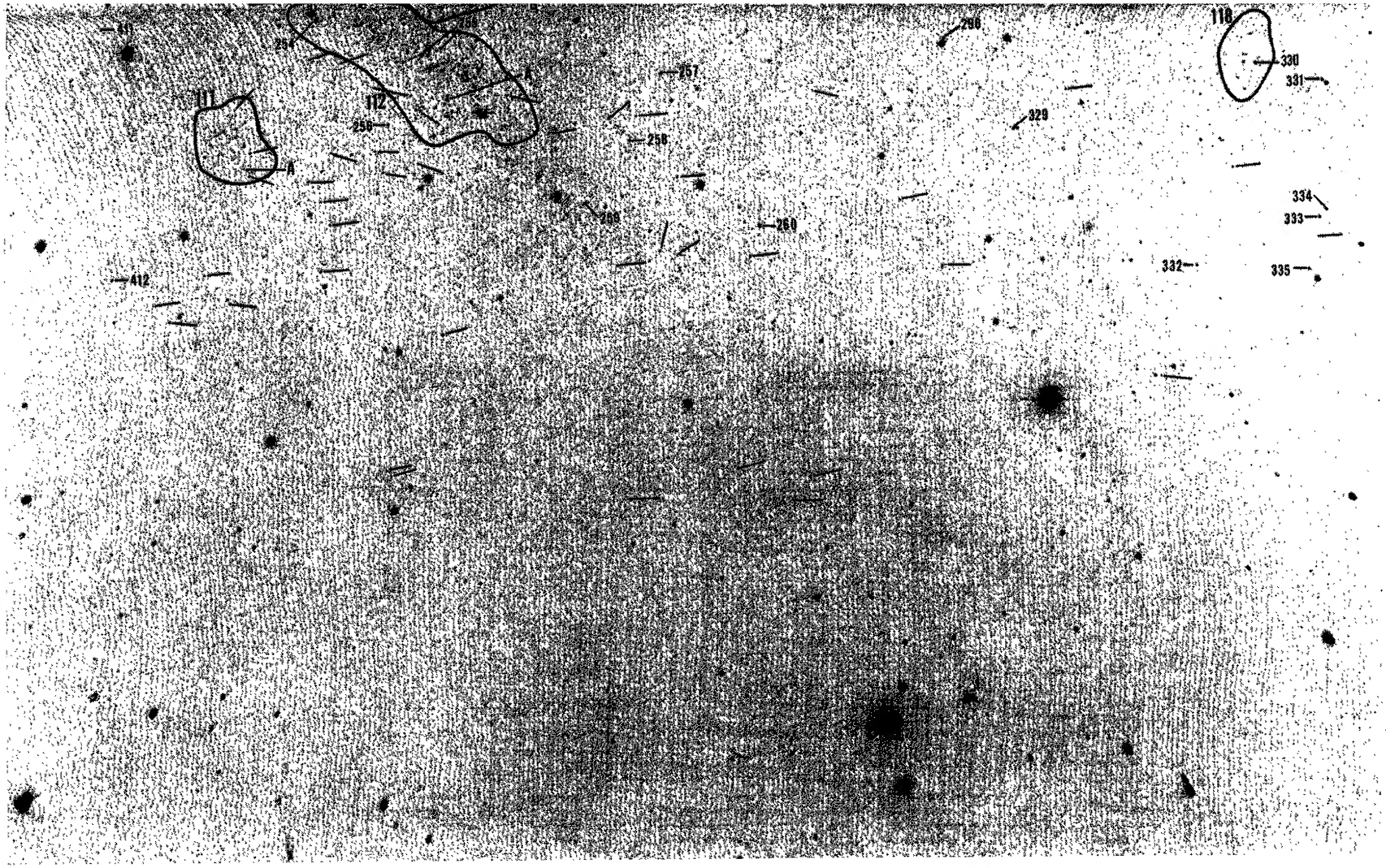

FIG. 12.—Finding chart for the red stars in field 8 from a Palomar 5 m 103aD+GG11 plate

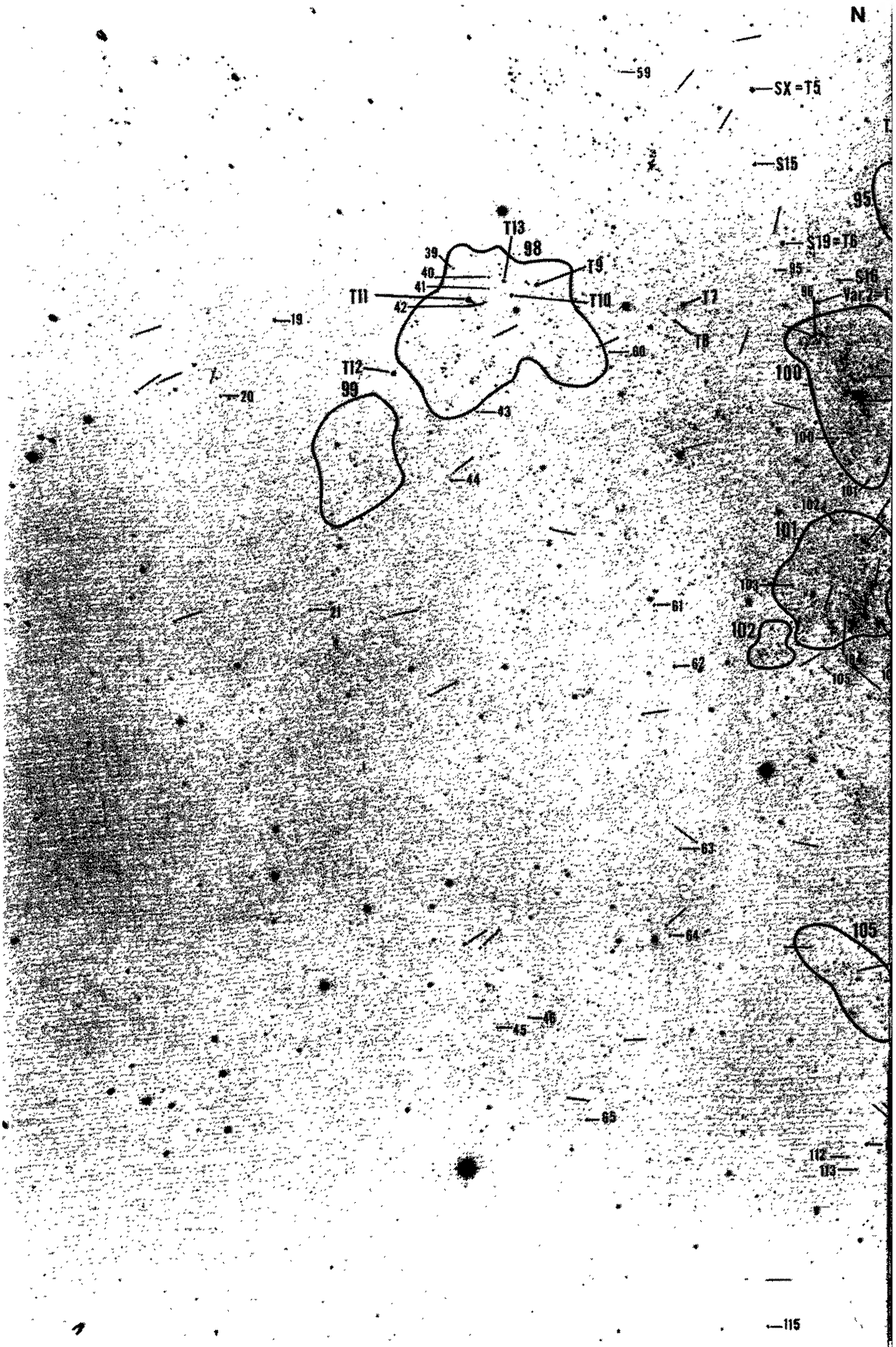

FIG. 13.—Finding chart for the red stars in field 15 from a Palomar 5 m 103aD+GG11 plate

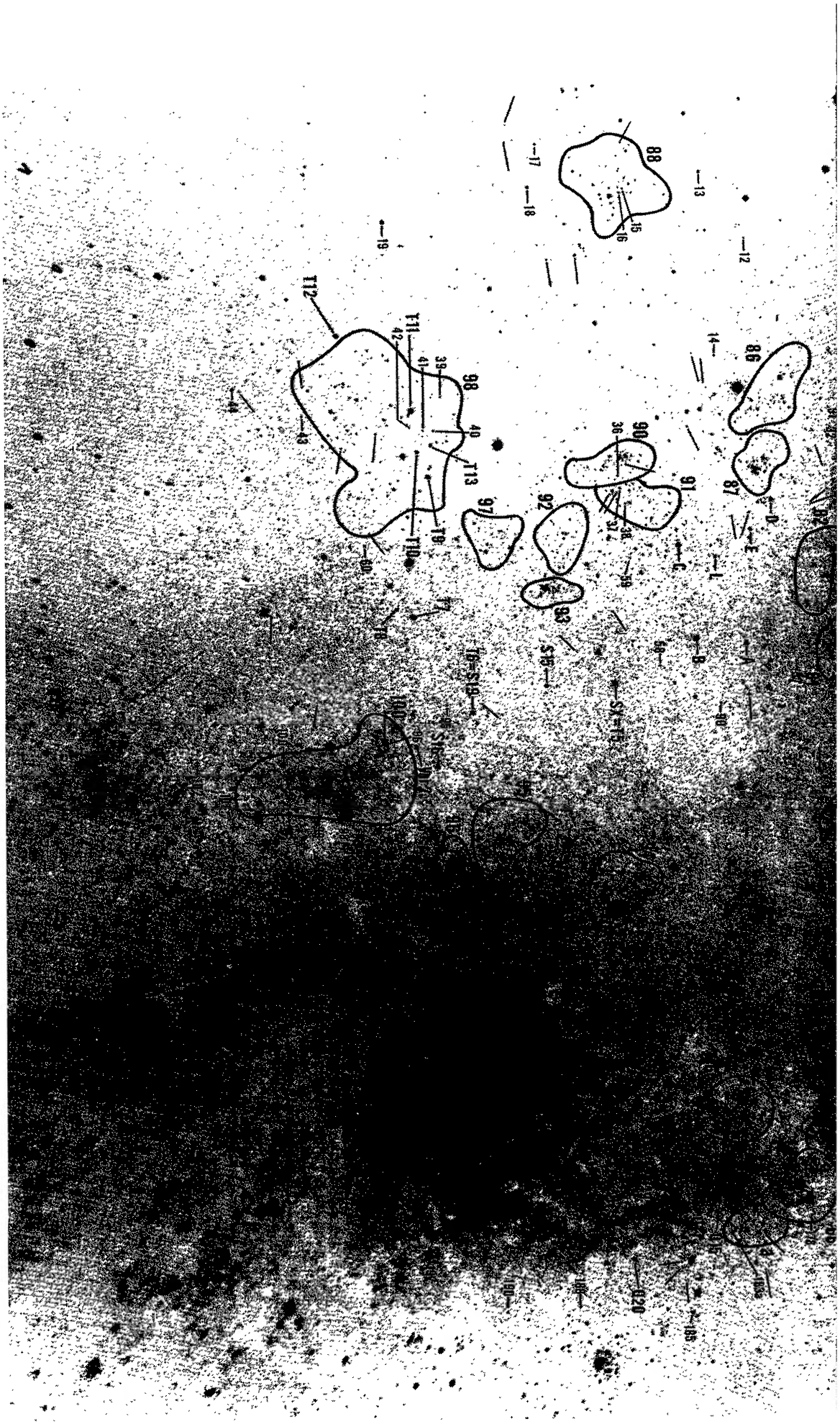

FIG. 14.—Finding chart for the red stars in field 16 from a Palomar 5 m 103aD+GG11 plate

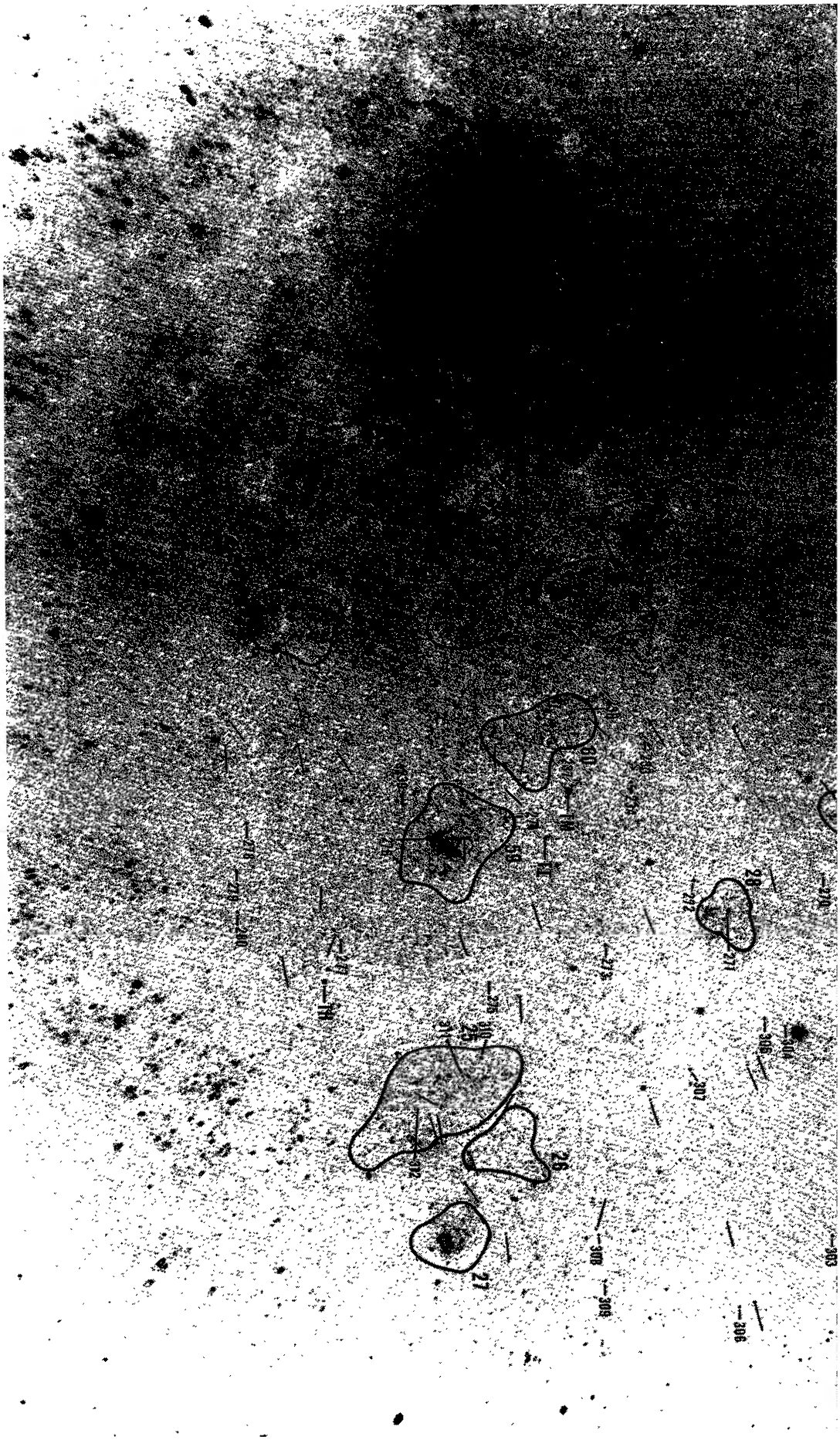

FIG. 15.—Finding chart for the red stars in field 10 from a Palomar 5 m 103aD+GG11 plate

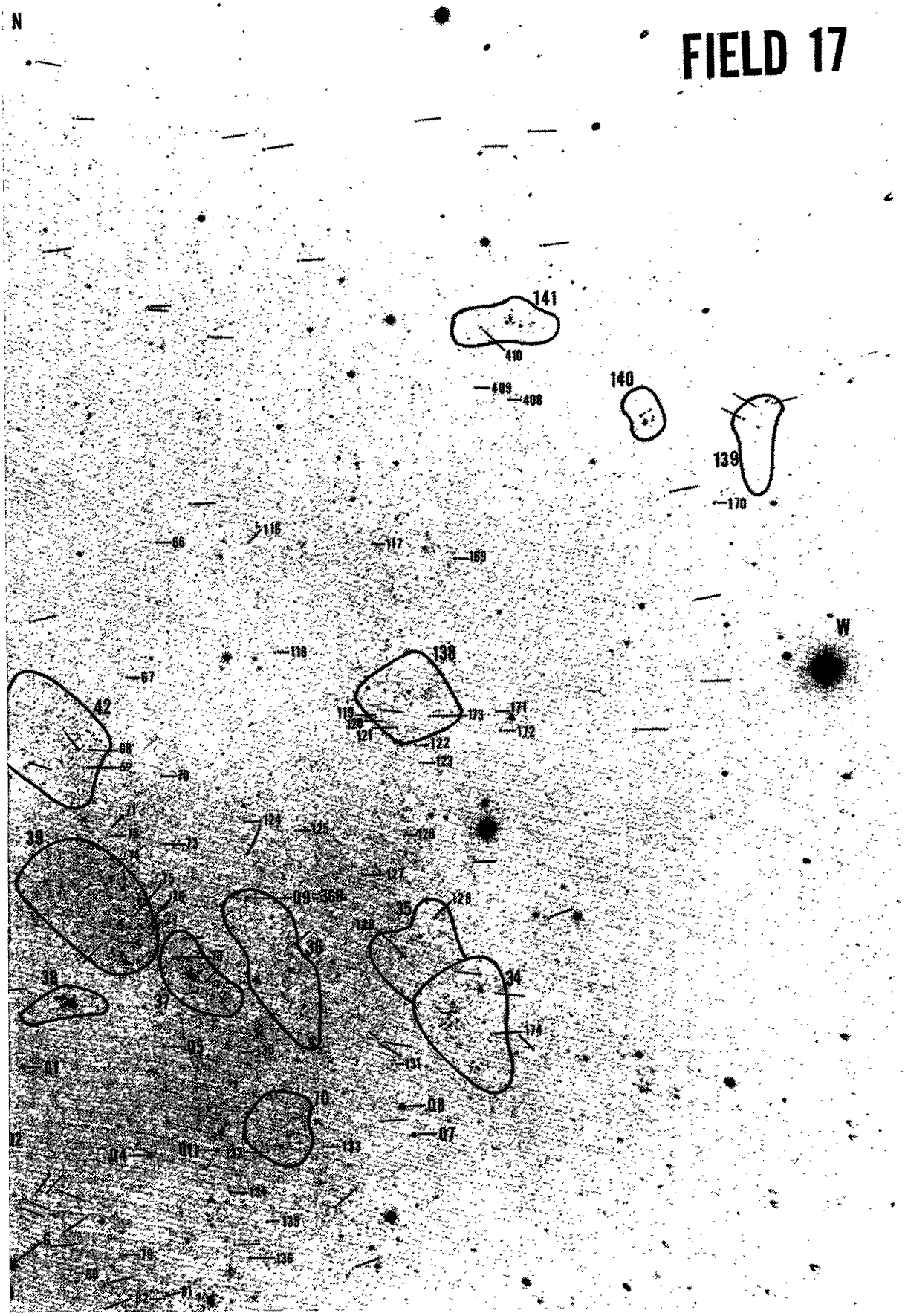

FIG. 16.—Finding chart for the red stars in field 17 from a Palomar 5 m 103aD+GG11 plate

to the diffuse background. Conventional photographic iris-photometry is usually out of the question.

The photometry of the candidate stars reported here was done by the method of Argelander eye estimates which eliminates, to first order, most of the problems due to background. A photographic step-scale was used, selected from a library of such scales made over the years with the Hale reflector. The scale was calibrated frequently relative to photoelectric standards taken from the two sequences set up earlier by SJ.

The bright sequence to the east of the nucleus (Fig. 2 of SJ) is in fields 15 and 16. The standards there cover the interval $12.7 < V < 17.6$ and are identified again in Figures 6, 7, 13, and 14. The fainter sequence (Fig. 3 of SJ) on the west side occurs in a clear region of field 25 and covers the interval $8.0 < V < 21.3$.

The spreading of these sequences over the face of M33 was done using the overlapping plates as follows. The step-scale was calibrated using the faint photoelectric sequence in field 25. From the curve of step-scale number versus the photoelectric magnitude, the candidate stars from the blink survey in field 25 were measured. The subset of those stars that occur in the overlap with field 9 was then used to calibrate the B and V plates of field 9. The other fields are then stepwise overlapped in the same fashion from 9 to 15, 15 to 16, 16 to 10, etc., until the circuit is closed.

This chain of overlaps was tested halfway through by making the calibration of fields 15 and 16 directly from the eastern photoelectric sequence itself and checking for consistency with the sequence brought in from field 25. A second test was made to determine the closing error of the entire chain by comparing the calibration of field 9 via the 9→15, 15→16, 16→10, and 10→9 circuit with the starting calibration of 9 via 25.

This method of spreading and checking the sequences was used primarily for the V Palomar plates. However, although the B magnitudes were also estimated via the step scale, most of the measurements were made on two Kitt Peak 4 m blue Mayall reflector plates of different exposure times in order to test the background effect. Here, as in Figure 1, the entire area is contained on a single plate; hence, overlaps are unnecessary.

The B magnitudes were measured in this way because the method of overlaps using the 5 m Hale plates, although more accurate due to the large plate scale ($11''$ mm^{-1} compared with 18) and the fewer field problems with radial distance, was too time-consuming and very tedious. The V measurements alone had taken 7 working months by the overlap method. However, when the reduced B measurements were completed using the two Kitt Peak plates, we found systematic errors on the long exposure 4 m blue plates that depend on background. The 4 m B magnitudes for such stars fainter than $B = 20$ are measured to be too faint, sometimes by as much as 0.7 mag. Stars that are brighter or in the clear or both are not so affected. As the problem exists in our final catalogs only for the fainter stars in B on the 4 m plates,[5] and as we are interested primarily in V for the brighter stars, we have allowed the problem in B to stand rather than to measure the remaining 5 m Palomar B plates by the overlap method. We return to the point again in § V in connection with a discussion of the colors.

The tests for the final photometric accuracy (i.e., [1] comparison of the independent calibrations of fields 15 and 16 from the overlaps and from the photoelectric sequence directly, and [2] the test for the closing error after the complete overlap circuit) show that our final magnitude system is on the SJ photoelectric system to better than $\sim \pm 0.2$ mag in V systematically for $V \lesssim 20.5$, except in regions near the center with high background where the systematic error may be as much as 0.5 mag.

We tested the transfer procedure for the bright part of the overlap sequences in still a third way. Most of the candidates from the blink survey are faint; hence if they had been used alone to transfer the scales through the overlap region we would have no information by which to transfer the bright end of the scale. For this reason we were forced to measure certain strategically placed bright foreground stars in the overlap regions. These, the so-called "area-transfer stars," are listed in Table 3 and are identified in Figures 3–16. The relevant finding charts are listed in column (2) by the field numbers. The adopted mean V and B values derived from the step-scale estimates, together with the number of independent estimates from all overlaps are listed in columns (3)–(6).

After the transfer procedure for the candidates in all fields had been completed, we made a direct photoelectric check to determine the zero-point accuracy of the transfers. Nineteen stars from Table 3 were observed photoelectrically in B, V, and R with the Mount Wilson 2.5 m Hooker reflector in 1978 November, and the results are listed in Table 4. The difference (pe-pg) between Tables 3 and 4 for the stars in common are $\langle \Delta V \rangle = +0.075 \pm 0.035$ (σ) mag with σ for a single difference of ± 0.15 mag and where the largest difference is $\Delta V = 0.35$ mag for star Q 14. The mean difference in B is $\langle \Delta B \rangle = +0.135 \pm 0.049$ (σ) mag with σ for a single difference of 0.21 mag and where the largest difference is $\Delta B = 0.50$ mag for stars Q2 and Q14. We consider this agreement to be highly satisfactory in that the final photometric system is reliable.

b) The Photographic Catalogs

The colors and magnitudes for most of the numbered blue objects marked in Figures 3–9 are given in

[5]The problem also exists for V magnitudes on the 4 m plates, as found by comparison of the measurements on our two 4 m V plates with the Palomar 5 m material, but we have discarded the affected Kitt Peak measurements in V for the final catalogs.

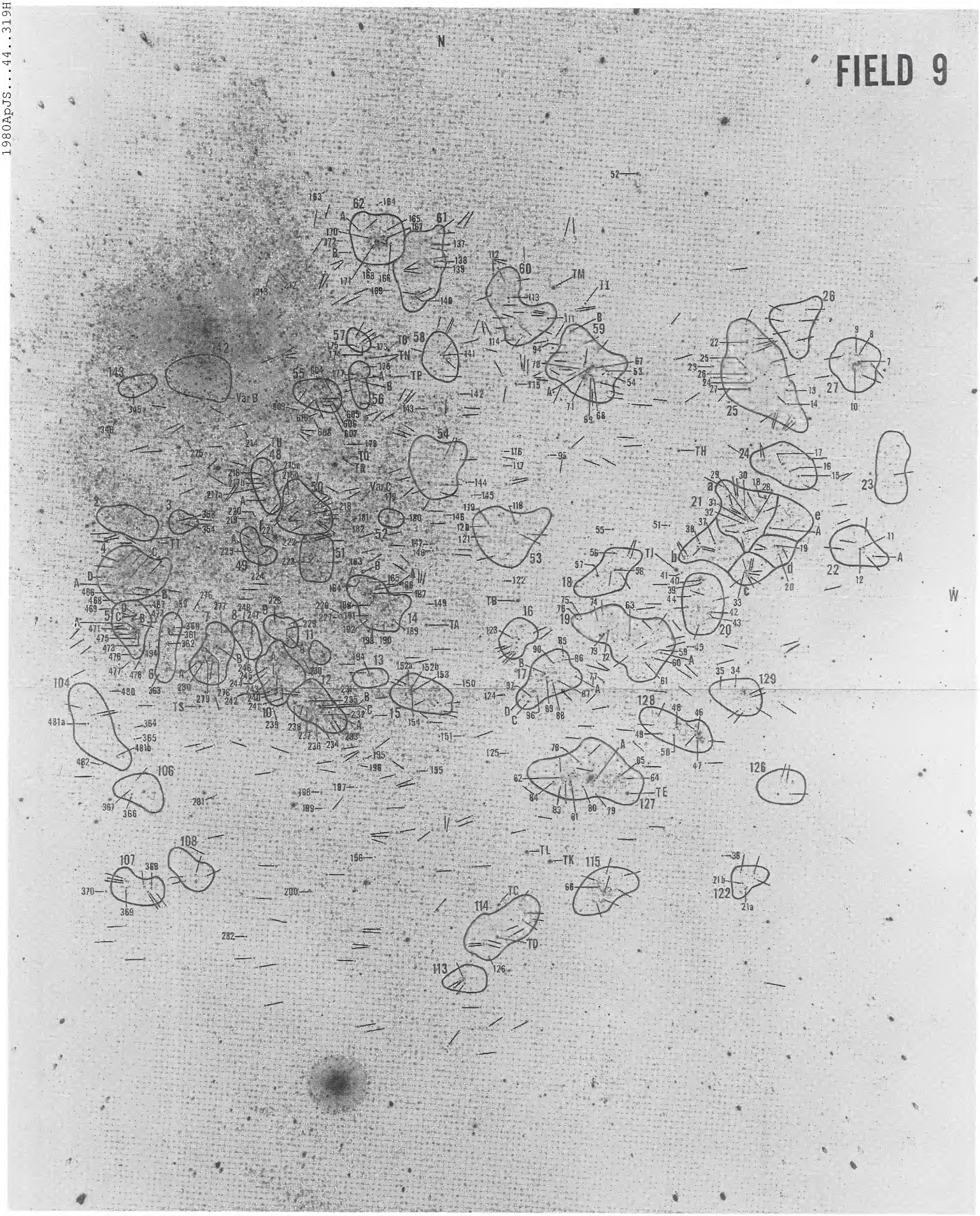

FIG. 4.—Finding chart for the blue stars in field 9 from a short exposure (10 min) 103aD+GG11 plate taken with the Palomar 5 m reflector. The approximate outlines of the associations from Fig. 2 are superposed on the field. Photometry of the numbered stars is listed in Table 4.

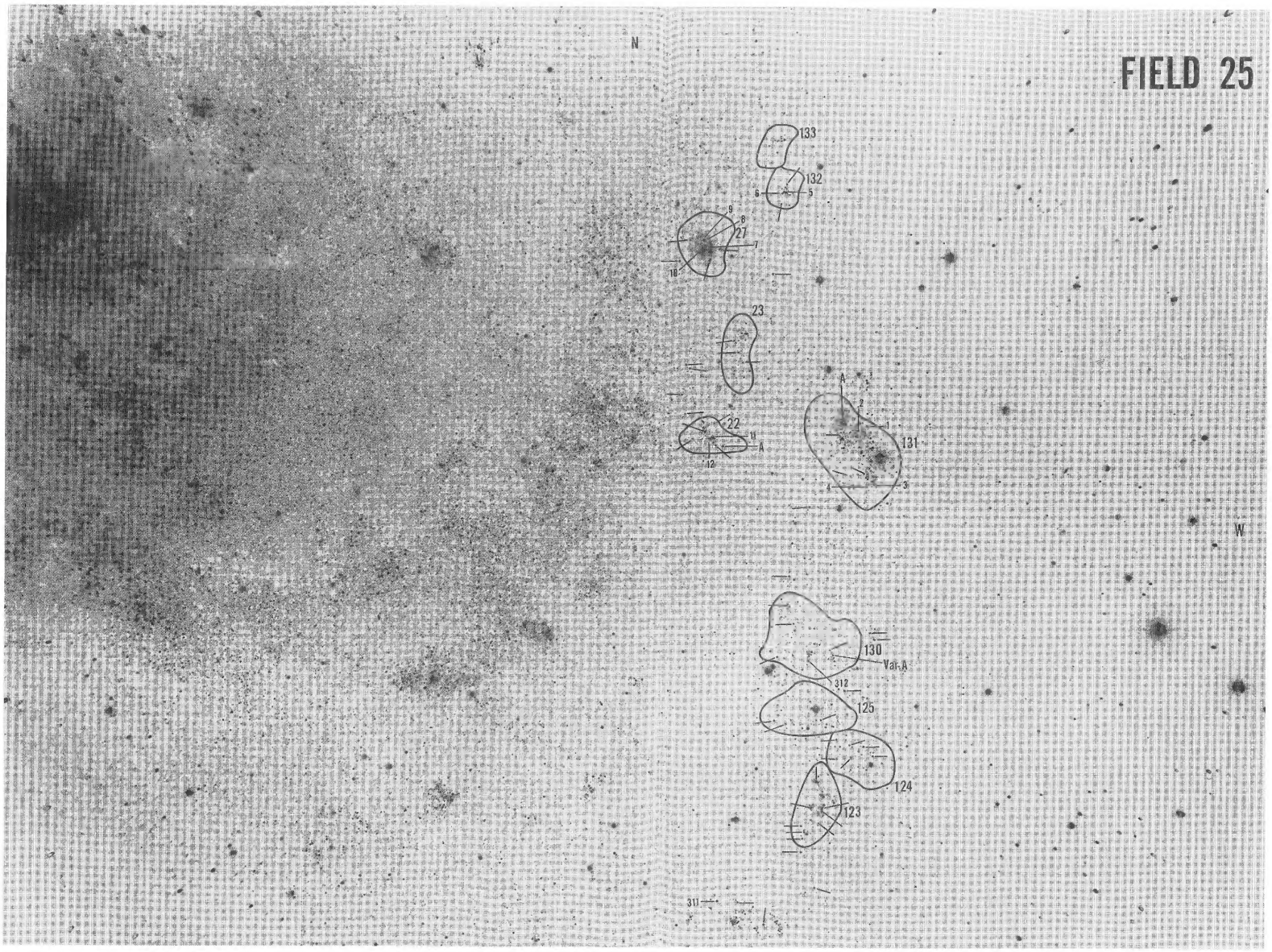

FIG. 3.—Finding chart for the blue stars in field 25 from a deep Palomar 5 m exposure on a 103aO+GG13 plate. The brighter stars are numbered and the photometry is given in Tables 5 and 7. The approximate boundaries of the associations on the western edge of Fig. 2 are outlined. The overlap with field 9 in Fig. 4 is substantial, but the duplicated regions are not generally identified again here.

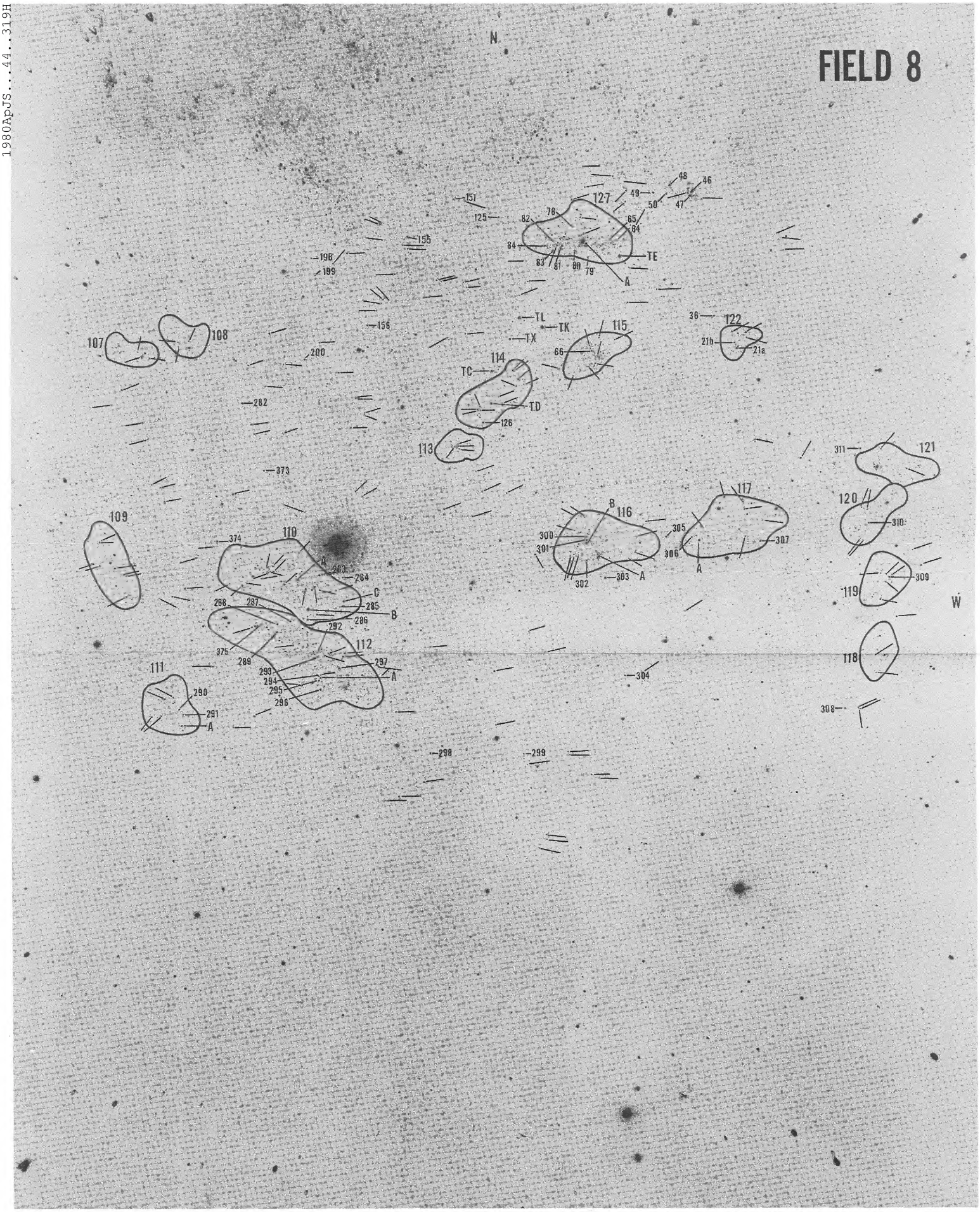

FIG. 5.—Finding chart for the blue stars in field 8 from a Palomar 5 in. IIIa-J + GG 1 plate.

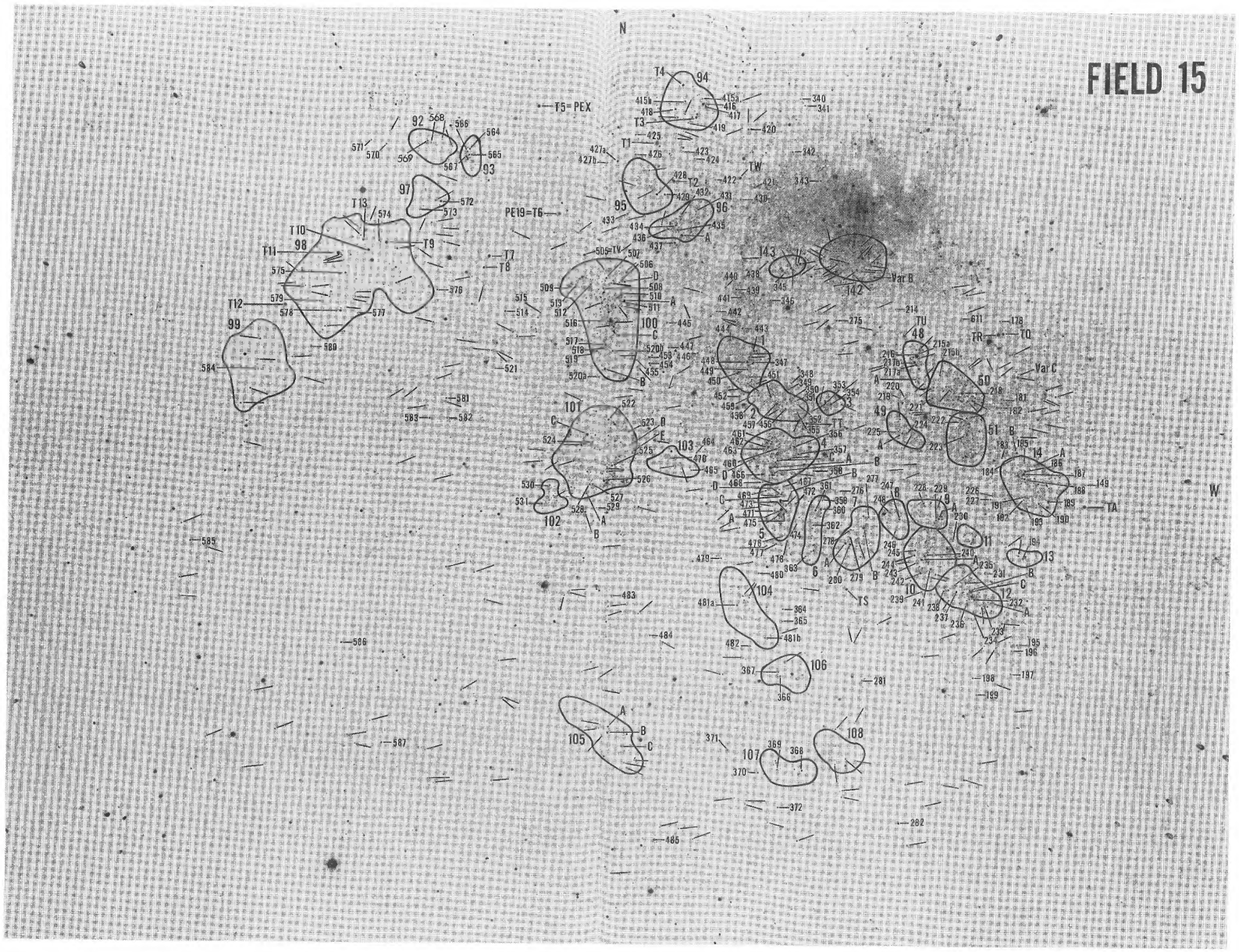

FIG. 6.—Finding chart for the blue stars in field 15 from a Palomar 5 m 103aD+GG11 plate

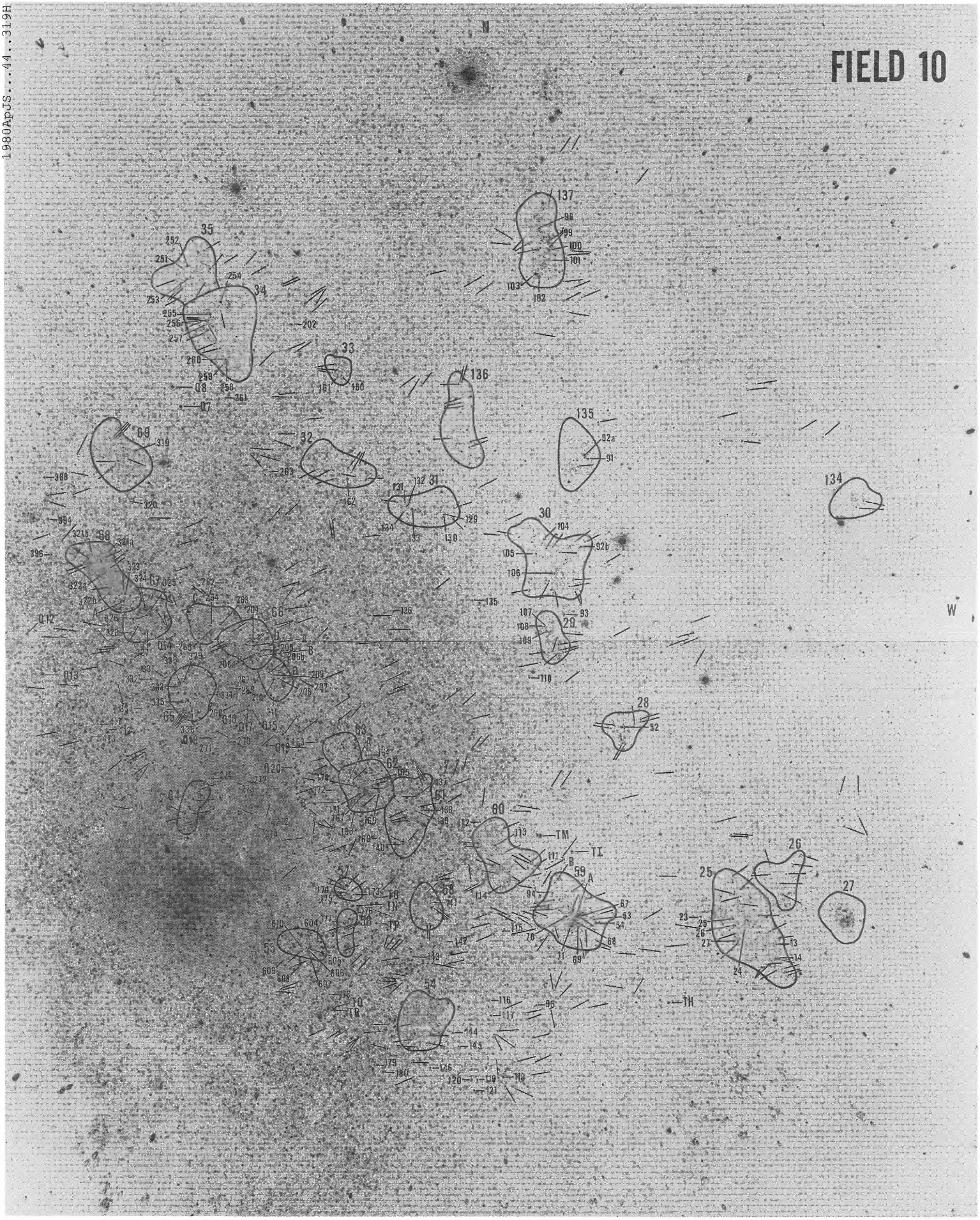

FIG. 8.—Finding chart for the blue stars in field 10 from a Palomar f on IIIaD + GG11 plate.

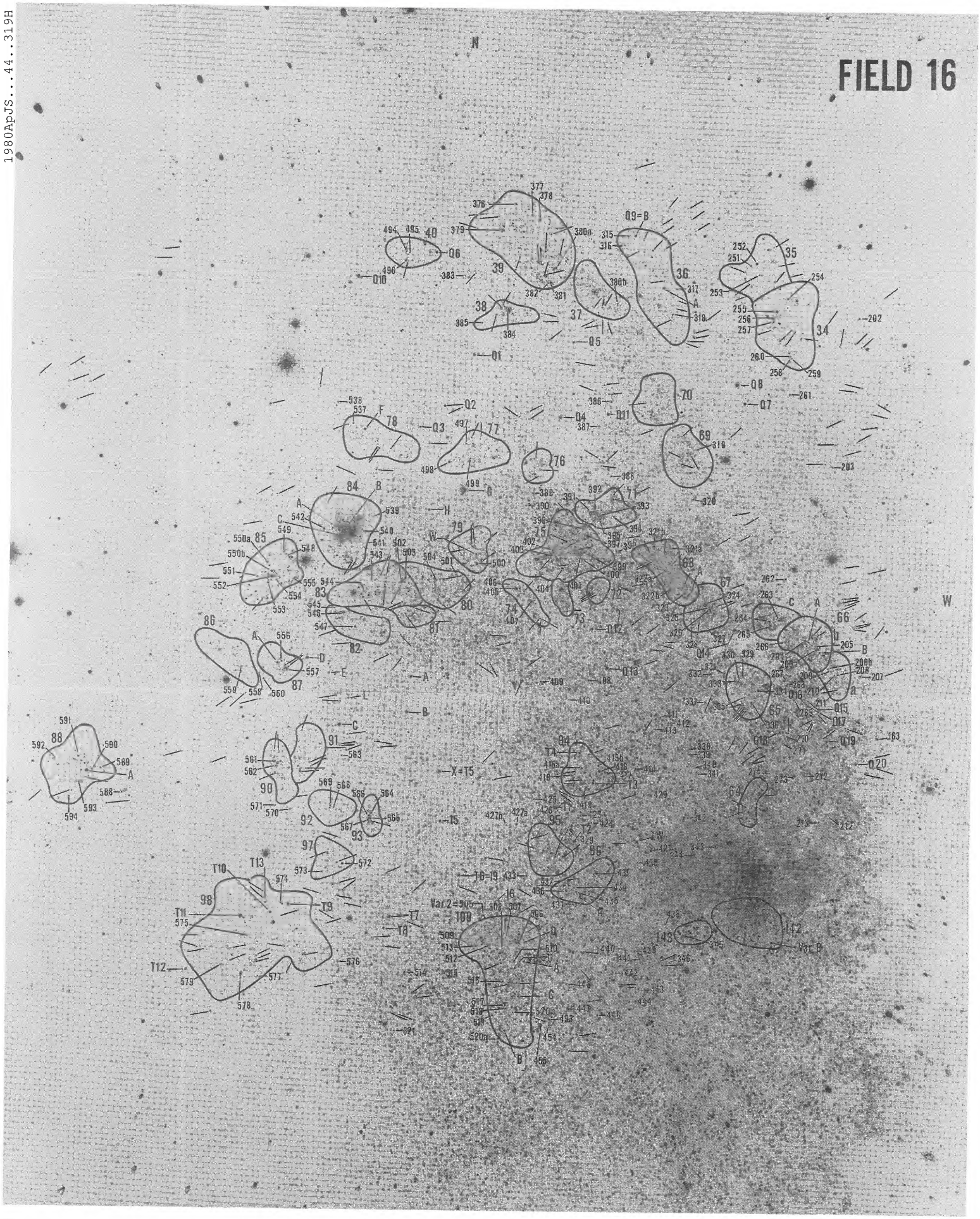

FIG. 7.—Finding chart for the blue stars in field 16 from a Palomar 5 m 103aD+GG11 plate.

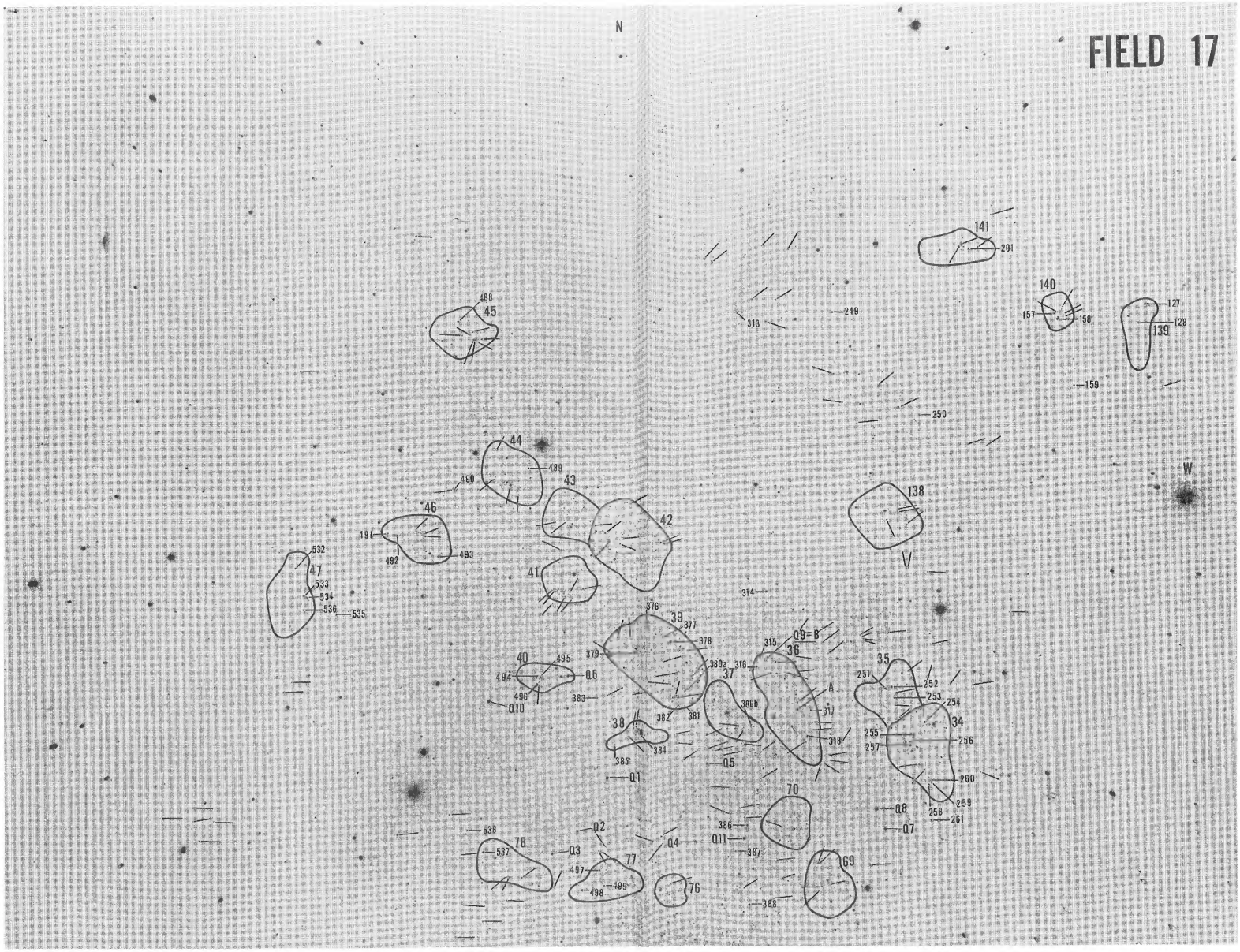

FIG. 9.—Finding chart for the blue stars in field 17 from a Palomar 5 m 103aD+GG11 plate

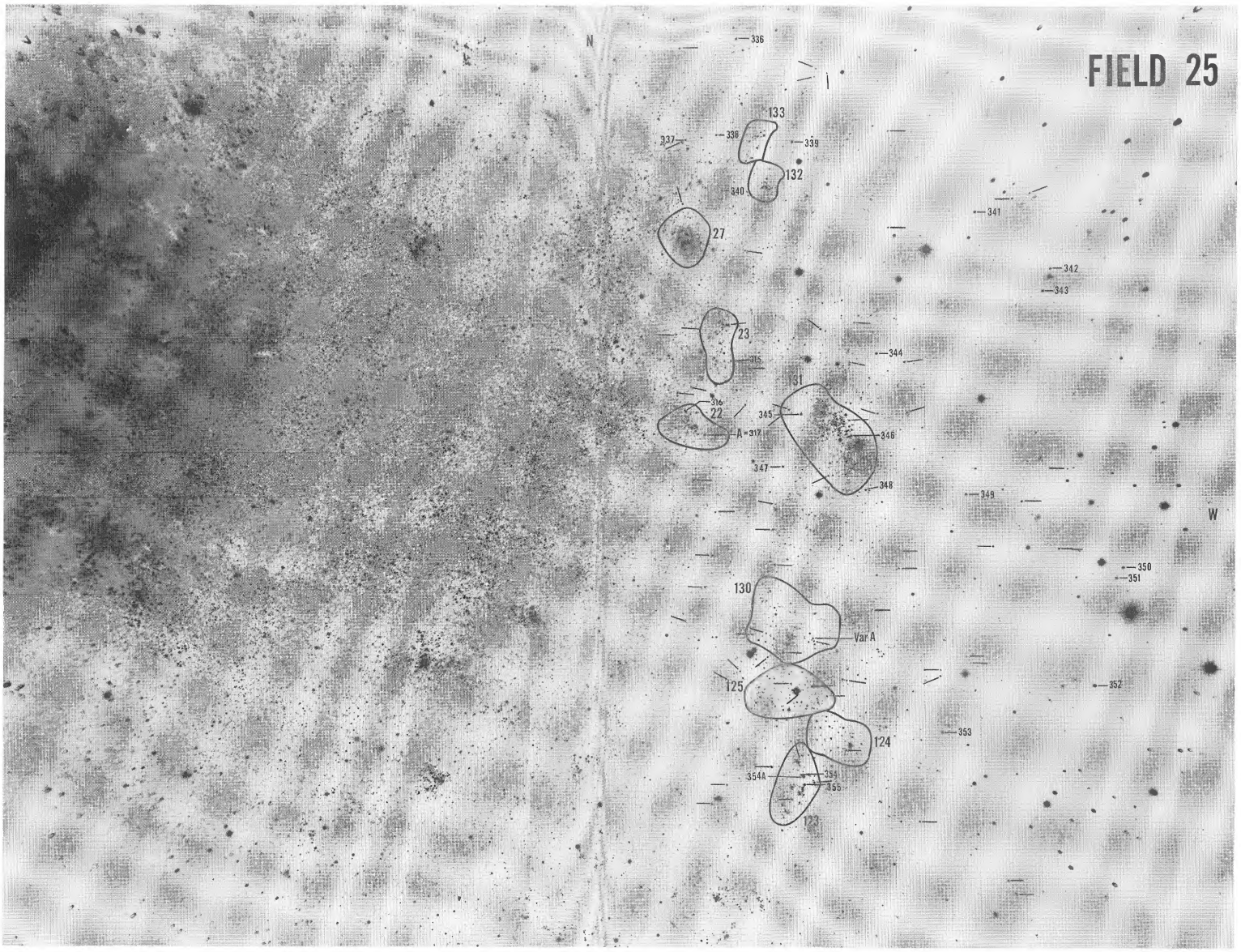

FIG. 10.—Finding chart for the red stars in field 25 from a Palomar 5 m 103aD+GG11 plate. Photometry for the numbered objects is listed in Table 6.

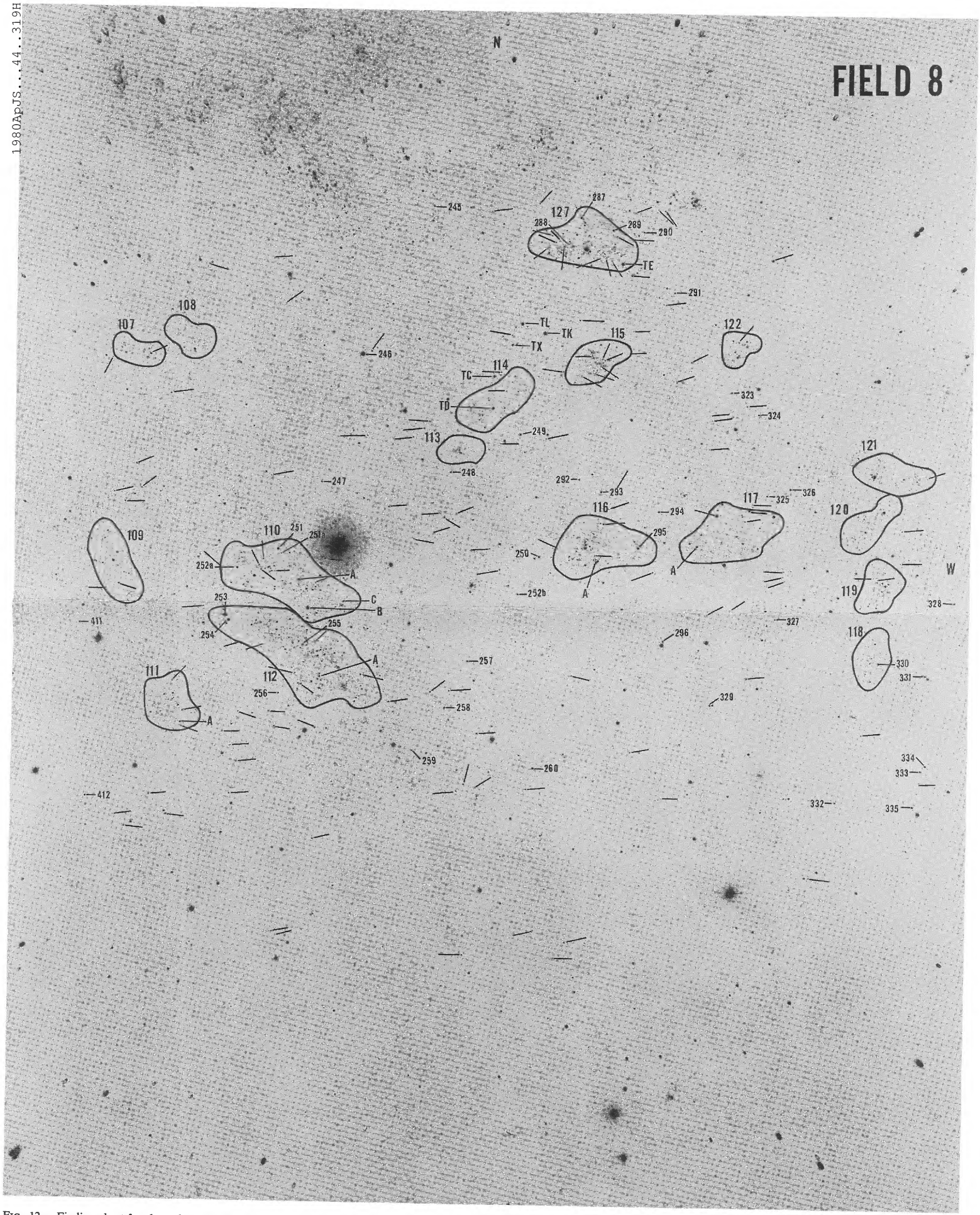

FIG. 12.—Finding chart for the red stars in field 8 from a Palomar 5 m IIIa-J + GG 1 plate.

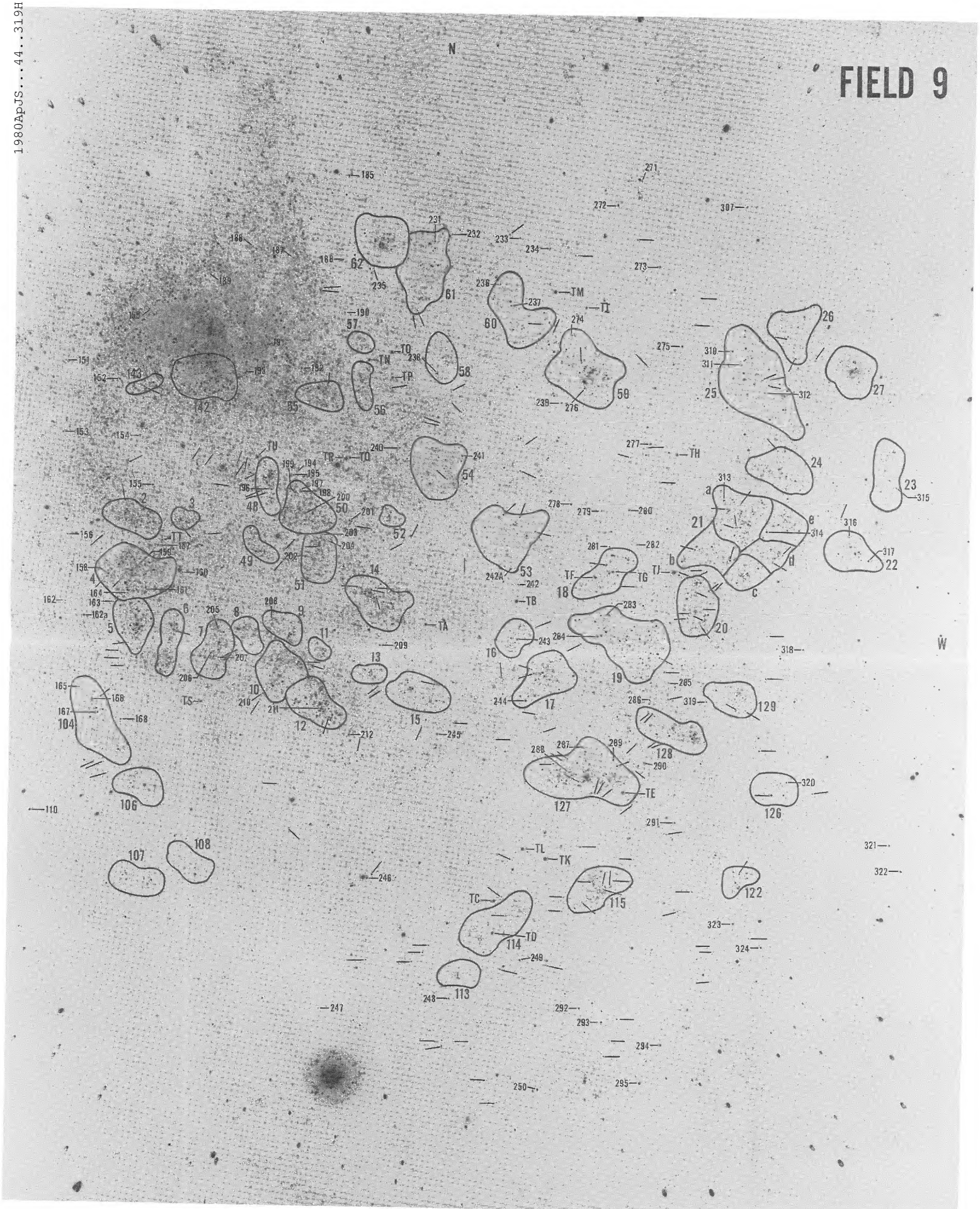

FIG. 11.—Finding chart for the red stars in field 9 from a Palomar 5 cm 103aD plate.

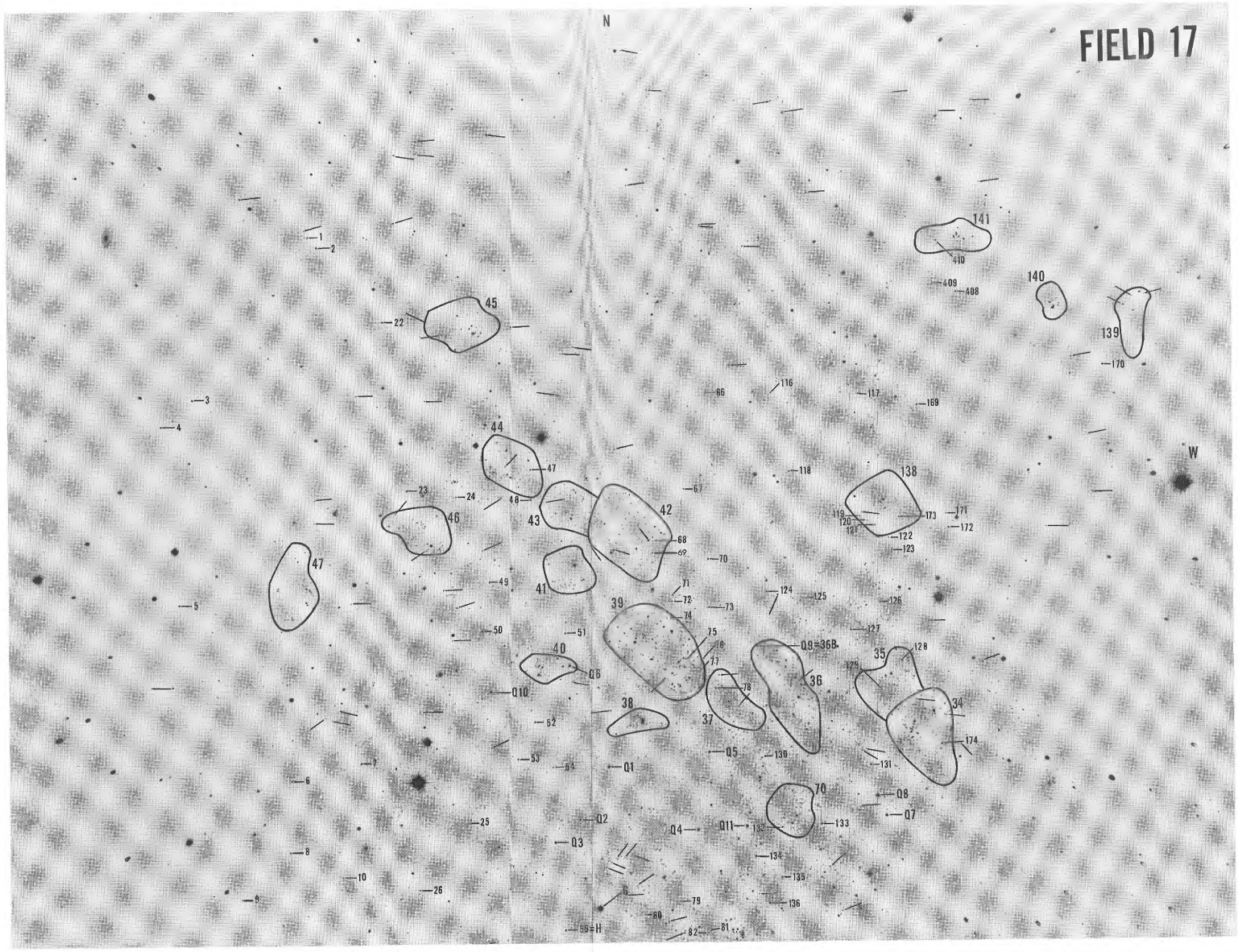

FIG. 16.—Finding chart for the red stars in field 17 from a Palomar 5 m 103aD+GG11 plate

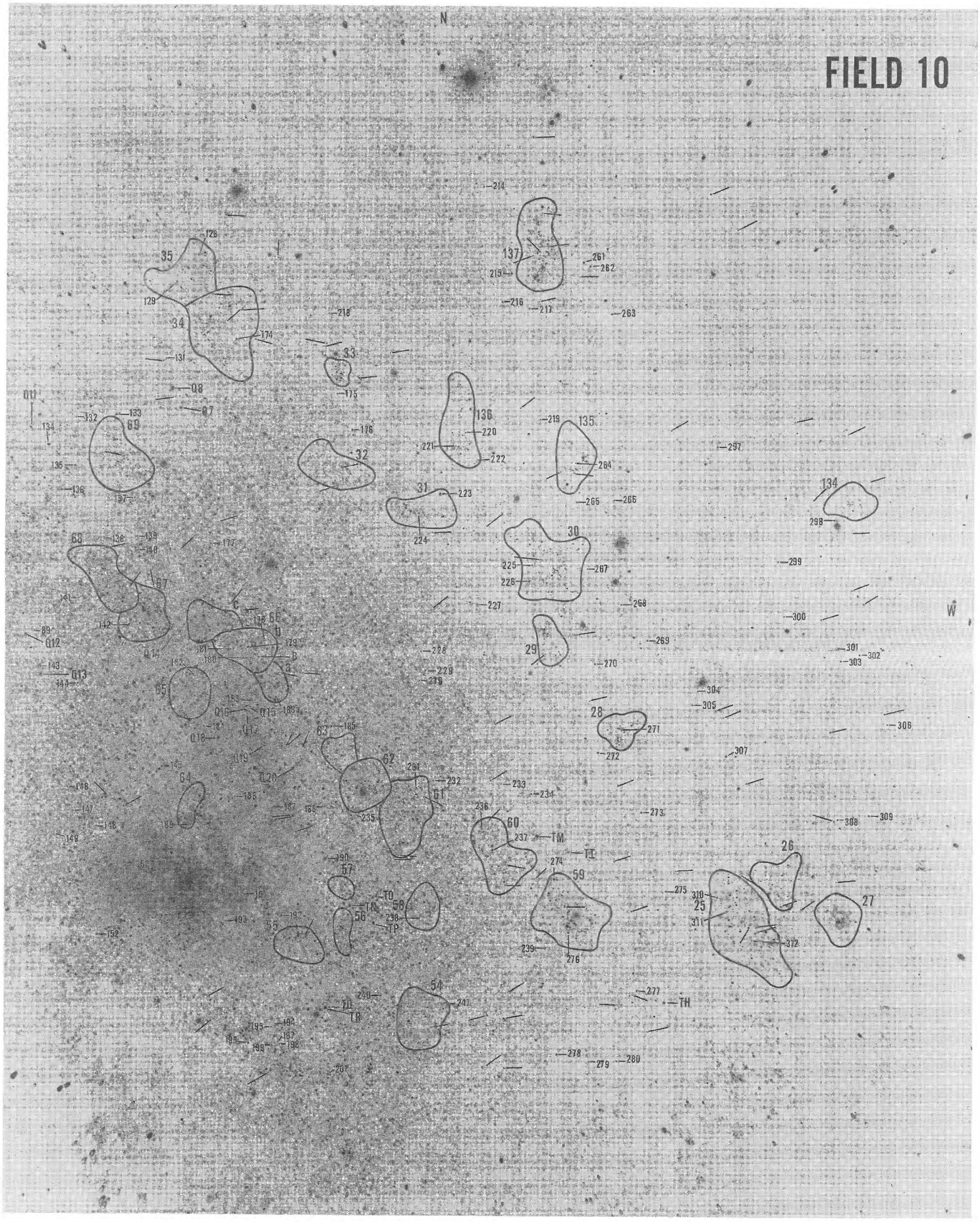

FIG. 15.—Finding chart for the red stars in field 10 from a Palomar 5 m 103aD+GG11 plate

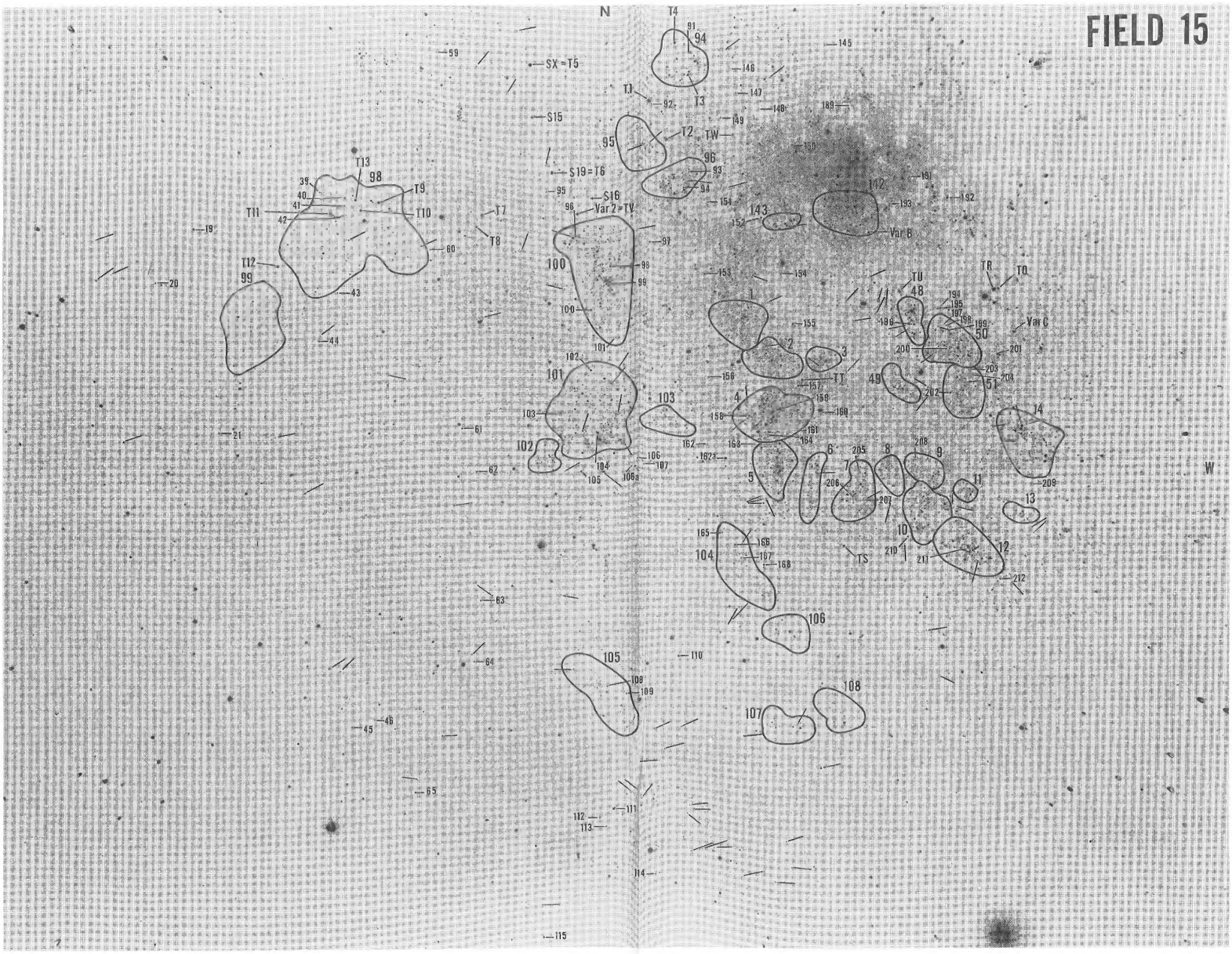

FIG. 13.—Finding chart for the red stars in field 15 from a Palomar 5 m 103aD+GG11 plate

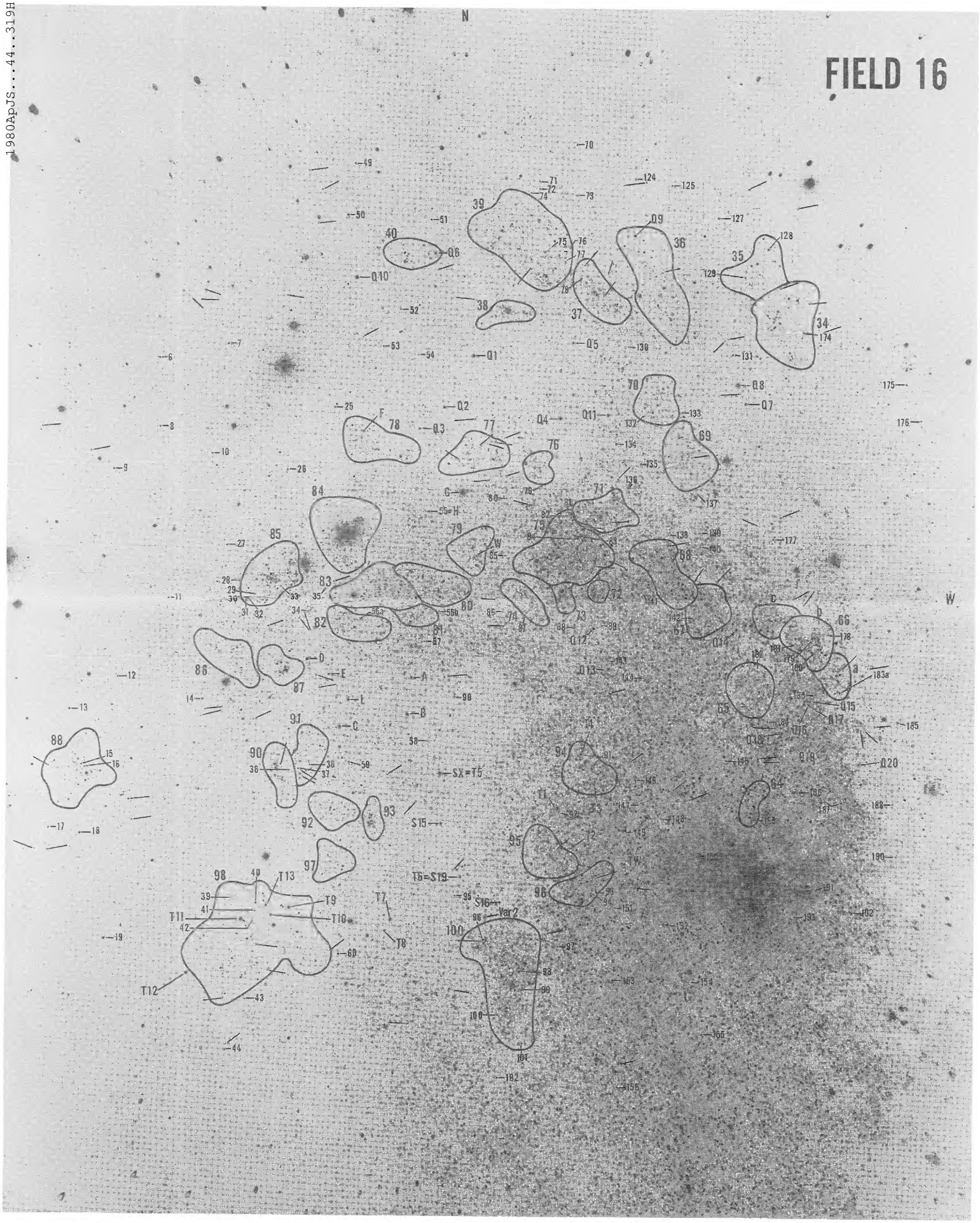

FIG. 14.—Finding chart for the red stars in field 16 from a Palomar 5 m 103aD+GG11 plate.

TABLE 3

ESTIMATED MAGNITUDES FOR THE AREA TRANSFER STARS[a]

NAME	AREA	⟨V⟩	n (V)	⟨B⟩	n (B)	⟨B⟩ - ⟨V⟩
TA	9	16.02	6	16.54	3	+0.52
TB	9, 25	14.95	6	15.26	3	+0.31
TC	8, 9, 25	15.96	6	16.65	3	+0.69
TD	8, 9, 25	15.61	6	16.33	3	+0.72
TE	8, 9, 25	14.84	6	16.08	3	+1.24
TF	9, 25	16.61	6	16.79	3	+0.18
TG	9, 25	17.21	6	17.20:	3	-0.01
TH	9, 10, 25	16.22	7	17.31	3	+1.09
TI	9, 10, 25	16.52	6	16.47	3	-0.05
B71	9, 10, 25	14.7:	6	15.3:	3	+0.06:
TJ	9, 25	14.13	5	14.97	3	+0.84
TK	8, 9, 25	14.45	5	15.02	2	+0.57
TL	8, 9, 25	14.89	6	16.28	3	+1.39
TM	9, 10, 25	14.77	7	15.10	2	+0.33
TN	9	15.51	6	16.35	1	+0.84:
TO	9	15.49	6	16.35	1	+0.86:
TP	9	16.18	5	17.46	1	+1.28:
TQ	9, 15	16.75	5	17.38	1	+0.63:
TR	9, 15	14.81	5	16.02	2	+1.21
TS	9, 15	16.51	4	17.63	1	+1.12:
TT	9, 15	17.02	5	17.70	1	+0.68:
TU	9, 15	16.15	5	16.72	1	+0.57:
TW	9, 15, 16	15.94	3	16.92	2	+0.98
T1	15, 16	14.54	5	15.44	2	+0.90
T2	15, 16	15.99	5	17.39	2	+1.40:
T3	15, 16	16.34	5	17.04:	2	+0.70:
T4	15, 16	16.43	5	17.22	2	+0.79
T5	15, 16	15.01	5	15.46	2	+0.45
T6	15, 16	16.00	5	17.85	2	+1.85
T7	15, 16	15.45	5	15.99	2	+0.54
T8	15, 16	17.35	5	18.01	2	+0.66
T9	15, 16	15.80	5	16.34	2	+0.54
T10	15, 16	16.85	5	17.59	2	+0.74
T11	15, 16	14.76	5	15.33	2	+0.57
T12	15, 16	15.59	5	16.06	2	+0.47
T13	15, 16	16.99	5	17.35	2	+0.36
Q1	16, 17	15.53	4	16.84	2	+1.31
Q2	16, 17	16.41	4	17.68	2	+1.27
Q3	16, 17	17.27	4	18.41	2	+1.14
Q4	16, 17	15.55	4	16.09	2	+0.54
Q5	16, 17	16.99	4	18.13	2	+1.14
Q6	16, 17	16.14	4	17.53	2	+1.39
Q7	10, 16, 17	15.69	4	16.29	2	+0.60
Q8	10, 16, 17	14.51	3	15.10	2	+0.59
Q9	16, 17	16.80	4	18.28	2	+1.48
Q10	16, 17	14.79	4	15.70	2	+0.91
Q11	16, 17	16.00	4	16.52	2	+0.52
Q12	10, 16	16.88	3	17.97	2	+1.09
Q13	10, 16	15.28	4	16.47	2	+1.19
Q14	10, 16	15.47	3	16.19	2	+0.72
Q15	10, 16	(17.21)	3	(17.90)	2	(+0.69)
Q16	10, 16	(17.40)	3	(17.86)	1	(+0.46)
Q17	10, 16	(18.31)	3	(18.80)	1	(+0.49)
Q18	10, 16	(16.64)	3	(17.04)	1	(+0.40)
Q19	10, 16	(16.07)	3	(17.04)	1	(+0.97)
Q20	10, 16	(15.89)	3	(16.70)	1	(+0.81)

[a] TF = B57; TG = B56; T5 = Photoelectric X; T6 = Photoelectric 19; Q9 = 36B

TABLE 4

PHOTOELECTRIC DATA FOR THE BRIGHT AREA TRANSFER STARS MEASURED WITH THE MOUNT WILSON 2.5 METER HOOKER REFLECTOR

Name	Area	V	$B-V$	$V-R$
TB.....	9, 25	14.74	0.50	0.55
TE.....	8, 9	15.05	1.14	1.23
TJ.....	9, 25	14.17	0.60	0.62
TK.....	8, 9	14.46	0.68	0.70
TL.....	8, 9	15.10	1.28	...
TM.....	9, 10	14.76	0.42	0.58
T1.....	15, 16	14.53	1.02	0.81
T7.....	15, 16	15.66	0.63	...
T11.....	15, 16	14.74	0.65	...
T12.....	15, 16	15.87	0.61	...
Q1.....	16, 17	15.49	1.50	1.57
Q2.....	16, 17	16.66	1.52	0.93
Q3.....	16, 17	17.34	1.50	0.93
Q4.....	16, 17	15.45	0.64	0.58
Q6.....	16, 17	16.22	1.28	0.92
Q7.....	16, 17	15.84	0.53	...
Q8.....	16, 17	14.39	0.51	0.51
Q10.....	16, 17	14.87	0.86	...
Q14.....	16, 17	15.82	0.87	...
B71.....	9, 10	14.46:	0.73:	0.61:
36-A....	17	16.49	1.05	0.92

Table 5. Column (1) lists the 488 blue stars sequentially, column (2) identifies the field and hence the finding charts among Figures 3–9, column (3) is the association number when the star is a member, column (5) and (6) list the adopted magnitudes and colors, column (7) is the number of independent estimates that have gone into $\langle V \rangle$. Special information such as image character or spectral type is contained in the final column. The omission of objects marked on the charts is noted by a special symbol in the left margin of column (1). The most common reason for omission is excessive crowding or clear multiplicity, or that the object is a cluster.

Note that magnitudes for most of the stars in Table 5 are based on more than one plate; in the overlap process many stars were estimated many times. Comparison of the individual values shows that the final $\langle V \rangle$ magnitudes are accurate at the $\sigma(V) \approx \pm 0.15$ mag level. (Note, therefore, that 2 $\sigma \approx \pm 0.3$ mag is an estimate of the accuracy of $\sim$95% of the entries of Table 5.) As fewer estimates were made for B, the *colors* have a somewhat larger deviation than $\sqrt{2}\sigma$. We estimate $\sigma(B-V) \approx \pm 0.3$ mag. Hence $2\sigma(B-V) \approx \pm 0.6$ mag is the range within which 95% of the Table 5 colors should lie.

Similar data for 360 red stars are listed in Table 6. Note that most of the red stars are not in associations but are spread more uniformly over the field. We show in § IV*b* that most of the listed red stars with $B-V \lesssim 2.0$ are, in fact, foreground K and M stars.

The errors of the listings in Table 6 are somewhat larger than those discussed for Table 5 because the number of separate measurements is less. Inspection of the internal consistency shows that $\sigma(V) \approx \pm 0.2$ mag and hence $\sigma(B-V) \approx \pm 0.35$ mag for a given entry in Table 6.

During the photometry, we noted a number of particularly interesting bright stars in associations that we had not previously marked as being red or blue. Magnitude estimates in B and V are listed for 55 such stars in Table 7 where the name is in an obvious notation (i.e., 4A is star A in association 4).

Spectra (Humphreys 1980*b*) have later shown that some of these stars are indeed members, as noted in the "Notes" column to Table 7. Of particular interest is star 14B which was bright in 1955 (the date of the charts) but which was not visible on any of the plates in 1977. The accuracy of the magnitudes in Table 7 is of the same order as previously discussed for Table 5.

We finally wish to comment on the appropriateness of the traditional photometric procedures used here so as to again emphasize our present purposes. Step-scale photometry is a powerful reconnaissance technique that overcomes to a large extent the problem of background contamination. However, one must *not* look for subtle details using such photometry. For example, because $\sigma(B-V) \approx \pm 0.2$ mag for all stars in Table 5, the listed $B-V$ colors for some entries are bluer than the infinite temperature black body value of $B-V=-0.37$, but clearly, most of this is due to the errors.

The photometry is, however, sufficiently accurate for estimating the ages and the luminosity functions of the associations and for our primary purpose of calibrating the blue and red candidates for the accompanying spectroscopy (Humphreys 1980*b*). It is with these purposes in mind that one should judge the level of accuracy of the present data.

IV. THE BRIGHTEST STARS

a) The Color-Magnitude Diagrams

i) *The Total Sample*

The data in Tables 5, 6, and 7 are plotted in the color-magnitude (CM) diagram, Figure 17, for all objects listed. Known variable stars are shown as tipped crosses, stars whose spectra show them to be supergiants are filled circles with vertical crosses, foreground dwarfs as determined from the spectra are open circles, and all others with no spectral information are filled circles.

The sequence of blue stars near $B-V=0$ is the dominant feature of the CM diagram. These blue supergiants begin at $V=15.2$ but have a scattering toward the red as shown by the two members whose spectra are A3Ia and F0–F5I. The brightest star is B324

TABLE 5

CATALOG OF BLUE STARS ACROSS THE FACE OF M33

Star No.	Field	Assoc.	⟨V⟩	⟨B⟩ - ⟨V⟩	n	Remarks
1	25	131	17.5	+.03	3	
2	25	131	18.5	-.25	3	
3	25	131	18.1	-.20	3	
>4	25	131	17.9	.00	3	
6	25	132	18.8	-.35	2	
7	25, 9	27	17.8	+.01	5	
8	25, 9	27	18.6	+.03	1	Double
9	25, 9	27	18.7	-.01	3	
>11	25, 9	22	18.3	-.21	3	
12	25, 9	22	17.0	-.20	5	
>						
14	9, 10	25	19.0	+.18	3	
15	9	24	18.7	+.19	3	
>16	9	24	18.5	-.04	3	
>18	9	21	17.7	+.13	3	
19	9	21	19.4	+.01	3	
20	9	21	18.5	+.33	3	
21a	9, 8	122	17.3	-.07	5	
21b	9, 8	122	18.1	-.12	4	
22	9	25	18.3	-.41	2	Cluster?
23	9, 10		17.7	+.07	5	
24	9, 10	25	18.6	+.16	4	
25	9, 10	25	18.0	+.15	4	
26	9, 10	25	17.2	+.03	5	
27	9, 10	25	17.5	-.10	2	Cluster?
28	9	21	18.5	-.06	3	
29	9	21	17.7	+.08	3	
30	9	21	18.7	-.26	3	
31	9	21	19.1	-.26	3	
32	9	21	18.9	-.17	2	
33	9	21	18.7	+.11	3	
34	9	129	18.8	-.53	3	Var. 67 (van den
35	9	129	17.9	-.10	3	Bergh et al. 1975)
36	9, 8		18.0	.00	4	
37	9	21	17.8	-.34	3	
38	9	21	17.5	-.11	4	
39	9	20	17.1	+.10	4	Probably double
40	9	20	16.8	+.77:	4	
41	9		18.0	-.08	4	
>42	9	20	18.6	+.26	3	
44	9	20	18.0	-.07	4	
>45	9		17.8	+.29	4	
>47	9, 8	128	17.1	+.23	2	
>48	9, 8	128	17.1	+.03	5	
>50	9, 8	128	17.3	+.73	4	
51	9		18.4	.00	4	
52	9, 10	28	17.3:	+.01:	3	Multiple, west
53	9, 10	59	17.8	+.35	5	component blue
54	9, 10	59	16.9	+.01	6	
55	9		18.5	-.11	3	
56	9	18	17.6	+.06	4	
57	9	18	16.7	+.32	5	
58	9	18	17.3	-.10	5	
59	9	19	18.2	+.11	2	Double
60	9	19	18.5	-.21	2	
61	9	19	18.6	+.02	1	
>						
64	9, 8	127	18.0	-.06	4	
>65	9, 8	127	17.5	+.04	4	
>68	9, 10	59	18.1	+.33	3	
69	9, 10	59	18.5	+.23	3	
70	9, 10	59	19.1	+.10	3	
71	9, 10	59	14.6	+.84	5	
>72	9	19	18.3	+.28	3	
>74	9	19	18.5	+.12	3	
75	9	19	19.3	+.44	3	
76	9	19	18.8	+.16	3	
77	9		17.8	+.13	4	
78	9, 8	127	18.2	+.15	5	
79	9, 8	127	18.6	+.21	3	Double
>80	9, 8	127	18.4	-.16	5	
>82	9, 8	127	18.4	-.02	4	
83	9, 8	127	18.2	+.03	5	
>84	9, 8	127	17.3	.00	5	
>87	9	17	17.9	-.14	4	
88	9	17	18.1	-.13	4	
89	9	17	17.9	+.23	4	
90	9	17	19.4	-.26	3	
91	10	135	17.1	+.98:	2	
92a	10	135	16.5	+.22	2	Multiple
92b	10	30	18.8	+.41	2	
93	10		17.9	-.11	2	
94	9, 10	59	18.8	+.07	4	Fuzzy
>95	9, 10		18.7	+.07	4	
>97	9	17	19.0	+.05	3	
>98	10	137	17.5	-.07	2	
>101	10	137	18.1	-.08	2	
>						
103	10	137	16.2	+.32	2	Emission line object
>104	10	30	18.6	+.07	2	
>106	10	30	19.0	+.10	2	
107	10	29	19.2	+.02	2	
108	10	29	19.2	-.09	2	
109	10	29	19.3	-.26	2	
110	10		18.2	+.03	2	
111	9, 10	60	17.7	-.15	5	
112	9, 10		17.9	+.20	4	
113	9, 10	60	16.9	+.07	5	
114	9, 10	60	18.0	+.22	4	
115	9, 10		18.0	+.23	4	
116	9, 10		19.1	-.10	4	
>117	9, 10		18.2	-.20	1	Variable
>119	9, 10	53	19.6	+.18	3	
>120	9, 10	53	19.2	-.06	3	
>123	9	16	18.6	-.04	3	
124	9		18.8	-.09	3	
125	9		18.7	-.12	3	
126	9	114	18.6	+.27	2	
>						
>128	17	139	18.5	-.44	1	
>130	10	31	18.9	+.14	2	
131	10	31	19.1	-.10	1	
132	10	31	18.3	-.26	2	
133	10	31	16.5	-.11	3	
134	10	31	18.6	+.22	2	
135	10		18.8	+.04	2	
136	10		19.1	+.13	2	
137	9, 10	61	19.0	-.19	2	
138	9, 10	61	18.8	+.25	3	
139	9, 10	61	18.1	+.44:	3	
140	9, 10	61	18.8	-.03:	3	Fuzzy
141	9, 10	58	18.1	+.07	3	
142	9, 10		19.2	+.07	4	
143	9, 10		19.2	+.25	3	
144	9, 10		18.4	+.13	4	
145	9, 10		19.3	-.05	3	Cluster
146	9, 10		19.4	-.22	2	Cluster
147	9		18.6	+.22	3	Fuzzy
148	9		19.1	+.10	3	
149	9, 15		19.4	-.16	3	
>150	9		18.3	+.08	3	
>152a	9	15	19.3	-.44	3	
>157	17	140	18.1	-.47	1	
158	17	140	16.3	-.23	2	Member (c B)
>159	17		18.5	+.34	1	
>162	10	32	17.2	-.04	1	
163	9, 10, 16		18.6	+.34	2	
164	9, 10		18.5	+.11	2	
165	9, 10	62	18.6	+.46	2	Cluster
166	9, 10	62	18.7	+.22	3	
167	9, 10	62	19.6	+.08	1	
>168	9, 10		18.3	+.33	3	
>171	9, 10	62	16.7	+.71	1	Single component only
172	9, 10	56	19.4	-.18	3	
173	9, 10	57	19.5	+.49	3	
174	9, 10	57	19.7	+.46	3	
175	9, 10	57	19.3	+.57	3	
176	9, 10	56	18.6	+.21	3	
177	9, 10	56	18.4	+.58	1	
179	9, 10	52	18.4	-.22	3	
>180	9, 10	52	19.4	-.43	3	
>182	9, 15		18.8	+.14	1	
183	9, 15		19.2	+.58	1	
184	9, 15	14	19.9	+.38	1	
185	9, 15	14	19.4	+.14	1	
186	9, 15	14	17.8	+.53	2	
187	9, 15	14	17.1	+.09	3	
>188	9, 15	14	19.2	+.03	1	
>190	9, 15	14	18.9	+.42	1	
191	9, 15	14	19.3	-.10	1	
192	9, 15	14	19.9	-.10	1	
193	9, 15	14	19.5	-.08	1	
194	9, 15	13	18.8	+.02	1	
195	9		19.0	-.05	1	

TABLE 5—*Continued*

Star No.	Field	Assoc.	⟨V⟩	⟨B⟩ - ⟨V⟩	n	Remarks
196	9		19.2	-.13	1	
197	9, 15		18.8	+.04	1	
198	9, 15, 8		19.0	+.03	2	
199	9, 15, 8		19.5	+.05	1	
200	9, 8		18.6	+.41	2	
201	17	141	17.6	-.18	2	
202	10, 16		18.4	+.24	2	
203	10, 16		19.2	+.10	3	
>204	10, 16	66	19.0	+.05	3	Cluster?
>206a	10, 16	66	18.6	+.44	3	
>206b	10, 16	66	19.5	+.42	3	
>208	10, 16	66	19.0:	+.05:	1	
209	10, 16	66	19.4	+.30	3	
210	10, 16	66	19.3	+.31	3	
211	10, 16	66	19.4	+.26	2	
212	9, 10, 16		19.5	+.11	3	
213	9, 10, 16		19.4	+.50	3	
214	9, 15		19.9	+.33	2	
215a	9, 15	48	17.1	+.49	1	
215b	9, 15	50	19.4	-.28	3	
216	9, 15	48	14.5	+.97	2	
217a	9, 15		18.6	+.12	1	Var? (V_{max} = 16.8)
>217b	9, 15	48	17.1	+.45	3	
>219	9, 15		19.8	+.14	3	Fuzzy
220	9, 15		19.5	+.26	1	
221	9, 15	50	17.4	+.12	1	
>222	9, 15	51	18.6	+.02	2	
>225	9, 15	49	19.1:	-.06	3	Fuzzy
226	9, 15		19.3	-.29	3	Fuzzy in V
227	9, 15		19.5	+.12	3	
228	9, 15	9	19.1	-.04	3	
229	9, 15	9	18.5	+.36	3	
230	9, 15		19.3	+.21	3	
231	9, 15		18.7	+.10	1	
232	9, 15	12	17.7	-.13	3	
>233	9, 15	12	17.1	+.02	3	
>237	9, 15	12	18.9	+.10	1	
238	9, 15	12	19.1	+.05	3	
>239	9, 15	10	18.8	+.15	3	
>241	9, 15	10	17.9	-.17	1	
242	9, 15	10	18.0	+.03	3	
243	9, 15	10	18.7	-.05	3	
244	9, 15	10	18.8	+.23	3	
>245	9, 15	10	18.7	+.16	3	
>247	9, 15	8	18.2	-.04	2	
248	9, 15	8	18.5	-.09	3	Fuzzy in V
249	17		18.4	-.38	2	
250	17		18.2	+2.00:	1	Red?
251	10, 17, 16	35	18.2	-.19	2	
252	10, 17, 16	35	16.8	+.30	4	
253	10, 17, 16	35	18.9	+.11	2	
254	10, 17, 16	34	17.8	-.41	3	Cluster in V?
255	10, 17, 16	34	16.2	+.19	5	Single!
257	10, 17, 16	34	19.0	+.37:	4	
258	10, 17, 16	34	19.2	-.03	3	
259	10, 17, 16	34	19.9	+.06	2	
260	10, 17, 16	34	19.6	+.01	3	
261	10, 17, 16		19.0	+.26	3	Fuzzy in blue, cluster?
262	10, 16		18.2	+.23	3	
263	10, 16	66	17.2	+.37:	3	
>269	10, 16		18.6	+.45	3	
270	10, 16		19.8	+.17	3	
271	10, 16		19.7	+.21	2	
>272	10, 16		19.6	+.65	3	
>274	10, 16		19.6	+.41	1	
275	9, 15		19.2	-.17	3	
276	9, 15		18.3	+.27	3	
>277	9, 15	7	18.8	+.41	3	
>279	9, 15	7	18.3:	+.18	1	
280	9, 15	7	17.2	+.18	2	
281	9, 15		18.8	+.56:	2	
282	9, 15, 8		18.0	-.36	3	
283	8	110	18.0	-.12	2	
284	8		18.7	+.29	1	
285	8	110	18.2	+.68	2	Close double
286	8	110	17.9	-.22	2	
287	8	112	18.1	-.31	2	
288	8	112	18.2	-.39	2	
289	8	112	18.2	-.31	2	
290	8	111	18.4	-.56	2	
291	8	111	18.9	+1.37	2	Variable?
292	8	112	18.4	-.40	2	
293	8	112	18.2	-.57	2	
294	8	112	17.6	+.02	1	
295	8	112	18.1	+.24	2	
296	8	112	17.1	-.01	2	
297	8	112	17.3	+.26	2	
298	8		17.6	+.04	2	
>299	8		18.5	-.48	2	
>301	8	116	18.2	-.16	1	
>302	8	116	17.8	+.15	2	
>304	8		18.4	-.26	2	
305	8		18.1	-.45	2	
>306	8	116	18.1	-.06	2	
>308	8		17.7	-.50	1	
309	8	119	18.0	+.08	2	
310	8	120	17.9	+.25	2	
311	8, 25		18.2	-.30	3	
312	25	130	18.1	-.21	2	
313	17		18.9	+.18	1	
>315	17, 16	36	19.2	-.09	1	
316	17, 16	36	19.5	-.10	1	
317	17, 16	36	19.0	+.15	3	
318	17, 16	36	19.2	-.09	1	Cluster?
319	10, 17, 16	69	18.5	+.32	3	
320	10, 16		18.4	-.18	2	Cluster?
321a	10, 16	68	18.9	+.17	3	
321b	10, 16	68	18.4	+.05	3	
>322a	10, 16	68	18.1	-.17	3	
>324	10, 16	67	15.2	-.05	4	Single! Member (A5eIa)
>325	10, 16	67	18.5:	+.55	2	
327	10, 16	67	19.2	-.09	3	
328	10, 16	67	18.7	+.15	3	
329	10, 16	65	19.3	+.37	3	
330	10, 16	65	19.6	+.19	3	
331	10, 16		18.1	+.43	3	
332	10, 16		17.2	+.41	3	
333	10, 16	65	19.7	+.31	3	
334	10, 16	65	19.4	+.34	2	Variable?
335	10, 16	65	19.4	+.21	2	
>336	10, 16	65	19.7	+.24	3	
>340	16, 15		19.6	+.24	1	
341	16, 15		19.2	+.22	1	
342	16, 15		18.5	+.46	3	
343	16, 15		19.8	+.58	1	
>>346	9, 16, 15		18.4	+.36	3	
>>348	15		19.2	+.15	1	
>350	15	2	19.5	.00	1	
351	15	2	19.4	+.26	2	
352	15	2	19.5	+.42	2	
353	9, 15	3	19.2	-.23	3	
354	9, 15	3	17.2	-.30:	2	
355	15	2	19.5	+.40	1	
>356	15	4	18.6	+.13	1	Double?
>358	15		19.7	+.22	1	
>361	9, 15	6	17.8	+.33	3	
362	9, 15	6	18.7	+.28	3	
>364	9, 15		19.4	+.01	3	
365	9, 15		18.7	+.15	3	
366	9, 15	106	18.6	+.22	3	
367	9, 15	106	18.7	+.55	3	
368	9, 15	107	17.4	.00	3	
369	9, 15	107	18.6	+.10	3	
>370	9, 15		18.2	+.44	2	
>372	15		18.1	-.10	2	
>373	8		18.4	+.58	2	
376	17, 16	39	19.1	-.01	2	
>377	17, 16	39	18.6	+.42	3	
>379	17, 16	39	16.5	+.39	4	
380a	17, 16	39	18.2	+.39	3	
380b	17, 16	37	18.7	+.29	3	
381	17, 16	39	17.8	+.52:	3	
382	17, 16	39	18.7	+.16	3	
383	17, 16		18.6	+.02	1	
384	17, 16	38	18.2	+.42	1	
>385	17, 16	38	18.8	-.17	3	
>387	17, 16		18.0	+.03	3	
>388	10, 17, 16		17.8	-.17	2	
>390	16		17.8	-.09	2	
391	16	71	18.2	+.41	2	

TABLE 5—*Continued*

Star No.	Field	Assoc.	⟨V⟩	⟨B⟩ - ⟨V⟩	n	Remarks
>392	16	71	18.6	~.8	2	
>394	10, 16	71	18.2:	.31	1	
395	16		17.6	+.02	1	
396	10, 16		18.1	+.15	1	
397	16	75	17.6	-.38	1	
398	16	75	17.1	+.18	2	
399	16	75	19.0	+.74	1	
400	16	75	18.8	+.20	1	
401	16	75	17.4	-.01	1	
402	16	75	18.2	-.10	1	
>403	16	75	16.0	+.68:	3	Single component
>405	16	74	18.5	+.10	2	
>406	16	74	18.4	+.27	2	
>409	16		19.3	+.14	2	
410	16		19.5	-.10	2	
> 413	10, 16		19.4	+.34	3	
>414	16		19.3	-.28	2	
>415b	16, 15	94	18.6	+.15	3	
>416	16, 15	94	16.3	+.29	4	
>418	16, 15	94	18.2	+.25	3	Fuzzy
419	16	94	19.0	+.37	3	
420	16		17.7	+.28	2	
>422	15		19.2	+.34	3	
>423	16, 15		19.4	+.21	3	
>425	16, 15		18.6	+.26	3	
>426	16, 15		18.6	+.10	2	
>427a	16, 15		17.4	+1.04	3	
>428	16, 15	95	17.6	+.28	2	
>430	16, 15		19.0	+.33	3	
431	16, 15	96	19.4	+.44	3	
> >434	16, 15	96	18.0	+.05	2	
>436	16, 15	96	18.2	+.28	3	Cluster
437	16, 15		18.1	+.40	3	
438	16, 15		18.4	+1.60	3	
439	16, 15		19.5	+.65	3	
441	15, 16		18.0	-.09	3	
>442	16, 15		18.7	+.04	3	
>445	16, 15		18.6	+.42	3	
446	16, 15		18.4	+.10	3	
447	16, 15		18.1	-.02	3	
>449	15	1	19.3	-.10	2	
450	15	1	19.7	+.49	2	
>451	15	1	18.8	+.10	1	Cluster?
>454	16, 15		18.4	+.36	3	
455	15, 16		19.0	-.15	3	
456	15	2	18.7:	+.30:	1	
457	15	2	16.6	-.13	2	Double?
458	15	2	19.6	+.12	2	
459	15	2	19.3	+.16	2	
460	15	4	18.6	-.01	2	
>461	15	4	18.4	+.46	2	
>464	15		18.9	+.12	2	
>465	15	103	19.3	-.03	2	
>468	9, 15	4	19.3	+.29	3	
469	9, 15	5	18.3	+.28	3	
> 471	9, 15	5	18.8	.26	1	
472	9, 15	5	17.3	+.31	2	
473	9, 15	5	17.6	+.33	2	
474	9, 15		19.3	-.01	3	
475	9, 15	5	17.0	-.35	3	
> >477	9, 15		19.3	-.28	3	
>479	15		18.8	+.18	3	
480	9, 15		19.3	+.19	3	
>481a	9, 15	104	18.3	-.13	3	
>482	9, 15		19.3	-.34	3	
483	15		18.2	+.02	2	
484	15		18.7	+.27	2	
>485	15		18.0	-.04	2	
>488	17	45	18.5	-.56	1	
489	17	44	18.8	-.31	2	
490	17		18.5	-.05	2	
491	17	46	18.6	-.03	2	
492	17	46	18.7	+.32	2	
493	17	46	18.9	-.24	2	
494	17, 16	40	18.8	+.05	3	
495	17, 16	40	19.3	-.24	2	Fuzzy?
496	17, 16	40	17.8	-.01	3	
497	17, 16	77	18.2	+.22	3	
498	17, 16	77	17.1	+.26	3	
>499	17, 16	77	19.1	+.13	3	
> >501	16	80	18.9	+.34	2	
>504	16	80	18.8	+.49	3	
505	16, 15		18.2	+.52	1	H.S. Var. 2 (16.63)
506	16, 15	100	19.5	+.46	3	
507	16, 15	100	19.0	+.31	3	
508	16, 15	100	19.4	+.78	3	
>509	16, 15	100	18.3	+.34	3	
>512	16, 15	100	18.4	+.27	3	
>513	16, 15	100	18.4	+.27	3	
>515	16, 15		19.5	.30	2	
516	16, 15	100	18.4	-.03	3	
517	16, 15	100	18.1	+.14	3	
518	16, 15	100	18.6	-.21	3	
>519	16, 15	100	18.5	+.32	3	
>520b	16, 15	100	19.6	-.29	3	
521	16, 15		18.7	+.02	3	
>522	15	101	18.7	+.40	2	Cluster?
>524	15	101	17.7	+.09	2	
>525	15	101	18.1	+.10	2	
>528	15	101	18.0	+.33	2	
529	15		18.7	+.27	2	
530	15	102	17.9	+.15	2	
531	15	102	18.0	+.18	2	
>532	17	47	18.7	-.15	2	
>534	17	47	18.8	+.05	2	
535	17		18.4	+.04	2	
536	17	47	18.1	-.24	2	
537	17, 16	78	18.0	-.08	3	
538	17, 16		18.5	+.26	3	
539	16	84	19.3	-.11	2	
540	16	84	19.2	+.10	2	
541	16	84	18.9	+.15	2	
542	16	84	18.2	+.18	2	
543	16	83	18.3	+.66	2	
544	16	83	18.2	+.53	2	
>545	16	82	18.7	+.37	1	
548	16	85	18.4	+.40	1	
549	16	85	18.2	+.60	1	
550a	16	85	17.4	-.20	1	
550b	16	85	18.2	-.56	1	
551	16	85	17.5	+.24	1	
552	16	85	16.1	-.07	2	Double: Member (B5I)
553	16	85	18.6	+.34	2	
554	16	85	18.9	+.16	2	
555	16	85	17.4	+.18	2	
>556	16	87	18.4	.00	2	
558	16		19.0	+.03	2	
559	16	86	18.7	-.08	1	
560	16		19.3	+.04	2	
561	16	90	18.0:	-.05:	1	
> 563	16		18.9	+.07	1	
>564	16, 15	93	18.2	+.20	3	
>566	16, 15	93	18.5	+.17	3	
567	16, 15	93	18.2	+.45	3	
568	16	92	19.1	+.11	1	
569	16	92	18.7	+.33	1	
570	16, 15		18.8	+.05	2	
571	16, 15		18.8	+.22	2	
572	16, 15	97	17.1	-.21	2	
573	16, 15	97	18.8	+.22	1	
574	16, 15	98	18.7	+.47	3	
>575	16, 15	98	18.0	+.50	3	
>577	16, 15	98	18.9	+.37	2	
578	16, 15	98	17.2	-.26	2	
579	16, 15	98	18.4	.00	2	
580	15		19.2	-.72:	2	
581	15		18.9	+.09	2	
582	15		19.1	-.38	2	Cluster
583	15		18.4	.00	2	
584	15	99	18.6	-.03	2	
585	15		18.2	-.17	2	
586	15		18.5	+.28	2	
587	15		18.1	+.93	2	
588	16		18.6	-.15	1	
589	16	88	18.9	+.07	1	
590	16	88	18.9	-.19	1	
591	16	88	18.2	-.22	1	
592	16	88	18.1	-.05	1	
593	16	88	19.2	-.22	1	
594	16	88	18.3	+.19	1	
595		89	18.8	-.09	1	
596		89	18.7	-.25	1	
597		89	19.0	-.03	1	
>598		89	17.9	-.07	1	
>600a		89	18.2	-.36	1	
>601			17.6	-.20	1	Blue variable - Asiago
609	9		19.4	+.03	3	
610	9	55	19.5	+.18	3	

TABLE 6

CATALOG OF RED STARS ACROSS THE FACE OF M33

Star No.	Field	Assoc.	⟨V⟩	⟨B⟩ - ⟨V⟩	n	Remarks
1	17		18.4	1.59	1	
2	17		17.6	1.80	1	
3	17		17.9	1.72	1	
4	17		18.2	1.45	1	
5	17		17.9	1.75	1	
6	16, 17		18.5	1.46	3	
7	16, 17		17.8	1.83	3	
8	16, 17		18.7	1.57	2	
9	16, 17		18.4	1.47	2	
10	16, 17		19.1	1.72	2	
11	16		18.4	1.60	2	
12	16		19.4	3.05	2	Var. 81 (van den Bergh et al. 1975)
13	16		17.4	1.67	2	
14	16		18.6	1.84	2	
15	16	88	19.1	2.49	2	
16	16	88	19.1	1.73	2	
17	16		18.4	1.84	1	
18	16		17.2	1.94	2	(M3 V)
19	16, 15		16.5	1.50	1	
20	15		18.4	2.87	2	Variable
21	15		17.5	2.16	2	
22	17		18.2	1.50	1	
23	17		18.3	1.64	1	
24	17		19.0	1.08	1	
25	17, 16		19.1	2.50	3	
26	17, 16		18.9	1.29	3	Fuzzy?
27	16		17.2	1.70	2	Variable?
28	16	85	17.5	1.28	2	
29	16	85	19.0	2.00	2	
30	16	85	20.5	2.10	1	
31	16	85	19.2	1.68	2	
32	16	85	19.8	2.68	2	
v 33	16	85	19.5	2.00	2	
35	16		19.0	2.54	2	Variable?
36	16	90	19.3	1.50	1	
37	16	91	19.2	2.40	1	
38	16	91	19.3	2.20	1	
39	16, 15	98	19.4	2.16	3	
40	16, 15	98	19.2	2.43	3	
41	16, 15	98	19.9	2.70	2	
42	16, 15	98	19.7	2.38	3	
43	16, 15	near 98	18.9	2.61	2	
44	16, 15		18.3	1.99	2	
45	15		19.1	2.43	2	
46	15		19.0	1.52	2	
47	17	44	19.1	1.39	2	
48	17	44	18.4	1.87	2	
49	17, 16		18.5	1.52	2	
50	17, 16		17.5	1.75	2	
51	17, 16		18.4	1.73	3	
52	17, 16		18.7	1.78	3	
53	17, 16		18.9	1.21	3	
54	17, 16		18.8	2.75	3	Variable
55	17, 16		17.5	2.14	2	photoelectric std. H, (M3 V)
56a	16	82	19.1	1.28	2	
56b	16		19.5	1.93	2	
57	16		18.7	1.16	2	Cluster?
58	16		19.5	2.10	1	
59	16, 15		18.4	3.10	2	Variable
60	16, 15	near 98	18.3	2.20	3	
61	15		18.2	1.32	2	
62	15		17.6	1.61	2	(M3 V)
63	15		18.0	1.47	2	
64	15		18.3	2.28	2	
65	15		17.5	1.44	2	
66	17		18.5	1.20	2	
67	17		18.6	1.62	2	
68	17	42	19.4	2.27	2	
69	17	42	19.3	2.72	2	Fuzzy?
70	17, 16		18.9	1.32	2	
71	17, 16		19.4	1.07	2	
72	17, 16		19.3	1.18	2	
73	17, 16		18.7	1.56	3	
74	17, 16	39	19.5	2.10	3	
75	17, 16	39	18.1	2.16	3	Var. 71 (van den Bergh et al. 1975)
76	17, 16	39	18.6	1.66	3	
77	17, 16	39	19.5	2.13	3	
78	17, 16	37	18.4	1.78	3	
79	17, 16		18.6	1.50	3	Fuzzy
80	17, 16		19.5	3.08	3	Variable?
81	17, 16	75	20.4	2.40	2	
82	17, 16	75	19.5	2.48	2	
83	16	75	18.2	1.52	2	
84	16	75	19.6	2.43	2	
85	16		19.3	0.98	2	
86	16		19.4	3.10	2	
87	16	74	18.9	1.75	2	
88	16, 10		17.5	1.72	2	Variable?
89	16, 10		18.5	1.49	2	
90	16		18.3	1.66	2	
91	16, 15	94	19.6	2.80	2	
92	16, 15		19.1	1.59	3	Fuzzy
93	16, 15	96	19.6	1.15	2	
94	16, 15	96	18.6	1.20	3	Variable?
95	16, 15		19.0	2.85	3	
96	16, 15	100	16.8	2.5:	4	M0Ia
97	16, 15		18.8	1.36	3	
98	16, 15	100	19.2	2.58	3	
99	16, 15	100	17.5	1.51	3	
100	16, 15	100	18.4	1.63	3	
101	16, 15	100	19.5	2.90	3	
102	16, 15	101	18.8	1.83	2	
103	15	101	18.4	1.78	2	
104a	15	101	18.6	2.26	2	Variable?
105a	15		17.4	1.52	2	= 101B
106	15		19.3	2.98	2	
106a	15		19.6	2.60	1	
107a	15		19.2	1.65	2	
108a	15	105	17.9	3.41	2	Var. ? = 105A
109	15	105	18.8	1.52	2	
110	15		16.4	2.00	2	
111	15		16.5	1.15	2	Close companion
112	15		18.2	1.24	2	
113	15		18.4	1.75	2	
114	15		18.0	1.98	2	
115	15		17.7	1.90	1	
116	17		19.2	1.33	2	
117	17		18.8	1.67	2	
118	17		18.6	1.32	2	
119	17	138	19.1	2.38	2	
120	17	138	19.5	2.48	2	Fuzzy?
121	17	138	18.8	2.76	2	
122	17	138	19.2	2.41	2	Cluster?
> 123	17		19.0	0.87	2	
> 125	17, 16		18.8	1.49	2	
126	17		19.0	1.64	2	
127	17, 16		18.2	1.18	2	
128	17, 16, 10	35	17.8	1.53	2	(M0 V)
129	17, 16, 10	35	19.0	1.35	3	
130	17, 16		19.0	1.00	3	
> 131	17, 16, 10		18.7	1.15	4	
> 133	17, 16, 10		18.4	1.62	4	
134	17, 16, 10		17.1	2.01	3	(M0 V)
135	17, 16, 10		18.1	2.00	4	(M2-M3Ia)
136	17, 16, 10		17.8	(1.27)	4	Elongated image
137	16, 10		19.8	2.14	3	
138	16, 10		19.9	2.01	3	
139	16, 10		19.4	2.70	3	
140	16, 10		19.4	2.88	3	Cluster?
141	16, 10		20.0	2.67	3	
142	16, 10	67	18.4	1.30	3	Var. 19 (Hubble, van den Bergh et al. 1975)
143	16, 10		19.3	1.10	2	
144	16, 10		20.0	1.58	2	
145	16, 15, 10		18.5	1.12	3	Double?
146	16, 15, 10		19.6	2.17	3	
147	16, 15, 10		19.6	1.78	3	
148	16, 15, 10		19.2	0.92	4	
149	16, 15, 10		18.6	2.17	3	
150	16, 15, 10, 9		19.8	1.02:	2	
151	16, 15, 9		19.4	2.05	3	
152	16, 15, 10, 9		18.2	1.52	3	
153	15, 9		19.5	2.13	1	Cluster?
154	15, 9		19.2	3.3:	3	In dust
155	15, 9		17.8	1.03	2	
156	15, 9		19.1	1.08	2	
157	15, 9		18.9	1.84	2	
158a	15, 9	4	17.2	2.26	3	Variable = 4D (c M)
159	15, 9	4	18.0	2.00	3	Variable (c M)
160	15, 9		19.5	2.41	3	
161	15, 9	4	19.5	2.36	3	

TABLE 6—*Continued*

Star No.	Field	Assoc.	⟨V⟩	⟨B⟩ - ⟨V⟩	n	Remarks
162a	15, 9		16.8	1.74	2	
162	15, 9		19.4	1.32	3	
163	15, 9	near 4	19.6	2.38	3	
164	15, 9	4	19.6	2.98	3	
165	15, 9	104	19.7	2.47	3	
166	15, 9	104	17.4	1.35	3	
167	15, 9	104	18.9	2.07	3	
168	15, 9		18.2	1.22	3	
169	17		18.4	1.76	2	
170	17		18.5	1.72	1	
171	17		19.0	1.20	2	
172	17		18.8	1.60	2	
173	17, 10	138	19.2	1.01	2	
174	17, 16, 10	34	19.2	2.08	3	
175	16, 10		19.1	1.08	2	
176	16, 10		18.2	1.56	2	(M0-M1 V)
177	16, 10		17.5	1.86	3	
178a	16, 10	66	20.2	2.00	3	
179	16, 10		17.8	1.59	3	= 66b A
180	16, 10	66	19.2	2.28	2	
181	16, 10	66	19.8	2.06	1	
182	16, 10	65	19.1	2.60	2	In dust
183	16, 10		19.2	2.50	3	
183a	16, 10		18.6	0.80	3	Fuzzy?
>185	16, 10, 9		(17.4)	1.82	3	Variable
186	16, 10, 9		19.3	1.50	4	Variable
>188	10, 9		19.1	0.97	3	
190	10, 9		18.9	1.65	2	In dust
191	16, 15, 10, 9		19.1	1.40	4	
192	16, 15, 10, 9		17.2	1.45	4	Variable?
193	16, 15, 10, 9		19.2	1.14	5	
194	15, 9		20.0	>2.2	3	
195	15, 9		19.6	>2.6	3	
196	15, 9	48	17.3	1.62	3	Variable
197	15, 9	50	19.6	0.46	3	
198	15, 9	50	19.3	1.27	3	
199	15, 9	50	19.5	2.83	3	Cluster?
200	15, 9	50	19.7	1.90	3	
201	15, 9		18.0	2.29	3	Variable: (cM)
202	15, 9	51	18.2	1.61	3	Variable?
203	15, 9	51	20.0	2.06	2	In dust
204	15, 9	51	20.2	1.99	2	In dust
205	15, 9	7	19.3	2.27	2	
207	15, 9	7	18.8	2.40	3	
208	15, 9	9	19.4	2.45	3	
209	15, 9		18.0	1.62	3	
210	15, 9		18.6	1.63	1	Var. 62 (van den Bergh et al.
*211	15, 9	12	16.5	2.18	3	(M1 Ia) 1975)
>212	15, 9		17.8	1.29	3	
214	10		18.8	1.90	2	
215	10		18.2	1.70	2	
216	10		18.6	1.42	2	
217	10		18.5	1.73	2	
218	10		19.4	2.60	2	
219	10		19.4	2.03	2	
220	10		19.3	2.30	2	Fuzzy
221	10		19.7	2.69	2	
222	10	136	20.0	1.92	2	
223	10	31	16.0	1.57	2	Visible proper motion
224	10	31	18.7	3.30	2	
225	10	30	19.3	2.23	2	
226	10	30	17.8	1.97	2	Cluster?
227	10		17.2	1.60	2	
>228	10		19.7	1.13	2	
>230	10		19.2	1.18	2	
231	10, 9	61	19.1	1.42	3	
232	10, 9		19.3	0.97	3	
233	10, 9		19.0	1.70	4	
234	10, 9		19.2	1.65	4	
235	10		20.2	2.01	2	
236	10, 9	60	19.4	3.13	5	Variable?
237	10, 9	60	19.2	2.33	5	
238	10, 9	58	18.6	0.77	4	
239	10, 9	near 59	18.3	1.69	5	
240	10, 9		18.7	1.12	5	
241	10, 9	54	17.9	1.80	4	
242	9		19.5	1.97	4	
242a	9		17.4	1.62	4	
243a	9	16	18.1	1.41	4	(K3-K5 V)
244	9	17	16.8	2.63	4	(M1 Ia)

Star No.	Field	Assoc.	⟨V⟩	⟨B⟩ - ⟨V⟩	n	Remarks
245	9, 8		18.8	1.51	5	
246	9, 8		17.1	1.81	3	
247	9, 8		18.5	1.29	3	
248	9, 8		18.0	1.73	3	(G5-G8 V)
249	9, 25, 8		17.3	1.64	4	
250	9, 8	110	16.9	1.83	2	(M4 V)
251a	8		19.5	1.50	1	
251	8	110	17.0	1.40	2	
252a	8	110	17.4	1.75	2	(M0 V)
252b	8		18.1	1.75	2	
253	8	112	14.3	1.49	2	
254	8	112	15.6	1.95	2	(M3 V)
255	8	112	18.1	—	2	
256	8	near 112	18.1	1.80	2	
257	8		17.3	1.71	2	
258	8		17.4	1.82	2	
259	8		18.5	2.26	2	Var. 64 (van den Bergh
260	8		16.8	1.59	2	et al. 1975)
261	10		17.3	1.74	2	
262	10		17.8	1.76	2	
263	10		18.4	1.70	2	
264	10	135	19.2	2.26	2	
265	10		19.3	2.42	2	
266	10		19.3	1.32	2	
267	10		19.3	2.38	2	
268	10		18.6	1.96	2	Var. 48 (van den Bergh
269	10		18.6	2.14	2	et al. 1975)
270	10		18.8	2.50	2	
271	9, 25, 10	28	18.9	3.01	3	
272	9, 25, 10		17.3	1.68	4	
273	9, 25, 10		17.4	1.92	5	(M3 V)
274	9, 25, 10	59	17.5	1.43	5	
275	9, 25, 10		17.8	1.27	5	
276	9, 25, 10	59	19.0	1.42	5	
277	9, 25, 10		17.8	1.86	5	Variable
278	9, 25, 10		17.1	1.58	5	
279	9, 25, 10		19.3	2.07	4	
280	9, 25, 10		18.6	1.66	4	
281	9, 25	near 18	18.6	1.30	4	
282	9, 25		18.6	2.74	4	Variable?
283	9, 25	19	19.8	2.50	4	
284	9, 25		17.5	2.69	4	(K3 V)
285	9, 25		19.0	2.60	4	Variable
286	9, 25		19.0	2.49	4	
287	9, 25, 8	127	17.9	1.81	5	Variable
288	9, 25, 8	127	18.1	—	5	Variable?, Multiple
289	9, 25, 8	127	17.9	2.13	5	
290	9, 25, 8		18.0	3.00		Variable
291	9, 25, 8		18.5	2.59	5	(cM)
292	9, 25, 8		18.1	2.32	5	
293	9, 25, 8		17.3	2.14	5	
294	9, 25, 8		16.9	0.78	4	Variable?
295	9, 8	116	17.3	1.50	2	
296	8		18.0	1.92	2	
297	10		18.7	1.73	2	
298	10	134	18.0	2.13	2	
299	10		18.0	1.02	2	
300	10		18.9	2.55	2	
301	10		18.3	1.30	2	
302	10		18.0	0.80	2	
303	10		18.3	0.56	2	
304	10		19.2	2.10	2	
305	10		18.0	2.03	2	(cM)
306	10		18.3	1.88	2	
307	25, 9, 10		17.7	1.70	3	
308	10		18.9	1.40	2	
309	10		18.4	1.52	2	
310	25, 9, 10	25	18.7	1.25	5	
311	25, 9, 10	25	18.8	3.14	5	
312	25, 9	25	19.4	1.88	4	
313	25, 9	21	18.5	2.12	4	
314	25, 9	21	17.7	1.57	4	
315	25, 9	23	18.6	1.23	2	
316	25, 9	22	18.5	3.03	4	Var. 55 (van den Bergh
317	25, 9	22	17.4	1.32	4	et al. 1975)
318	25, 9		17.9	2.14	4	Variable?
319	25, 9	129	19.2	2.56	4	
320	25, 9	126	18.8	0.87	4	
321	25, 9		17.6	1.16	3	
322	25, 9		17.2	1.19	3	

TABLE 6—*Continued*

Star No.	Field	Assoc.	⟨V⟩	⟨B⟩ - ⟨V⟩	n	Remarks
323	25, 9, 8		18.5	1.64	5	
324	25, 9, 8		18.2	1.67	5	
325	8		18.4	1.88	2	
326	8		16.8	2.04	2	(M3 V)
327	8		18.4	1.88	2	Variable
328	8		17.3	1.76	1	
329	8		18.5	1.77	2	
330	8	118	17.3	1.15	2	
331	8		16.8	1.84	1	
332	8		17.9	1.93	2	
333	8		17.6	1.39	1	
334	8		18.3	1.97	1	
335	8		17.2	1.56	1	
336	25		18.3	1.96	1	(= 306)
337	25		18.9	1.48	1	(= 308)
338	25		18.5	1.55	1	(= 309)
339	25		17.6	1.88	1	
340	25		18.4	1.64	1	
341	25		17.2	1.70	1	
342	25		18.5	1.72	1	
343	25		17.6	1.68	1	
344	25		17.7	1.52	2	
345	25	131	17.8	1.89	3	
346	25	131	18.5	0.73	2	
347	25		17.7	1.38	2	
348	25		18.6	1.69	2	
349	25		17.6	2.17	2	Variable?
350	25		17.8	1.77	1	
351	25		17.6	2.12	1	
352	25		16.2	2.05	1	
353	25		17.1	1.82	2	
354a	25	123	16.5	0.40	1	(F8: I)
354	25	123	18.5	2.46	3	
355	25	123	18.2	2.25	2	(cM:)
408	17		18.8	1.36	1	
409	17		19.2	1.54	1	
410	17	141	18.2	1.30	1	
411	8		18.2	1.73	1	
412	8		18.2	2.07	1	
Var. #66	9, 25		19.2	2.44	1	(van den Bergh et al. 1975) (M3 Ia)

a#105 Independent Measurement V = 17.2, B - V = 1.63 (Association 101B)
a#108 Independent Measurement V = 18.4:, B - V = 3.25 (Association 105B)
a#158 Independent Measurement V = 17.3, B - V = 2.61 (Association 4D)
a#179 Independent Measurement V = 17.5, B - V = 0.69 (Association 66bA)
a#244 Independent Measurement V = 16.9, B - V = 2.28 (Association 17C)

TABLE 7

ESTIMATED MAGNITUDES FOR SPECIALLY MARKED BRIGHT STARS IN PARTICULAR ASSOCIATIONS

NAME	V	n(V)	B	n(B)	B - V	NOTES
4A	15.24	3	15.25	1	+0.01	Field (A0V)
4B	17.26	3	17.65	1	+0.39	
4C	17.16	3	18.15	1	+0.99	
4D	17.27	3	19.88	1	+2.61	R158 (cM)
5A	15.40	3	(15.98)	1	(+0.58)	Member (A3Ia)
5B	16.77	3	17.16	1	+0.39	
5C	17.12	3	17.04	1	-0.08	
7A	16.60	3	17.22	1	+0.62	
7B	15.94	3	16.99	1	+1.05	
9A	17.30	2	18.22	1	+0.92	
10A	16.95	3	18.10	1	+1.15	
12A	16.28	2	17.63	1	+1.35	
14A	17.11	2	17.53	2	+0.42	
14B	Fainter than V = 22 in 1977: V = 17.2 in 1955.					
17A	16.99	3	17.75	2	+0.76	
17B	16.84	2	17.16	1	+0.32	
17C	16.94	2	19.22	1	+2.28	R244 (M1Ia)
17D	17.65	2	18.22	1	+0.57	
19A	17.04	3	17.27	2	+0.23	
21A	17.50:	3	19.07	2	+1.57	
22A	17.38	3	18.82	2	+1.44	
36A	16.04	3	17.16	2	+1.12	
36B	16.71	3	18.15	1	+1.44	Q9
48A	17.17	2	17.78	1	+0.61	
49A	17.10	2	17.46	1	+0.36	
56B	17.12	1	17.86	1	+0.74	
59A	15.88	3	16.93:	2	+1.05	Field (G2 V)
59B	17.55	3	19.30	2	+1.75	
62A	17.16	2	18.38	1	+1.22	
62B	17.04	2	17.80	2	+0.76	
66bA	17.77	4	19.25	1	+1.48	R179
66bB	17.53	3	18.22	1	+0.69	
68A	16.31:	3	17.04	1	+0.73:	
87A	17.17	2	17.61	2	+0.44	
88A	15.12	3	16.16	2	+1.04	Field (G8 V)
96A	16.11	3	16.10	1	-0.01	Member (B5-B8I)
100A	16.50	3	18.13	2	+1.63	Field (K0 V)
100B	17.01	4	17.54	2	+0.53	
100C	16.78	3	17.82	2	+1.04	
100D	17.84	2	18.22	1	+0.38	
101A	17.12	2	17.05	1	-0.07	
101B	17.22	2	18.85	1	+1.63	R105
101C	16.42	3	16.83	1	+0.41	
101D	16.31	2	17.04	1	+0.73	
101E	17.62	2	18.10	1	+0.48	
105A	18.35:	3	21.60	1	+3.20	R108
105B	17.05	3	18.06	2	+1.01	
110A	16.04	2	16.09	2	+0.05	Member (cB)
110B	15.03	2	16.36	2	+1.33	Field (M0 V)
110C	16.84	3	17.10	2	+0.26	Member (A3-A5Ia)
111A	17.40	3	17.88	2	+0.48	
116B	15.33	2	16.25:	1	+0.92	Member (F0-F5I)
117A	16.55	3	16.34	2	-0.21	Member (A2I)
127A	17.01	2	17.53	2	+0.52	
131A	17.39	3	18.22	1	+0.83	

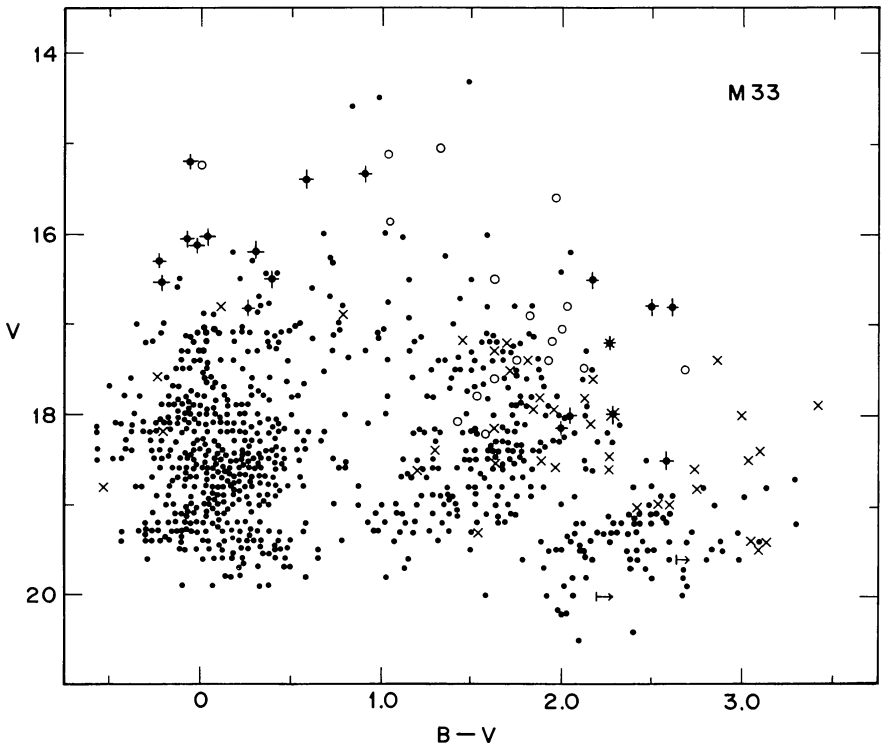

FIG. 17.—Color-magnitude diagram for all stars listed in Tables 5, 6, and 7. Confirmed supergiant members as determined from spectra are closed circles with vertical crosses. Variable stars are tipped crosses. Foreground dwarfs as determined from spectra are open circles. All others from Tables 5, 6, and 7 are closed circles.

(Table 5) in association 67 on Figures 7 and 8 of fields 16 and 10. Adopting the apparent visual modulus of $(m-M)_{AV}=24.65$ from ST1 (Table 2), using $E(B-V)=0.03$ gives $M_V=-9.4$ for B324. Close rivals are 116B and 5A from Table 7 at $M_V=-9.0$, but they are redder, and in the absence of spectra, would have been considered as probable foreground stars.

The bulk of the blue supergiant sequence begins near V = 16.0 (i.e., $M_V=-8.6$), and the luminosity function rises rapidly fainter than V = 17. Our blue star photometry is fairly complete brighter than $V\approx 18.3$, and counting Table 5, from $V=16$ to $V=18$, gives the rise of the differential $\phi(M)$ for the blue stars as $\log\phi(V) \propto 0.68V$. This rate is the same as Hubble's (1926) for blue magnitudes between $m_{pg}=16$ and $m_{pg}=18$ (no correction for the errors in the 1926 magnitude scale have been applied for this comparison as the corrections are small, and at the moment, uncertain).[6]

Four other features of Figure 17 are noteworthy.

(1) The gap between $B-V\approx 0.5$ and $B-V\approx 1.0$ is largely artificial because the blink surveys isolated only the bluest and reddest stars; those of intermediate color were not marked.

[6]We postpone a discussion of whether a stellar luminosity function with this slope at the bright end can produce the observed correlation of M(brightest star) with M(galaxy) as a purely statistical number effect (Holmberg 1950; ST 2) until work now in progress on $\phi(M)$ for the nearby dwarf galaxies Sextans A, Sextans B, Leo A, WLM, NGC 3109, and IC 5152 is completed.

(2) Most of the stars with colors between $B-V\approx 1.0$ and 2.0 and brighter than $V\approx 18$ are probably foreground stars. This is shown by the large number of candidates that were tested by spectra (*open circles*) and found to be K and M dwarfs. It is also shown by the statistics of the CM diagram of nearby Selected Area 45 discussed in § IV*b*. Hence, although the gap mentioned in item (1) *is* artificial, the true number of member red stars is so small in the interval $1.0 < B-V < 2.0$, $V < 18.5$ that the distribution in Figure 17 redward of $B-V\approx 0.5$ is totally misleading in any case. It will be a formidable task to obtain the true frequency distribution of late-type members brighter than say even $V=18.5$ because of the contamination problem. Hence, a comparison of the observed ratio of blue to red supergiants at any given magnitude with calculated time scales of evolution (see Robertson 1974*b*; Chiosi, Nasi, and Sreenivasan 1978) is not possible in M33 with the present data.

(3) The three brightest confirmed M supergiants in M33 occur at $V=16.5$, 16.8, and 16.8; hence $M_V(3)=-7.95$ if the mean apparent modulus of $(m-M)_{AV}=24.65$ is assumed to apply to each star individually. Note also that the number of red supergiants increases rapidly fainter than $V\approx 17.5$ as shown by those stars that are variable (crosses in Fig. 17) and are therefore probable members.

(4) The gap in Figure 17 for red stars fainter than $V\approx 19$ redward of $B-V\approx 2.0$ is not real but, as men-

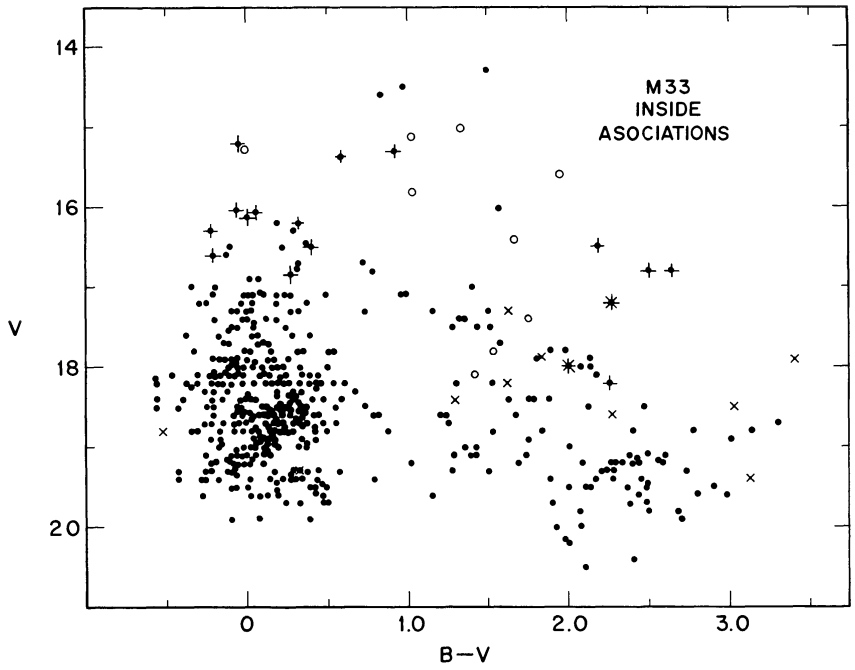

FIG. 18.—Color-magnitude diagram for stars in Tables 5, 6, and 7 that are inside the association boundaries. The coding is the same as for Fig. 17.

tioned earlier, is a result of the systematic errors in the B photometry for stars fainter than $B=21.5$ in regions of moderate to strong background. Nothing should be made of this quite artificial feature, and we have permitted the B photometry of the affected stars to stand for reasons discussed earlier.

ii) *Inside Associations Only*

The CM diagram for stars inside the association boundaries is shown in Figure 18. Three features of this diagram that concern the contamination should be noted.

(1) The brightest blue star (B324 in association 67) remains, as do the other two brightest stars (116B and 5A), and indeed most other blue stars brighter than $V=17$. Hence, the *brightest* blue stars in M33 occur almost exclusively in the associations.

(2) The brightest *red supergiants* are also present, which means that the contamination is substantially reduced by considering only stars in associations—a potentially important point in studies of the brightest stars as distance indicators in nearby galaxies such as M101, members of the NGC 4214 group, members of the South Pole group, etc.

Concerning these points, recall the discovery by Roberts (1957) that most of the O and early B stars in our galaxy (and hence their red supergiant descendents) can be accounted for as having originated in O associations.

(3) The total number of red stars brighter than $V\approx 18$ ($M_V\approx -6.5$) is much reduced in Figure 18 compared with Figure 17. Clearly the percentage of members-to-field brighter than $V\approx 18$ is greater inside associations than out.

iii) *Outside Associations*

The CM diagram for stars outside the associations is shown in Figure 19. Note the following points in a comparison with Figure 17 and 18.

(1) The population of red stars relative to blue is now different from Figure 18. Nearly all the *bright* red stars ($V\approx 18$) found outside the associations for which we have spectra *are foreground dwarfs*.

(2) The brightest blue stars, although clearly members, now begin only at $V\approx 17.5$ ($M_V\approx -7$) which is considerably fainter than $V=15.2$ ($M_V\approx -9.4$) for the brightest blue stars inside the associations. Nevertheless, nonassociation OB stars do exist, as the presence of the blue sequence for $V>17.5$ in Figure 19 shows. Among the brightest examples, well away from association borders, are the stars B95, B117 (probably variable), B282, B298, B299, B304, B308, B313, etc.,

b) Statistics of the Foreground Contamination

Selected Area 45 is within 0°.50 of the center of M33 on the west side, and part of SA 45 can be seen in the extreme western 1/3 of Field 25. In 1924 Hubble (1926) used the then unpublished Seares, Kapteyn, and van Rhijn (1930) standards in SA 45 to transfer to his individual comparison stars for M33 cepheids. As part of an effort to recalibrate the Hubble photometry, work

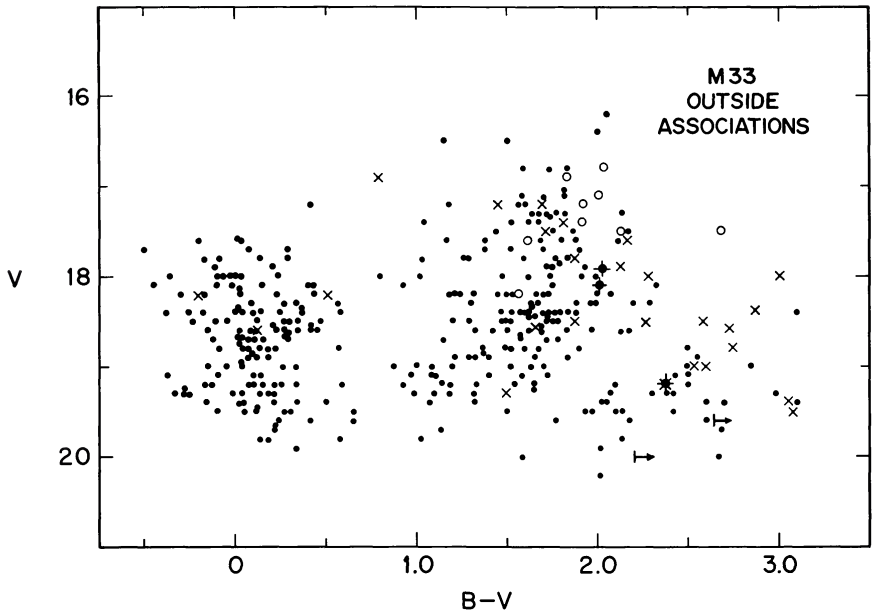

FIG. 19.—Color-magnitude diagram for stars outside the associations, coded the same as in Figs. 17 and 18.

was begun by one of us (A.S.) in 1973 to obtain photoelectric magnitudes for many of the Seares SA 45 stars using the Mount Wilson 2.5 m Hooker reflector. This bright calibration is now largely complete to $V \approx$ 17.5, and Sandage and Katem (1977) have extended their SA 45 sequence to faint magnitudes with visual Palomar 5 m reflector plates taken at the prime focus with a Racine (1969) wedge. The 5 magnitude ratio of the wedge permits calibration of the plates to $V = 22.5$.

The resulting CM diagram for SA 45 is shown in Figure 20. Although SA 45 is very close to M33, it is outside its borders, and all stars in Figure 20 are in the Galaxy. This CM diagram then provides the data from which the foreground contamination in Figures 17, 18, and 19 can be estimated.

Figure 20 is complete to $B = 21.8$ over the good photometric area of 0.056 square degrees for the Palomar prime focus plates. Therefore, counts in the diagram give a representative distribution of galactic field stars at the position of M33 over the stated area.

The expected contamination in M33 follows by noting that the combined area of the M33 region plotted in Figure 17 is approximately an ellipse whose semimajor and semiminor axes are ~25′ and 13′, respectively, which is an area of 0.28 square degrees. The combined area of the M33 associations plotted in Figure 18 is measured to be 0.050 square degrees, which is only slightly less than that for SA 45 itself.

Consider first the contamination for stars between $V = 17$ and $V = 19$ in the color range $1.0 < B - V < 2.0$ over the area covered by our blink survey. Counts in Figure 17 show that 180 such stars exist in M33 within the entire area. There are 38 stars in the SA 45 control field between the same intervals. Since the ratio of the areas is $0.28/0.056 = 5.0$, we expect 190 foreground dwarfs in M33 in the stated photometric intervals. As 180 are observed, it follows that there are few if any

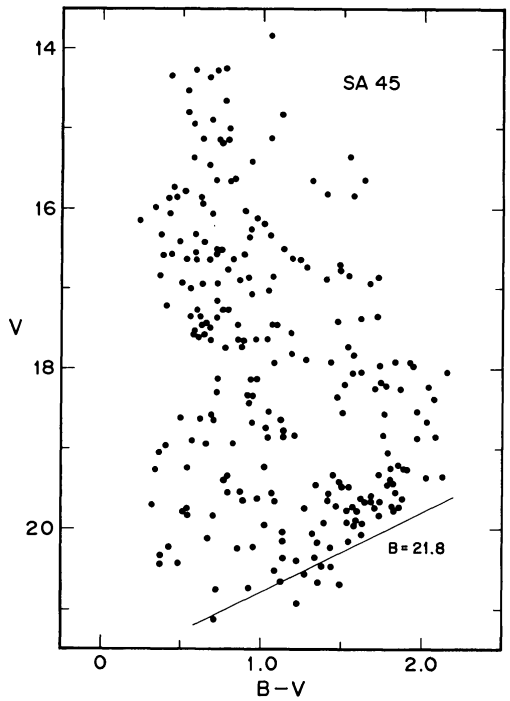

FIG. 20.—Color-magnitude diagram for all stars in selected area 45 within the 0.056 square degree area of Palomar 5 m reflector plates. The photometry is the mean of measurements on two plates in each color, photoelectrically calibrated. The data are from work in progress on the galactic halo (Sandage and Katem 1977).

M33 members in this magnitude ($M_V = -5.6$ to $M_V = -7.6$) and color ($1.0 < B-V < 2.0$) range.

The same conclusion follows from Figure 18 for stars within the association boundaries alone. There are 34 stars between $17 < V < 19$, $1.0 < B-V < 2.0$ in the 0.050 square degrees plotted in Figure 18 for M33. This number is to be compared with the 38 stars in SA 45 over 0.056 square degrees. The agreement of numbers shows again that foreground dwarfs dominate Figure 18 at intermediate colors. Hence, the Hertzsprung gap does indeed exist in M33 from at least $M_V \approx -8$ to $M_V = -5$. The gap is almost empty until stars as red as $B-V \approx 2.0$ are reached. In this regard, M33 is similar to the Milky Way and the LMC where few supergiants exist between spectral types G0 and M1 (Humphreys 1978, 1979*a*).

However, as few stars exist in SA 45 redder than $B-V = 2.0$, and as many are present in Figures 17, 18, and 19, it follows that most of the observed stars this red in M33 are probable members.

c) *The Brightest Stars Calibrated*

A listing of the blue stars from Tables 3, 5, and 7 brighter than $V = 17.0$ and generally bluer than $B-V = 0.50$ is given in Table 8. A few redder stars of special interest are listed for completeness. The available spectra (Humphreys 1980*b*) summarized in column (6) show that most of the stars brighter than $V = 16.2$ are members.

These data supersede those given by ST2 (Table 11) where they list B (brightest) $= 15.5$ and $B(3) = 15.72$ for M33. From Table 8 here we now obtain $B(1) = 15.2$, $B(3) = 15.73$, $V(1) = 15.2$, and $V(3) = 15.3$. Hence, $M_B(1) = -9.5$, $\langle M_B(3) \rangle = -8.95$, $M_V(1) = -9.4$, $\langle M_V(3) \rangle = -9.3$ for the brightest *blue* stars.

Note that two of the three brightest stars are redder than their spectral type and may therefore be reddened by dust. Correction for individual absorption is not attempted here, but rather, as previously mentioned, the mean apparent moduli of $(m-M)_{AB} = 24.68$ and $(m-M)_{AV} = 24.65$ are assumed to apply to all the candidates. A discussion taking individual reddening into account is given elsewhere (Humphreys 1980*b*).

The red stars brighter than $V = 18.5$ with colors redder than $B-V = 1.90$ are listed in Table 9. For completeness, R354a (F8I, $B-V = 0.40$) is also included. As shown by the spectra summarized in column (6), many more of these red stars are foreground dwarfs than in Table 8.

The three brightest M supergiants, R211 ($V = 16.5$, M1 Ia), R96 ($V = 16.8$, K5–M0 Ia), and R244 ($V = 16.8$,

TABLE 8

BRIGHTEST BLUE STARS
$V \leq 17.0$ AND $B-V \lesssim 0.50$

Name (1)	Chart (2)	Association (3)	V (4)	$B-V$ (5)	Spectrum (6)	Remarks (7)
4-A	9, 15	4	15.2	+0.01	A0V	
B324	10, 16	67	15.2	−0.05	A5eIa	Single
116-B	8	116	15.3	+0.92	F0-F5I	
5-A	9, 15	5	15.4	+0.58:	A3Ia	Elongated
B403	16	75	16.0	+0.68:	...	Data for single star
110-A	8	110	16.0	+0.05	cB	
B552	16	85	16.1	−0.07	B5I	Double
96-A	15, 16	96	16.1	−0.01	B5-B8I	Variable?
B103	10	137	16.2	+0.32	...	Emission line object
B255	10, 16, 17	34	16.2	+0.19	...	Single!
B158	17	140	16.3	+0.23	cB	
B416	15, 16	94	16.3	+0.29	...	
101-C	15	101	16.4	+0.41	...	
B92a	10	135	16.5	+0.22	...	Multiple
B133	10	31	16.5	−0.11	...	
B379	16, 17	39	16.5	+0.39	...	
TI	9, 10, 25	...	16.5	−0.05	...	
B457	15	2	16.6	−0.13	...	Double?
117-A	8	17	16.6	−0.21	A2I	
B57	9	18	16.7	+0.32	...	
110-C	8	110	16.8	+0.26	A3-A5Ia	
B252	10, 16, 17	35	16.8	+0.39	...	
5-B	9, 15	5	16.8	+0.39	...	
17-B	9	17	16.8	+0.32	...	
B54	9, 10	59	16.9	+0.01	...	
B113	9, 10	60	16.9	+0.07	...	
B12	9, 25	22	17.0	−0.20	...	
B475	9, 15	5	17.0	−0.35	...	

TABLE 9

BRIGHTEST RED STARS, $V \geq 18.5$ AND $B-V \geq 1.90$

NAME	CHART	ASSOC	V	B-V	SPECTRUM	REMARKS
(1)	(2)	(3)	(4)	(5)	(6)	(7)
R 254	8	112	15.6	1.95	M3V	
R 352	25		16.2	2.05		
R 110	15		16.4	2.00		
R 211	9, 15	12	16.5	2.18	M1Ia	
R 354a	25	123	16.5	0.40	F8:I	
R 96	15, 16	100	16.8	2.5:	M0Ia	
R 244	9	17	16.8	2.63	M1Ia	= 17-C
R 326	8		16.8	2.04	M3V	
R 134	10, 16, 17		17.1	2.01	M0V	
R 18	16		17.2	1.94	M3V	
R 158	9, 15	4	17.2	2.26	M	= 4-D: Variable
R 293	8, 9, 25		17.3	2.14		
R 273	9, 10, 25		17.4	1.92	M3V	
R 21	15		17.5	2.16		
R 55	16, 17		17.5	2.14	M3V	Photoelectric H
R 284	9, 25		17.5	2.69	K3V	
R 349	25		17.6	2.17		Variable?
R 351	25		17.6	2.12		
R 115	15		17.7	1.90		
R 226	10	30	17.8	1.97		Cluster?
R 108	15	105	17.9	3.41		= 105-A: Variable?
R 289	8, 9, 25		17.9	2.13		
R 318	9, 25		17.9	2.14		Variable?
R 332	8		17.9	1.93		
R 114	15		18.0	1.98		
R 159	9, 15	4	18.0	2.00	cM	
R 201	9, 15		18.0	2.29	cM	Variable
R 290	8, 9, 25		18.0	3.00		Variable
R 296	8		18.0	1.92		
R 298	10	134	18.0	2.13		
R 305	10		18.0	2.03	cM	
R 75	16, 17	39	18.1	2.16		Var. 71 of vd B et al. (1975)
R 135	10, 16, 17		18.1	2.00	M2-MeIa	
R 292	8, 9, 25		18.1	2.32		
R 355	25	123	18.2	2.25	cM	
R 412	8		18.2	2.25		
R 60	15, 16	Near 98	18.3	2.20		
R 64	15		18.3	2.28		
R 44	15, 16		18.3	1.99		
R 334	8		18.3	1.97		
R 336	25		18.3	1.96		= 306
R 20	15		18.4	2.87		Variable
R 59	15, 16		18.4	3.10		Variable
R 259	8		18.5	2.26		Var. 64 of vd B et al. (1975)
R 291	8, 9, 25		18.5	2.59	cM	
R 313	9, 25	21	18.5	2.12		
R 316	9, 25	22	18.5	3.03		Var. 55 of vd B et al. (1975)
R 354	25	123	18.5	2.46		

M1 Ia) give $M_V(1) = -8.15$ and $\langle M_V(3) \rangle = -7.95$. The data continue to show the remarkably well defined luminosity and the small dispersion about the mean of $M_V(1) = -8.0 \pm 0.2(\sigma)$.

The rather tight upper limit to the visual luminosities of the M supergiants may be explained by the role of extensive mass loss (Morton 1967; Snow and Morton 1976; Hutchings 1976; Conti 1978) on the post–main-sequence evolution of the most massive hot stars (>50–$60\ \mathfrak{M}_\odot$). Humphreys and Davidson (1979) discussed the evolution of the most massive stars in the Galaxy and the LMC and especially noted the very tight luminosity limit for the later-type supergiants (late B to M) at $M_{\rm Bol} \approx -9.5$ mag, corresponding to an initial mass of $\sim 50\ \mathfrak{M}_\odot$. Neither evolutionary models without mass loss (Stothers and Chin 1969, 1976) or with mass loss (Chiosi, Nasi, Sreenivasan 1978) nor neutrino processes in the red supergiant stage (Stothers 1969, 1972) can adequately account for this observation. Consequently Humphreys and Davidson (1979) suggested than instabilities and the accompanying mass loss observed in the hotter supergiants effectively limits the evolution of the most massive hot stars (>50–$60\ \mathfrak{M}_\odot$) to cooler temperatures. The observed upper bound

to the luminosities of the later-type supergiants near $M_{Bol} \approx -9.5$ mag very likely corresponds to the upper limit to the initial mass of stars which can evolve to the region of the M supergiants. This luminosity limit translates into a visual luminosity of ~ -8 mag for the M supergiants. The results of a spectroscopic study (Humphreys 1978; 1979*a*, *c*; 1980*a*) of the brightest red stars in nearby galaxies suggest that their maximum visual luminosities have little or no dependence on metallicity at least within the range represented by Local Group spirals and irregulars.

d) *Previously Known Variables*

A few of the variables found previously by Hubble (1926), by Hubble and Sandage (1953), or by van den Bergh, Herbst, and Kowal (1975) are identified on the finding charts of Figures 3–16 or have information given in Table 10, or both. Variable A of Hubble and Sandage is identified on Figure 3 in association 130; variable B is in association 142 and is marked in Figures 4, 6, 13, and 17; variable C is near association 52 in Figure 4; variable 2, which is our blue star 505 and also the transfer star TV, is near association 100 in Figures 6, 7, 13, and 14.

Another blue variable of the same type, discovered at Asiago (Romano 1978) is located in association 89 and can be identified from the chart in the reference just cited. Color information for some of the van den Bergh *et al.* variables that we found during the blinking is also in Table 9.

V. THE SPIRAL PATTERN

The spiral arms in M33 are not very well defined, a general characteristic of late type spirals of luminosity

TABLE 10

PREVIOUSLY KNOWN VARIABLES

NAME HERE	NAME OTHER	CHART	ASSOC	REMARKS
	HUBBLE - SANDAGE (1953) STARS			
B 505	HS - 2		Near 100	
...	HS - A		130	
...	HS - B		142	
...	HS - C		...	
	HUBBLE (1929) OR VAN DEN BERGH ET AL. (1975)			
R 12	vd B 81	16		
B 34	vd B 67	9	129	Marked as blue!
R 75	vd B 71	16, 17	39	
R 142	Hubble 19	10, 16	67	
B 181, R 201	vd B 60	9, 15	...	Marked both as red and blue!
R 210	vd B 62	9, 15	10	
R 259	vd B 64	8	...	
R 268	vd B 48	10	...	
R 316	vd B 55	9, 25	22	
B 378	vd B 68	16, 17	39	Marked as blue. Called fuzzy!
	VAN DEN BERGH ET AL. (1975)			
...	vd B 50		42	Marked as red
...	52		41	" " blue
...	56		...	" " red
...	57		...	" " "
...	58		17	" " "
...	61		...	" " blue
...	63		112	" " red
...	65		Near 88	" " "
...	66		...	" " "
...	69		...	" " "
...	70		...	" " "
...	73		34	" " "
...	74		139	" " "
...	75		39	" " "
...	76		101	" " blue
...	77		...	" " "
...	79		...	" " red
...	80		...	" " "
...	83		Near 103	" " blue

class II–III. Although the two principal arms closest to the center have a moderately high surface brightness, they are thick, branched, and massive in the sense of Reynolds (1927*a*, *b*).

The arms do, however, form a definite spiral pattern which was measured by de Groot (1925, 1926), Danver (1942), and others, and which is outlined well by the inner associations as seen by inspection of Figure 2 from a distance. In this section we discuss the spiral pattern defined by the brightest stars, the associations, the dust, and by the general enhancement of surface brightness by young stars fainter than those we have cataloged but whose effect is visible on small scale photographs.

a) *Distribution of the Blue and Red Stars*

The distribution of the 1778 blue stars found from the blinking is shown in Figure 21, and the association pattern is superposed. This diagram should be viewed from a distance to best see the spiral structure of the inner arms. The pattern of these inner arms is clear enough, but its overall noncoherence (called the geometrical entropy by Gerola and Seiden [1978]) is more evident. Many of the blue stars exist outside the association boundaries as discussed earlier (§ IV*a* [iii]). Figure 21 can be compared with a similar diagram by Madore (1978) which shows the same features.

The distribution of the 828 red stars found in the blink survey does not show the spiral arms so prominently. Those listed in Table 6 are plotted in Figure 22 as dots; the additional very red stars found from blinking the 4 meter IV N–103aO plates are plotted as crosses. The more uniform distribution across the field of Figure 22 compared with Figure 21 betrays again the large contamination by foreground K and M stars.

A somewhat cleaner but more meager distribution is given in Figure 23 which shows only those stars in Table 6 with $B-V \gtrsim 1.9$. Although some foreground dwarfs will be included here because errors in the colors put them beyond $B-V=1.9$ in the listings, most stars plotted in Figure 23 are expected to be M supergiants. Note their higher concentration to the associations.

b) *The System of Arms*

Long exposure plates taken with the Palomar 1.2 m Schmidt show a system of 10 arms; 5 on each side of the center (SH). The four outer arms on each side of the center (II N–V N and II S–V S) were first traced from the integrated light on the small scale Schmidt plates. The reader is referred to Figure 1 of SH for assurance that these outer arms do exist. They are hard to trace from the associations alone, and it was only after the global pattern was found from the deep Schmidt plates that we became convinced of their reality.

We have adopted the positions of the ten arms given by SH and put them on the composite map shown in Figure 24 (Plate 5). This diagram is made from an overlay of the associations but with the H II regions from an earlier survey (Sandage and Sersic 1960) shown in red. Note that arms I N and I S *are* well defined by the associations alone.

Arm III N is also convincing from the associations, as is the segment of IV in the south and perhaps even II S, but by the time we reach arms IV N, V N, IV S, and V S, the underlying surface brightness of the faint young stars must be used to define them.

Note that other interpretations of the arm system might seem possible using only the associations. One such would be to connect associations 28 through 47 into a coherent arm. However, the long exposure Schmidt prints do not admit this. The problem is, of course, important for our claim (SH) that the optical plane is warped, for if such a northern "arm III" were correct, then the *inclination of the disk* at arm III would be the same as at arm I, and our warp for the inner region would largely disappear. Hence, the reader should make a comparison of Figures 2 and 24 here with the deep Schmidt plate reproduced by SH to judge the reality of the 10 arm system.

c) *The Dust Pattern*

Dust in many highly symmetrical, late type spirals is often an arm tracer. To test the relations between the dust pattern, the associations, and the blue supergiants in M33, we have outlined the obvious dust patches that are visible in silhouette against the background disk. The dust can be traced over much of the central 25′ diameter and is shown both as superposed on a photograph and alone on facing pages in Figures 25 and 26 (Plates 6 and 7).

The pattern is more chaotic than regular. Given Figure 26 alone, no clear spiral pattern is evident. There are no obvious outlines even of the I N and I S arms that are so evident from the associations. In particular, the pattern preferred by the density wave theory where dust and gas is expected on the *insides* of the association arms (see Toomre 1977 and W. W. Roberts 1977 for reviews) is not apparent in Figures 25 and 26. There is an indication of this proper sequence in the south-preceding arm (I S) where dust is on the inside of the major concentration of light and where many small Strömgren spheres exist on the inside edges of association, 7, 8, 9, 11, 13, and 15. However, the dust on the north side is more prominent on the outside of arm I N; hence no generalizations about the location of the dust are possible from M33 taken as a whole.

Of course, M33 has never been claimed to be the major arena for testing the density wave theory. The arms themselves are too massive and ill defined. Nevertheless, the incoherent dust pattern and the general lack of significant neutral hydrogen enhancement especially

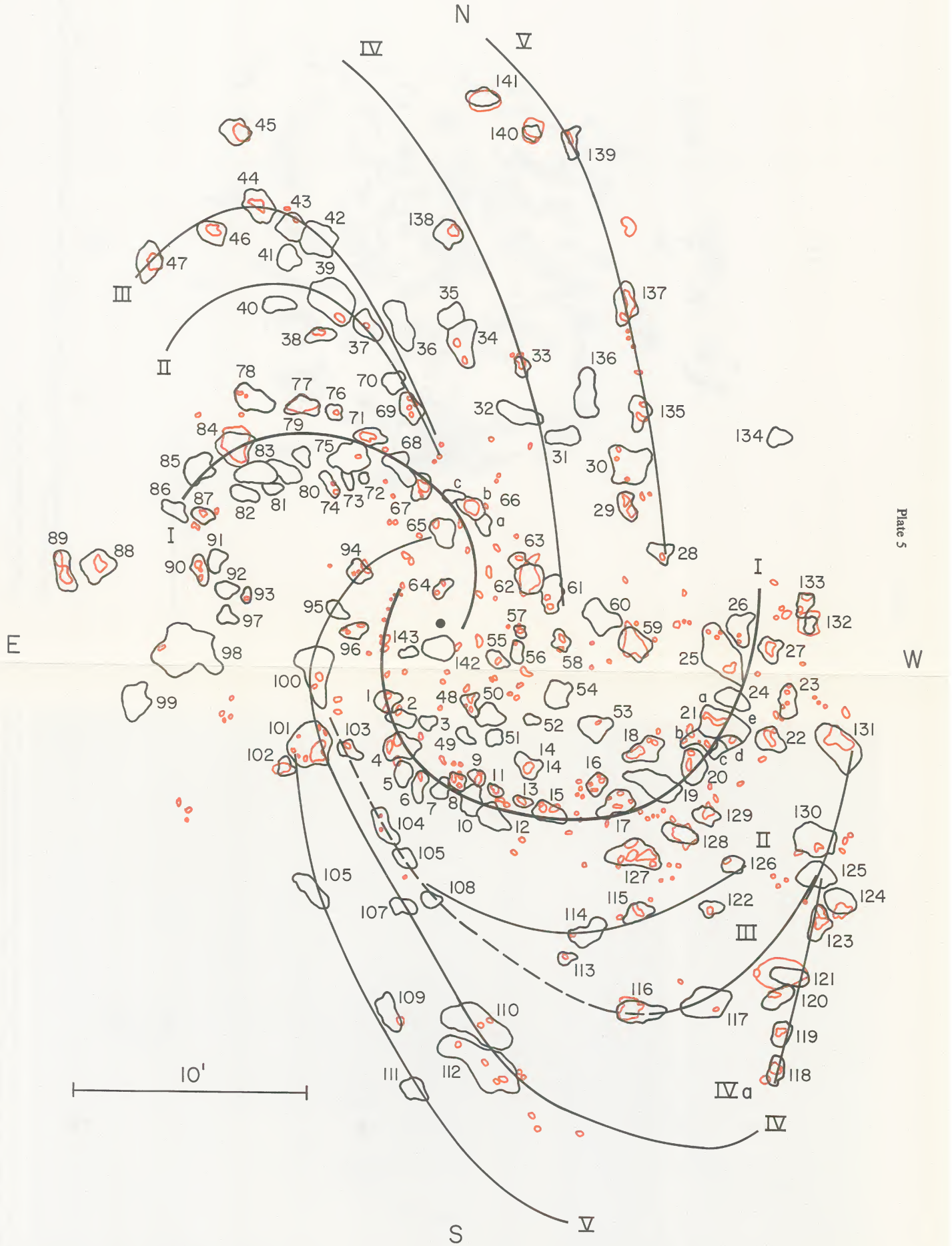

Plate 5

FIG. 24.—Positions of the associations compared with H II regions (in red) from an unpublished study (Sandage and Sersic 1960). The adopted system of five arms is also shown.

HUMPHREYS AND SANDAGE (*see* page 366)

Plate 6

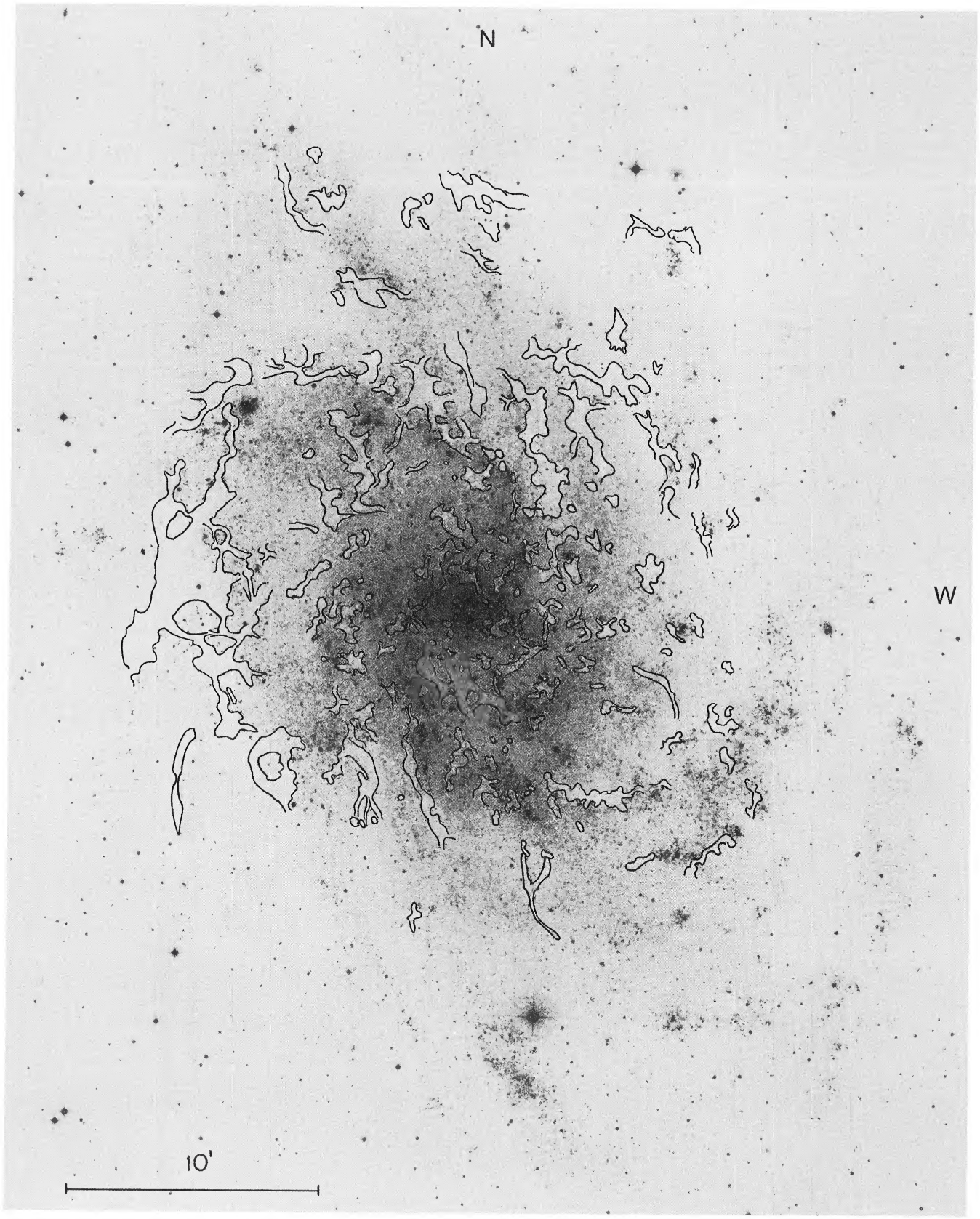

FIG. 25.—Dust patches as found by their silhouette against the background disk, superposed on a blue photograph taken with the Palomar 1.2 m Schmidt. The scale is the same as for the accompanying line drawing in Fig. 26, so that a direct comparison can be made more easily.

HUMPHREYS AND SANDAGE (*see* page 366)

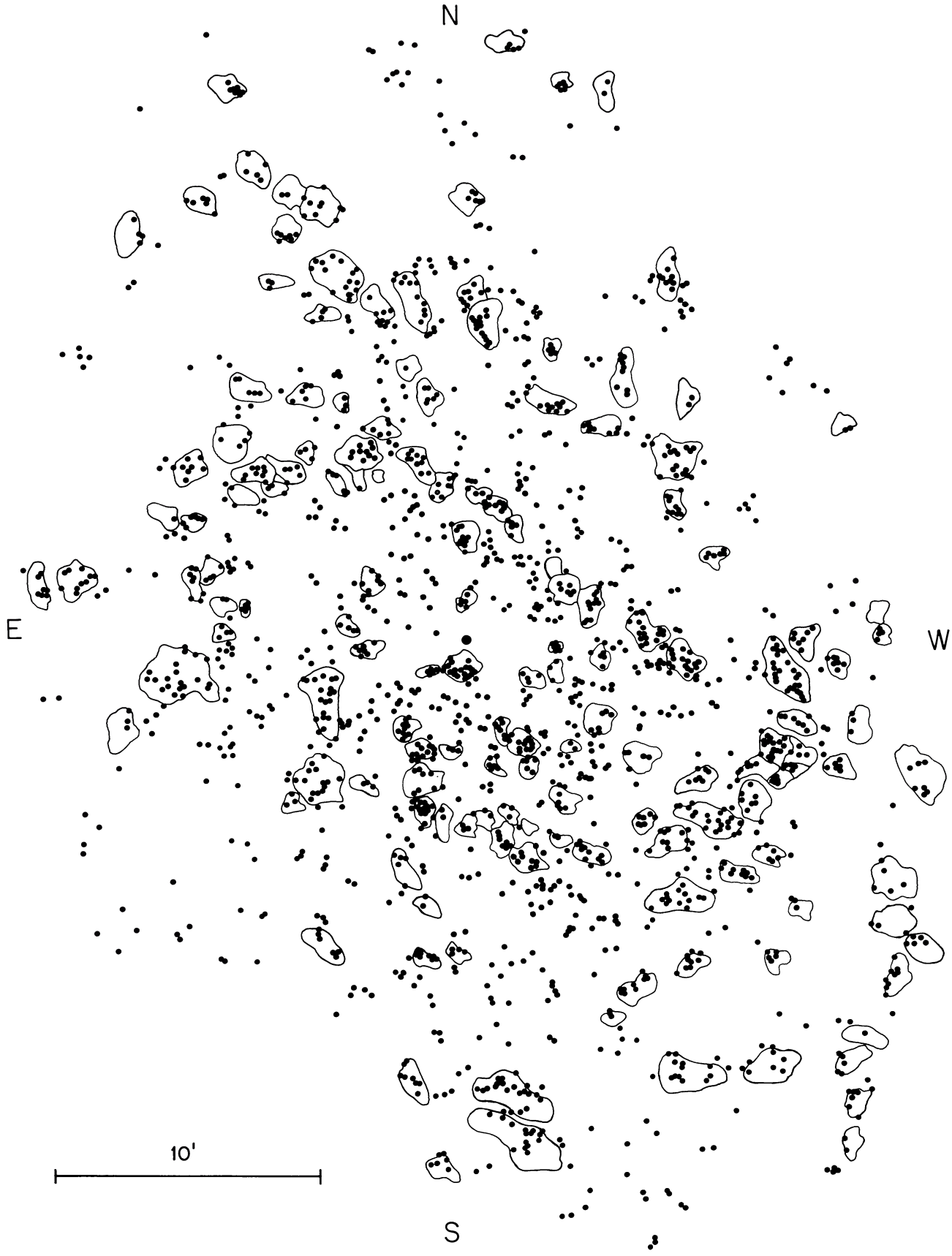

FIG. 21.—Surface distribution of blue stars listed in Table 5, plus all others marked as blue in the blinking but not photometered. The outlines of the associations is superposed.

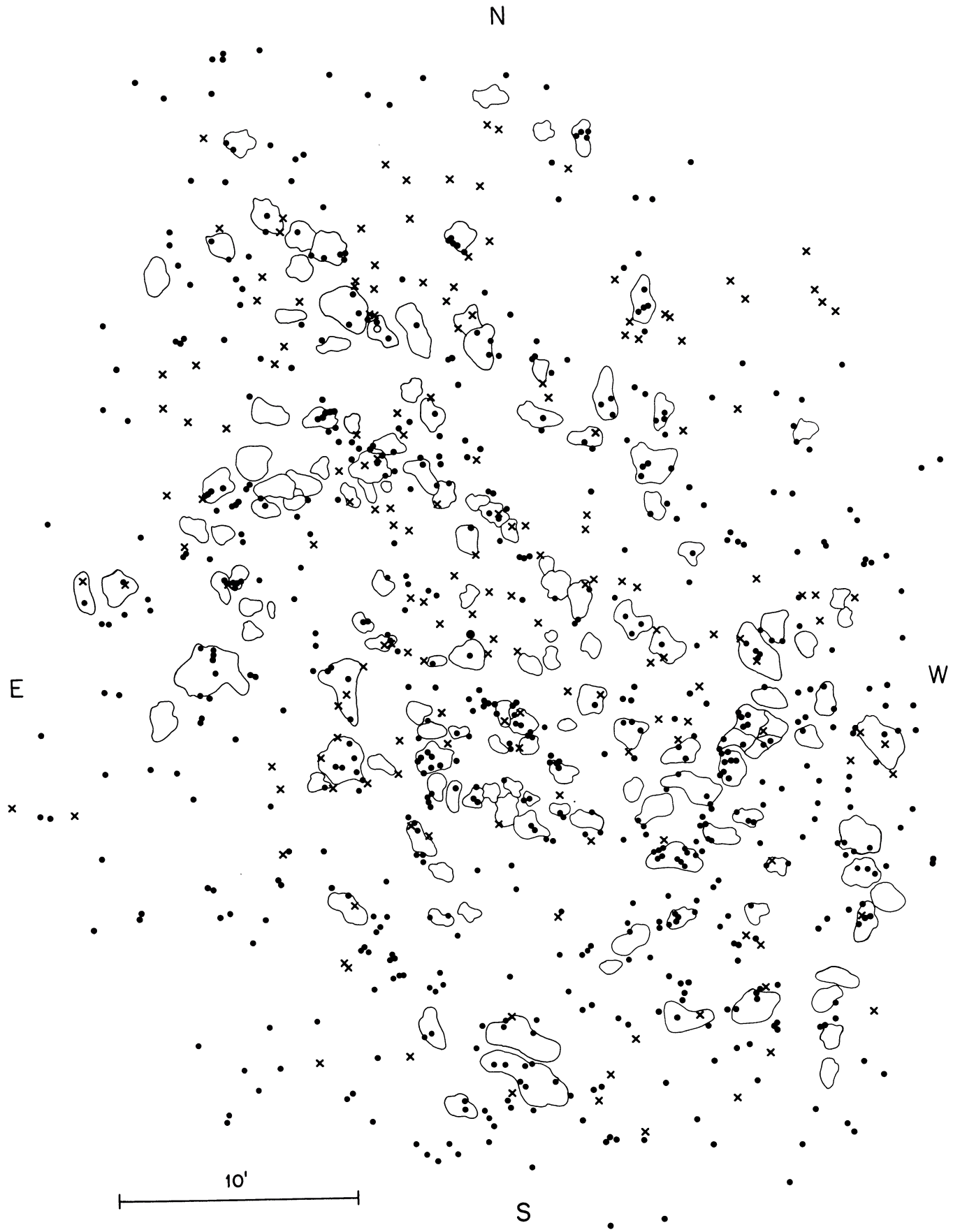

FIG. 22.—Surface distribution of red stars listed in Table 6 plus all others marked as red in the blinking but not photometered. Red stars found in the blink survey using the Kitt Peak IV N − 103aO plate pair are marked as crosses.

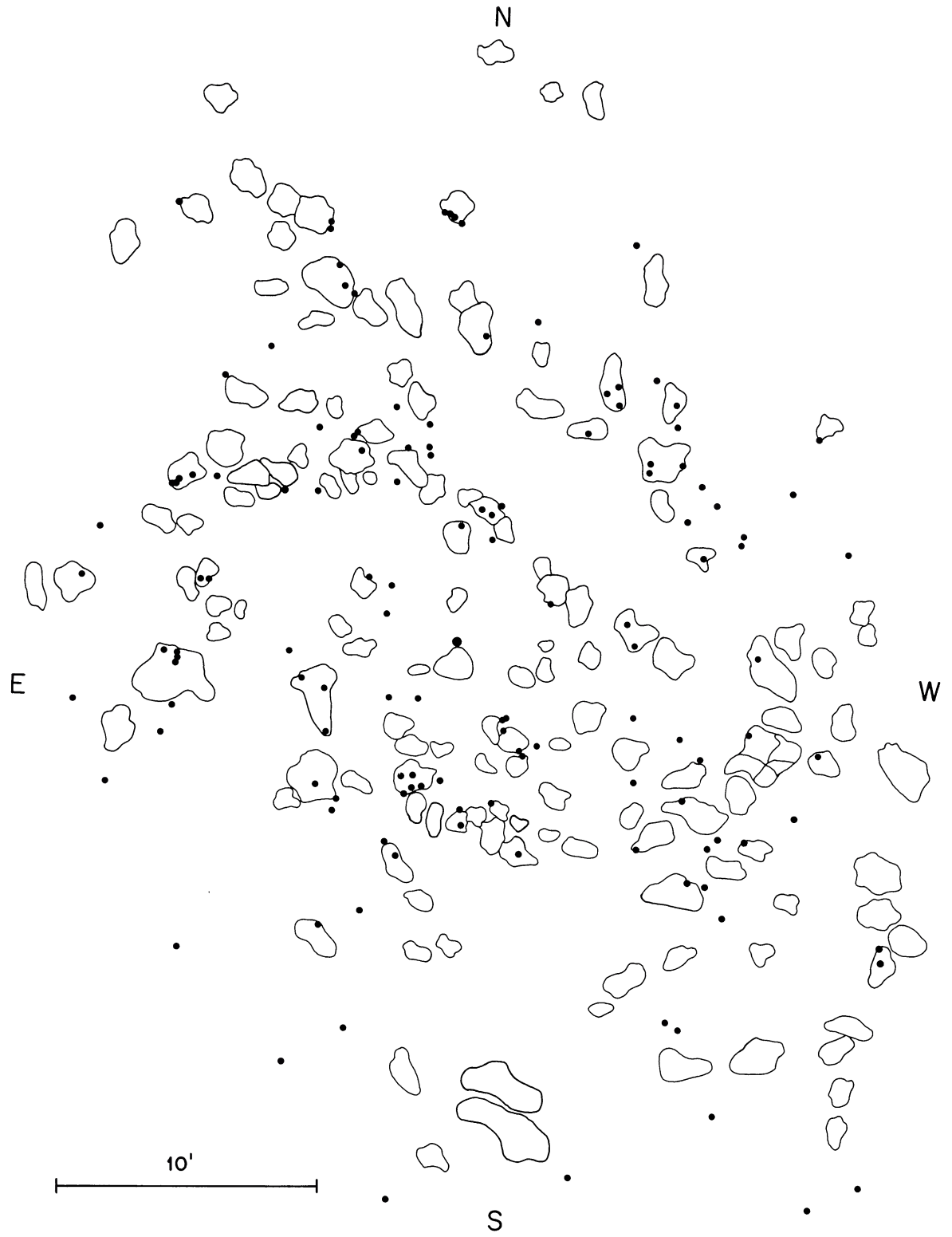

FIG. 23.—Surface distribution of red stars in Table 6 that have $B-V>1.9$, with the association boundaries superposed.

in the outer features of M33 (Wright, Warner, and Baldwin 1971; Warner, Wright, and Baldwin 1973; Rogstad, Wright, and Lockhart 1976) emphasize again that the density waves, if they exist, are weak in M33. And since copious star formation is observed to occur not only in M33 but in all late galaxies of types Sc III, Sc IV, Sd, Sm, etc., where galactic shocks by density waves (W. W. Roberts 1969, 1970*a*, *b*; Roberts and Burton 1977) hardly exist (Roberts, Roberts, and Shu 1975), it follows that other mechanisms of star formation are operating in these types of galaxies.

This point is made again in Figure 27 (Plate 8) where the adopted arm pattern is superposed on the dust distribution alone. Clearly, the dust is spread more evenly over the inner region of M33 than it is concentrated to any parts of the arms, although one does have the impression that the dust lanes are elongated in the direction of the spiral features. We should also mention the large prominent dust feature on the east side of M33 at the end of arm I N. This feature and its southern extensions given an asymmetrical appearance to M33 especially on long exposure photographs and may affect our interpretation of the spiral pattern on this side. We have no suggestions as to the origin of this very large dust cloud.

There is, however, one important aspect of the dust distribution, shown best in Figure 26. Over the inner disk, defined here as the region from the center to the outsides of arms I N and I S, the dust lanes form an elliptical pattern whose major axis is at position angle (N through E) $\sim 45° \pm 5°$ and whose axial ratio is ~ 1.40. Assuming that the dust lies in the plane of the inner disk, this axial ratio gives an inclination to the plane of the sky of $\omega = 44°$ ($\omega = 90°$ for edge-on orientation). These values are consistent with those derived from arms I N and I S by Danver (1942) of PA = 49° and $\omega = 40°$. As they differ from those by de Vaucouleurs (1959) of PA = 23°, $\omega = 55°$ that apply to the *outer* regions beyond arms I, we take this observation to be consistent with the warped optical plane model discussed by SH.

d) *Associations*, H II, *and Dust in Arms I N and I S*

Some of the points made in the last section are shown in more detail for arms I N and I S in Figure 28 (Plate 9). The associations are plotted in black, H II regions in red, and the regions of dust as shaded areas. It is, of course, expected that the H II regions and the associations should appear together as the OB stars in the associations provide the excitation of the gas.

The small classic Strömgren H II spheres are generally on the inside of the south arm, as are most of the dust lanes. This is the region of M33 most often cited to support density-wave star formation in part of the galaxy (see Courtes 1977, Figure 5, etc.; Dubout-Crillon 1977). Arm I S is also the only region of M33 where there is a strong correlation between peak H I features (Wright, Warner, and Baldwin 1971) and the optical spiral tracers. Many of the strongest H I features in M33 correspond with the stellar associations in arm I S. But convincing as Figure 28 and Courtes's Figure 5 may be for the south arm, the required ordering of the various components, i.e., gas and dust on the inner edge, the tight, small H II regions next, with the associations and elder H II regions on the outer edge, is not present in its northern counterpart. Furthermore, star formation, large, young associations, and well-defined pieces of spiral arms in the outer parts of M33 far from the two principal arms are not consistent with star formation by density-wave shocks in as clean a way as in the idealized models (W. W. Roberts 1969). The density-wave and alternative models are discussed further in § VII.

VI. THE ASSOCIATIONS

Because associations are principal arm tracers, a study of their age distribution may provide a key to their origin and possible mechanisms of arm formation and maintenance. With this in mind we have begun a study of particular associations to find luminosity functions and ages. The work is incomplete, but we discuss first results in this section to illustrate future possibilities.

a) *Color-Magnitude Diagrams*

CM diagrams have been obtained for six associations, chosen so as to sample a variety of positions within the M33 spiral pattern. Associations 10, 12, and 17 are along the ridge-line arm I S at its brightest part, close to the center of the galaxy. Association 127 is a large region of active star formation on the outer boundary of arm I S, or is in the inter-arm region between arms I S and II S (see Fig. 2 here and Fig. 1 of SH). The very large and dense association 131 is far from the center and is probably at the end of the arm II S, although it may be on the arm IVa extension. Association 137 is also far from the center and is the most prominent optical feature of arm V N.

Finding charts of the individual stars are given in Figures 29 (Plates 11 and 12) and 30 (Plate 10), made from the Palomar 5 m Hale reflector 103aD+GG11 plates. Stars that appear in the blue and red catalogs of Tables 5 and 6 or in Table 7 are identified once again by the prefix *B* and *R* or by the original capital letter from the Table 7 notation. The new stars measured here for the first time have running numbers without prefix in each association.

The very large scale of the charts is shown by the 60″ bar in the lower left. With this in mind, note that the surface density of the bright stars in associations 10, 11, 12, and 17 is nearly the same, but that it is considerably

Plate 9

FIG. 28.—Composite diagram of the two inner arms I N and I S showing the H II regions (in red), the dust patches (in grey), the association boundaries, the ridge-line, and inner and outer boundaries of the arms.

HUMPHREYS AND SANDAGE (*see* page 370)

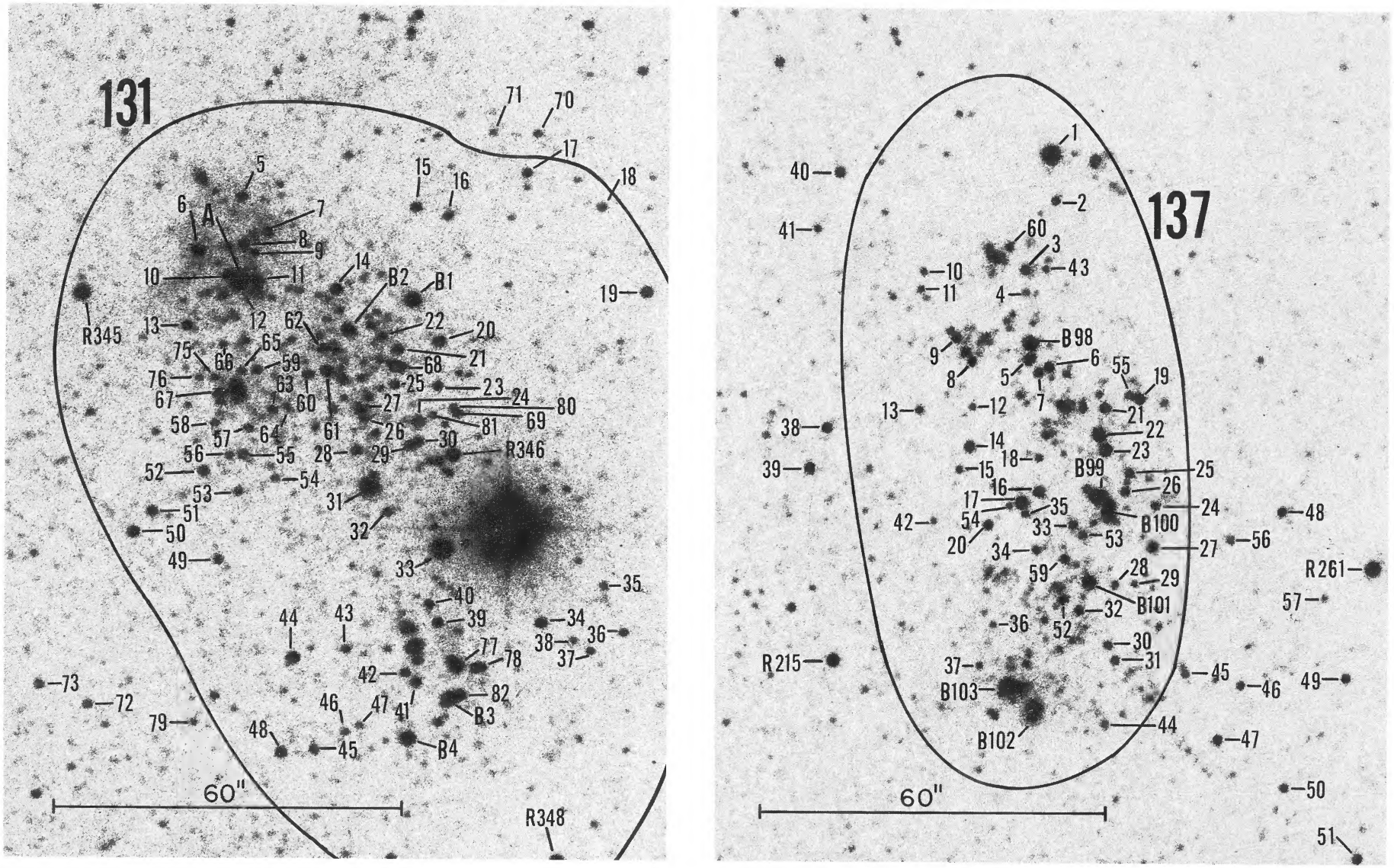

FIG. 30.—Identification chart for stars in associations 131 and 137 whose photometry is listed in Table 11. Chart is from a Palomar 5 m 103aD+GG11 plate.

HUMPHREYS AND SANDAGE (*see* page 370)

Plate 11

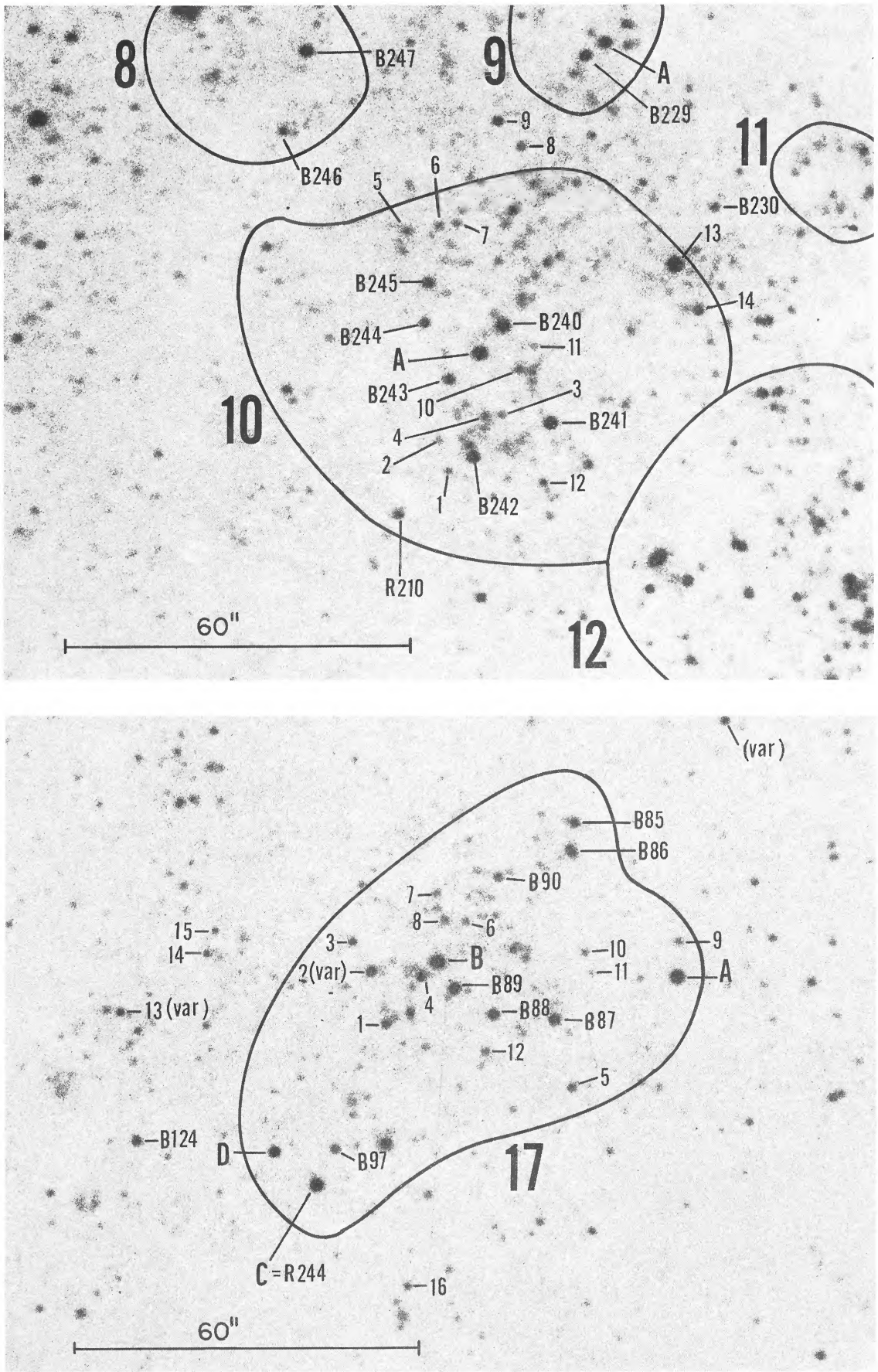

FIG. 29.—Identification of stars in the extended sample within associations 10, 12, 17, and 127. The reproduction is from a Palomar 5m 103aD+GG11 plate. The 1′ scale is marked. The photometry of the stars is listed in Table 11.

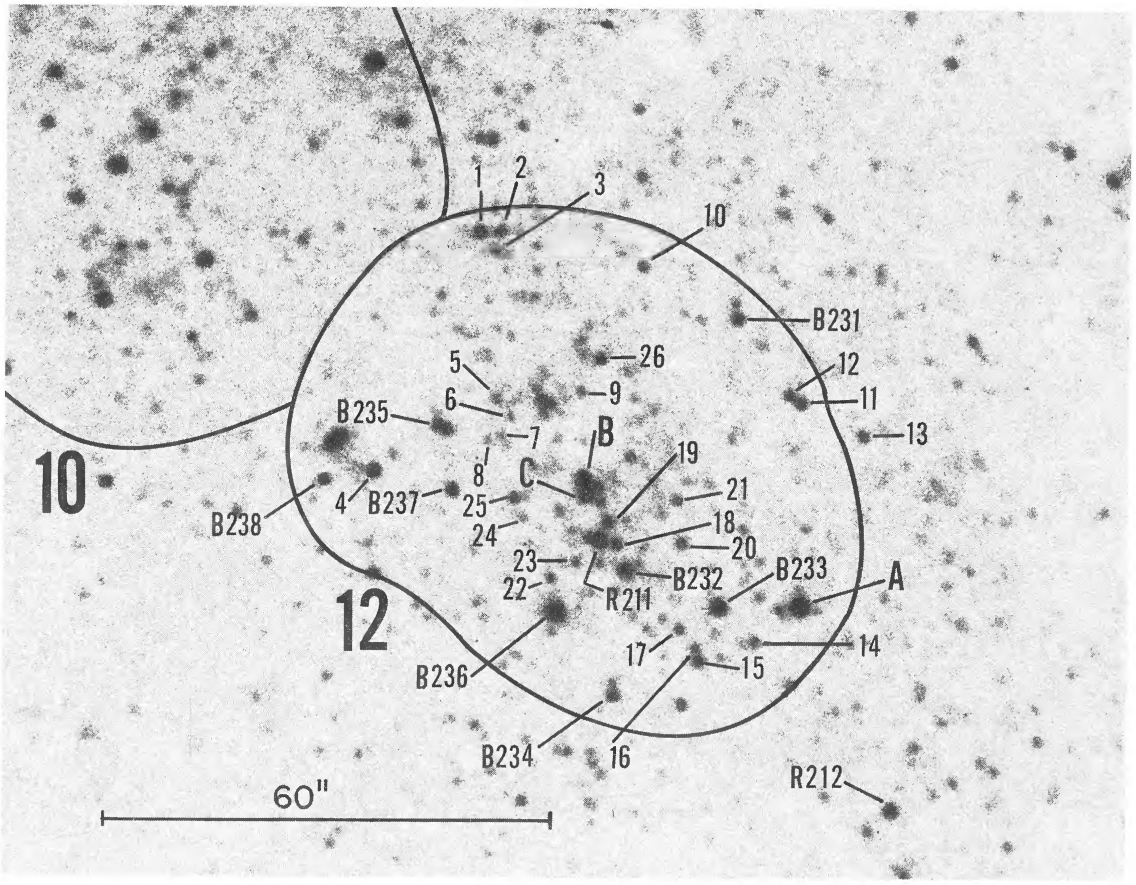

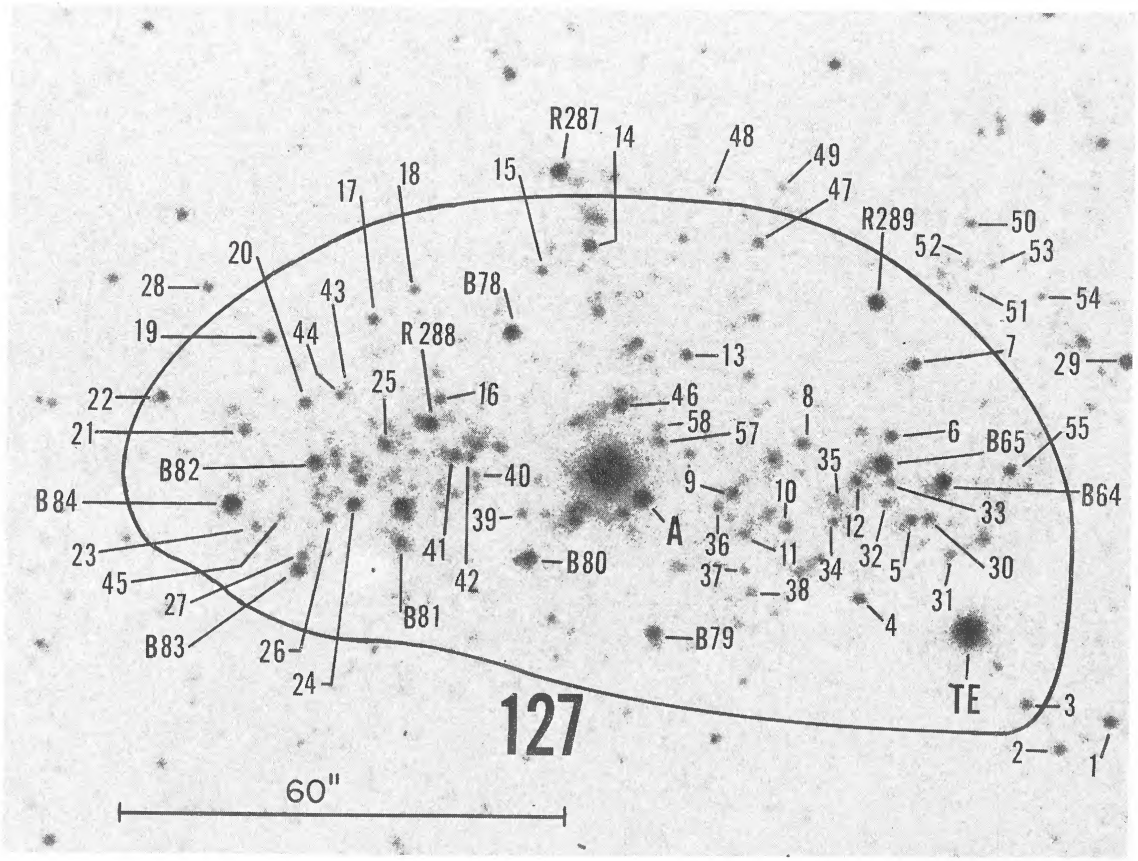

FIG. 29.—*Continued*

TABLE 11

ADOPTED PRELIMINARY MAGNITUDES FOR STARS IN SIX ASSOCIATIONS

Star	V	B-V	Star	V	B-V	Star	V	B-V
				ASSOCIATION #10				
A	17.26	1.15	B 245	18.63	-0.03	7	19.75	3.25
R 210	18.47	1.68	1	19.60	0.60	8	19.29	0.71
B 230	19.39	-0.11	2	19.75	0.50	9	19.22	1.13
B 241	17.59	0.06	3	19.75	0.19	10	19.60	0.50
B 242	17.67	0.00	4	19.66	1.34	11	19.98	0.22
B 243	18.65	-0.29	5	19.60	0.20	12	19.50	0.12
B 244	18.80	0.12	6	19.66	0.24	13	16.65:	1.00:
						14	18.80	0.15
				ASSOCIATION #12				
A	16.22	1.00	B 238	19.11	-0.13	12	19.5	1.25
B	17.25	(0.21)	1	18.3	-0.19	13	19.2	-0.20
C	17.05	(0.41)	2	19.0	-0.16	14	19.2	-0.16
R 211	16.50	2.40	3	(19.6)	(-0.28)	15	Crowded	
R 212	18.00	1.34	4	18.2	-0.16	16	19.9	>1.1
B 231	18.88	-0.28	5	19.2	0.05	17	19.3	-0.23
B 232	17.28:	0.12	6	19.9	-0.02	18	~19.0	(-0.19)
B 233	16.95	0.09	7	20.2	0.25	21	19.5	-0.23
B 234	Elongated		8	20.3	>1.70	22	19.4	-0.11
B 235	Multiple		9	19.7	0.67	23	19.5	-0.27
B 236	Cluster		10	19.0	0.38	24	19.5	0.08
B 237	18.93	-0.13	11	18.9	0.33	26	18.9	0.33
				ASSOCIATION #17				
A	17.10	0.70	B 124	18.77	-0.09	9	19.75	-0.16
B	17.07	0.59	1	19.03	0.87	10	19.90	0.30
C= R244	16.98	2.63	2	19.16	2.48	11	20.75	0.45
D	18.00	0.65	3	19.22	2.66	12	19.32	0.78
B 87	17.93	-0.14	4	18.61	0.21	13	20.03	2.67
B 88	18.05	-0.13	5	19.16	0.10	14	19.98	-0.09
B 89	17.87	0.23	6	19.50	0.70	15	19.60	0.78
B 90	19.37	-0.26	7	19.75	0.50	16	20.20	1.44
B 97	19.01	0.05	8	19.32	0.58			
				ASSOCIATION #127				
A	17.44	-0.14	11	Not seen 1978		34	20.03	0.07
R 287	17.83	2.27	12	19.75	-0.05	35	19.98	-0.06
R 288	18.14	1.64	13	19.29	-0.01	36	20.45	-0.67
R 289	17.90	2.06	14	18.85	0.02	37	20.45	-0.57
R 290	17.96	3.74 var	15	19.50	0.06	38	20.20	-0.42
B 64	17.97	-0.06	16	19.50	-0.09	39	19.75	-0.43
B 65	17.54	0.06	17	19.48	2.42	40	20.75	-0.83
B 78	18.21	0.06	18	20.45	~2.55	41	19.60	-0.38
B 79	18.62	0.10	19	19.29	1.81	42	19.46	0.46
B 80	18.38	-0.45	20	19.46	-0.39	43	20.75	-0.05
B 82	18.40	-0.25	21	19.60	-0.29	44	20.20	-0.28
B 83	18.26	-0.17	22	19.29	(0.29)	45	20.45	-0.35
B 84	17.28	-0.05	23	20.45	-0.67	46	19.22	-0.42
1	18.70	1.55	24	18.50	-0.08	47	19.46	0.15
2	19.22	-0.13	25	19.22	1.08	48	20.75	-0.35
3	19.32	0.03	26	19.32	0.09	49	20.75	-0.17
4	19.16	0.94	27	(19.3)	(0.00)	50	20.20	>1.4
5	19.60	-0.38	28	19.60	0.28	51	20.45	0.15
6	19.32	-0.06	29	18.28	-0.05	52	20.58	-0.28
7	19.22	2.68	30	19.75	-0.50	53	20.58	-0.18
8	19.41	-0.25	31	19.90	0.02	54	20.45	-0.15
9	19.29	0.06	32	20.02	-0.32	55	19.46	0.07
10	19.41	0.05	33	20.45	-0.05			

TABLE 11—*Continued*

Star	V	B-V	Star	V	B-V	Star	V	B-V
			ASSOCIATION #131					
A	17.44	1.38	24	19.10	0.80	55	19.66	0.28
R 345	17.71	1.87	25	20.03	0.32	56	20.75	-0.40
R 346	18.46	0.76	28	19.81	0.09	57	20.75	0.05
R 248	18.54	1.74	29	19.66	2.22	58	21.08	0.56
B 1	17.42	0.10	30	19.50	2.38	59	20.75	0.25
B 2	18.46	-0.20	31	16.59	0.88	60	(19.98)	0.12
B 3	18.26	-0.36	32	19.98	-0.08	61	19.24	-0.07
B 4	17.93	-0.05	33	16.22	0.15	62	19.82	0.20
5	19.63	-0.27	34	19.41	-0.09	63	19.75	0.45
6	19.12	3.08	35	20.75	-0.50	64	21.08	-0.73
7	20.47	-0.22	36	20.20	0.00	65	21.60	0.28
8	20.21	0.27	37	21.08	-0.73	66	20.75	>2.2
9	20.99	0.65	38	21.08	-0.83	67	19.65	-0.39
10	19.55	0.25	39	19.66	2.54	68	19.35	-0.09
11	19.63	0.72	40	19.82	0.20	70	20.58	0.04
13	19.60	0.42	42	(19.75)	(0.06)	71	21.60	0.04
14	19.29	0.07	43	20.58	>2.0	72	20.03	2.57
15	19.63	0.72	44	19.09	0.19	73	19.90	0.00
16	19.82	2.06	45	19.98	-0.04	74	17.50	1.57
17	19.90	2.50	48	19.36	2.28	75	20.95	0.67
18	20.58	-0.23	49	20.45	0.97	76	21.08	0.34
19	19.33	2.55	50	19.30	-0.04	77	19.00	0.36
20	19.39	2.25	51	19.65	-0.06	78	(19.50)	(0.40)
21	19.43	2.77	52	19.46	0.13	79	21.30	>1.3
22	19.98	0.50	53	20.45	-0.10	82	19.26	2.94
23	19.60	0.20	54	21.08	0.34			
			ASSOCIATION #137					
R 215	18.37	1.57	16	19.20	2.68	39	19.06	-0.06
R 261	17.47	1.48	17	18.50	0.20	40	19.41	2.23
R 262	17.91	1.59	18	20.15	0.15	41	20.35	-0.30
B 98	17.79	-0.30	19	19.40	-0.05	42	(20.80)	0.84
B 99	17.80	0.55	20	19.43	2.97	43	20.36	-0.03
B 100	18.70	-0.35	21	19.25	-0.10	44	20.06	0.11
B 101	18.22	-0.20	22	18.20	0.80	45	19.86	0.84
B 103	16.23	0.51	23	18.48	3.24	46	19.73	2.67
1	16.35	0.64	24	20.23	-0.16	47	19.37	0.09
2	19.81	2.59	25	19.80	-0.20	48	19.70	0.24
3	19.45	-0.19	26	19.80	0.45	49	19.53	1.84
4	20.36	0.44	27	19.09	0.31	50	19.73	0.16
5	19.18	-0.07	28	20.04	-0.04	51	19.56	-0.32
6	19.31	0.39	29	20.15	0.75	52	(19.72)	-0.12
7	19.68	0.12	30	20.16	-0.06	53	19.91	0.24
8	19.61	0.09	31	19.74	0.16	54	20.21	0.44
9	19.40	-0.15	32	19.84	0.06	55	20.02	0.02
10	20.40	2.00	33	19.91	0.09	56	20.06	0.09
11	20.15	0.00	34	20.00	1.88	57	21.2	(-0.8)
12	20.50	-0.06	35	20.36	-0.36	58	19.56	-0.21
13	20.02	-0.02	36	20.36	1.06	59	20.02	2.38
14	19.00	0.02	37	20.21	0.79	60	20.25	-0.36
15	20.06	0.21	38	19.26	-0.31			

higher in associations 137 and 131, which are among the brightest associations in integrated luminosity.

The colors and magnitudes for stars in the six associations, again measured by the Argelander step-scale method, are listed in Table 11. The stars already in Tables 5 and 6 are reentered at the top of each listing. The CM diagrams are shown in Figure 31 where data for associations 10, 12, and 17 are combined into the single diagram at the upper left. The stars previously measured (Tables 5, 6, and 7) are plotted as filled circles; the new, mostly fainter additions are open circles.

In interpreting the CM diagrams, recall that the photometric errors are of order $\sigma(V)\approx\pm0.2$ mag, $\sigma(B-V)\approx\pm0.3$ mag. Hence, fine structure along the color axis is generally smeared out for features smaller

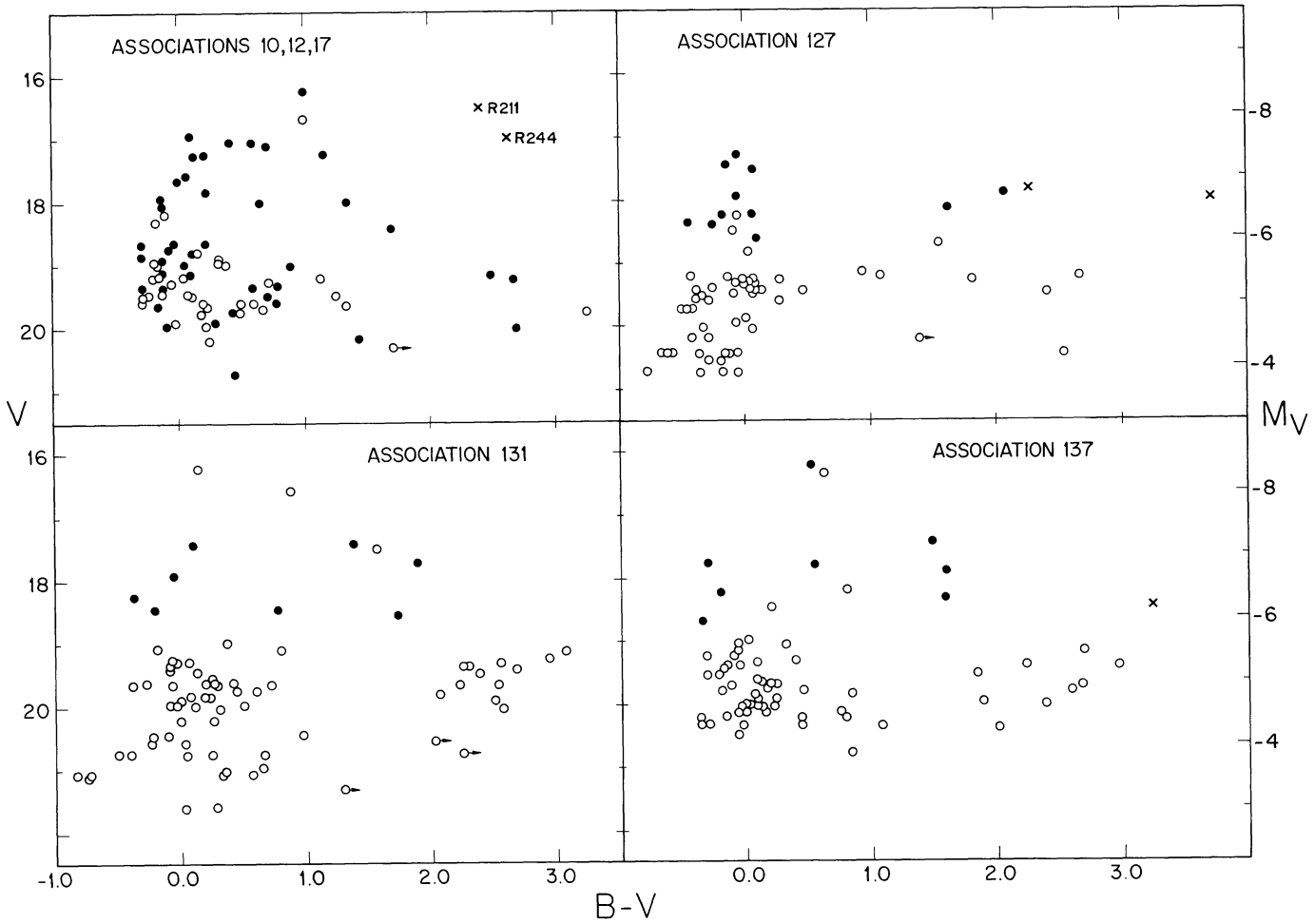

FIG. 31.—Color-magnitude diagrams plotted from the data in Table 11. The data have been combined for associations 10, 12, and 17. Closed circles are for the blue and red stars found in the blink surveys and listed in Tables 5 and 6. Open circles are for the stars newly listed in Table 11.

than the $\sim \pm 0.4$ mag level; however, any fine structure in magnitude is preserved to at least the ± 0.5 mag level.

b) *Ages*

The features that are similar in the four CM diagrams of Figure 31 are (1) a dominant blue sequence that terminates at $V \approx 17$ at the bright end, (2) a gap, or at least an abrupt change in the luminosity function at $V \approx 18.5$ to 19.0 ($M_V \approx -6$ to -5.5), and (3) a sequence of red supergiants that begins at $V = 19$ ($M_V = -5.5$), which is very prominent in associations 131 and 137, and to some extent in the upper two diagrams. The absolute magnitudes follow from our adoption of $(m - M)_{AV} = 24.65$.

Assuming that the observed gap at $V \approx 18.5$ to 19.0 in the CM diagrams of Figure 31 is caused by core hydrogen exhaustion at the main sequence turnoff, we can estimate the ages of the associations. For this purpose we have used the recent models for massive stars by Chiosi, Nasi, and Sreenivasan (1978). Their Figure 12 gives a relation between log T_e (or spectral type) at the main sequence turnoff and age and also between M_{Bol} at the turnoff and age based on their models with mass loss. With the information from this figure and bolometric corrections by Code *et al.* (1976) and Morton (1969) for main-sequence stars we can determine a relation between M_V (turnoff) and age which we have used to estimate the ages of the six associations in Figure 31. With this method the age estimates for associations 10, 12, and 17 are about 4×10^6 years and 5×10^6 years for associations 127, 131, and 137.

Alternatively, we can also estimate the ages of the M33 associations by scaling the evolutionary tracks computed by Robertson (1972, 1974*b*) for his LMC cluster CM diagrams (Robertson 1974*a*). The CM diagrams for the M33 associations, while $\sim$2.5 mag brighter in M_V than the LMC cluster diagrams, are similar enough (especially to NGC 1854) to suggest that the same physical processes operate over this mass interval in both galaxies.

Robertson (1974*b*) suggests that the clump of blue stars above the gap at 18.5–19.0 are evolved stars in the

core helium-burning stage. These stars appear in the observed diagrams as an extension of the main sequence, but with a gap. In this interpretation, the main sequence termination point is between $V=18.5$ and $V=19$ (Fig. 31) rather than at $V\approx17$.

Robertson's age of 3.3×10^7 years for NGC 1854 can then be scaled to the M33 associations by noting that all features in the diagrams are 2.6 magnitudes brighter in M_V than in Figure 2 of Robertson (1974*b*), assuming the modulus to the LMC to be $(m-M)_{AV}=18.9$. The ages scale approximately as $\mathfrak{M}/\mathfrak{L}$ which with $\mathfrak{L}\approx\mathfrak{M}^4$ from the mass-luminosity relation, gives $t\approx\mathfrak{L}^{-3/4}$. The resulting ages for the M33 associations in Figure 31 would be $t(\mathrm{M33})=(11)^{-3/4}\ (3.3\times10^7)=5.5\times10^6$ years.

The agreement between the two independent methods is very good. These ages are very much like those determined for the young OB associations in our region of the Galaxy and are also similar to the ages recently estimated for some associations in field IV in M33 (Humphreys 1979*b*).

c) The Blue-to-Red Ratio

Walker (1964) discovered that the ratio of blue to red supergiants in M33 varies with distance from the center, and a similar variation may exist in the Milky Way (Humphreys 1978). Our present M33 data suggest the same trend. The total number of blue and red stars found in the blink surveys and lying within the association boundaries are used to determine the blue to red supergiant ratio as a function of distance from the center. The B/R ratio for each distance interval is shown as a solid line in Figure 32. Those stars with photographic photometry are restricted to have $B-V\leq0.5$ and ≥1.9 to eliminate most of the foreground stars. The red stars for which no colors are known will suffer significant foreground star contamination and a correction for this possible contamination has been estimated statistically from the relative fraction of stars which had to be rejected with known colors bluer than $B-V\approx1.9$ mag. The same percentage of stars was subtracted from those red stars in association boundaries without color data. The B/R ratios so corrected are shown in Figure 23 as a dashed line. The data used for Figure 32 are summarized in Table 12. Each association is given by number with the numbers of blue and red stars, and the number of red stars corrected for possible field stars is given in parenthesis. We estimate that the surveys for candidate blue and red supergiants and the B/R ratios are complete to $m_V\approx19$ ($M_V\approx-5.5$). The mean B/R ratio for M33 to $M_V\approx-5.5$ is 5.7 using the red star numbers corrected for possible field star contamination.

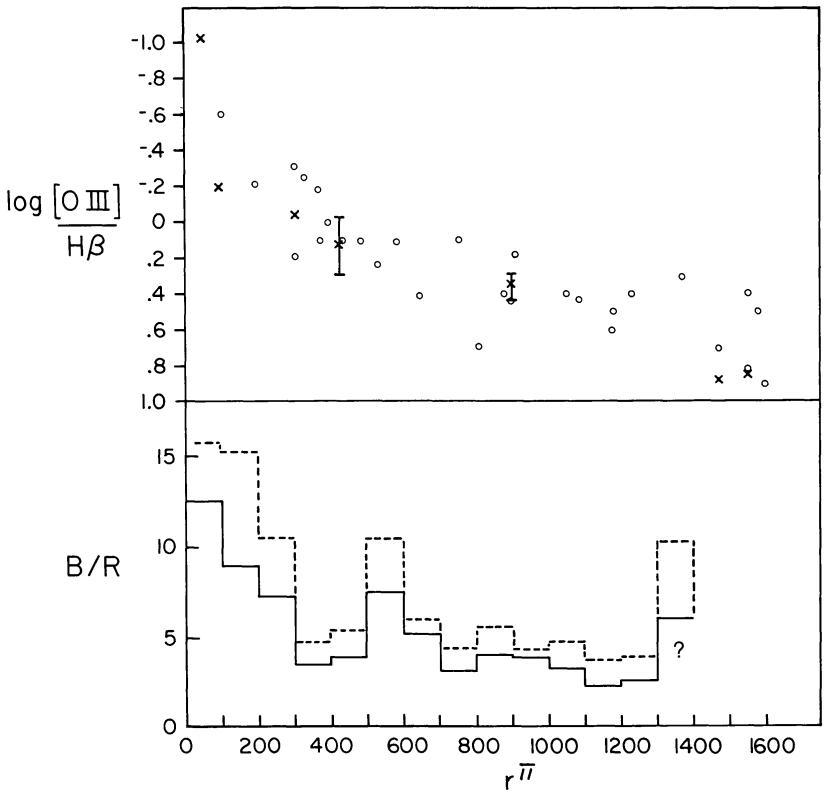

FIG. 32.—(*Upper*) Observed log [O III]/Hβ in the H II regions as a function of distance from the center. Data are from Searle (1971, *open circles*), and Smith (1975, *crosses*). (*Lower*) The ratio of the number of blue and red supergiants in the associations that are brighter than $M_V=-5.5$ as a function of distance (in arcsec) from the center.

TABLE 12

THE BLUE-TO-RED SUPERGIANT RATIO IN THE ASSOCIATIONS

Dist. (π)	Assoc.	Blue	Red[a]	B/R
0–100.....	64	5	1	
	142	20	1	
		25	2 (1.6)	12.5(15.7)
100–200....	143	6	1:	
	55	4	1	
		10	1 :(.6:)	19(15.2)
200–300....	1	11	0	
	2	9	1	
	3	4	1	
	48	9	3	
	49	5	0	
	50	12	3	
	56	5	0	
	57	7	0	
	61	14	3	
	62	8	0	
	63	0	0	
	65	13	1	
	94	8	1	
	95	4	2	
	96	6	1	
		115	16 (11.1)	7.2 (10.4)
300–400....	4	7	7	
	5	11	0	
	51	6	3	
	52	2	0	
	54	7	1	
	58	5	0	
	66	16	4	
	67	6	0	
	100	19	4	
		79	22 (16.1)	3.6(4.9)
400–500....	6	3	1	
	7	4	3	
	8	2	1	
	9	3	1	
	10	8	0	
	11	0	0	
	14	9	5	
	53	6	3	
	59	20	1	
	60	17	2	
	68	11	2	
	72	3	0	
	73	1	0	
	74	6	1	
	75	10	6	
	101	14	6	
	103	3	0	
		120	31 (22.4)	3.9(5.4)
500–600....	12	9	2	
	13	2	0	
	15	11	1	
	16	8	1	
	29	10	1	
	31	8	2	
	32	9	2	
	69	5	0	
	71	4	1	
	79	6	0	
	80	5	0	
	81	2	0	
	92	2	0	
	93	5	0	
	97	5	0	
	102	3	0	
	104	4	3	
		98	13 (9.3)	7.5(10.5)
600–700....	17	9	3	
	18	7	2	
	19	18	2	
	28	8	1	
	30	17	3	
	70	1	0	
	76	3	0	
	77	5	4	
	82	3	0	
	83	10	1	
	84	7	0	
	87	5	0	
	90	6	1	
	91	5	4	
	98	22	5	
	106	2	0	
	136	10	3	
		138	27 (22.9)	5.1(6.0)
700–800....	20	5	8	
	21	43	9	
	24	7	1	
	25	23	5	
	26	6	2	
	34	15	3	
	35	9	0	
	36	12	2	
	37	4	3	
	78	5	0	
	85	7	4	
	86	1	0	
	105	6	2	
	107	8	2	
	108	3	0	
	127	13	11	
	135	2	3	
		169	54 (37.8)	3.1(4.5)
800–900....	22	6	1	
	27	7	0	
	33	5	0	
	38	5	0	
	39	17	4	
	99	5	0	
	114	12	1	
	115	8	7	
	128	9	4	
	129	5	3	
		79	20 (13.9)	4.0(5.7)
900–1000...	23	3	1	
	40	4	0	
	88	9	2	
	89	7	2	
	113	3	0	
	126	3	0	
	132	5	0	

TABLE 12—*Continued*

Dist. (π)	Assoc.	Blue	Red[a]	B/R
	133	0	0	
	134	2	1	
	137	8	4	
	138	6	5	
		50	13 (11.3)	3.9(4.4)
1000–1100..	41	7	0	
	42	8	5	
	43	3	1	
	109	9	2	
	110	21	6	
	122	5	1	
	131	7	4	
		60	19 (12.4)	3.2(4.8)
1100–1200..	44	6	1	
	46	6	2	
	47	4	0	
	111	6	3	
	112	17	8	
	116	12	3	
	117	8	4	
	125	3	4	
	130	5	4	
		67	30 (17.5)	2.2(3.8)
1200–1300..	120	5	0	
	121	2	1	
	123	8	5	
	124	6	1	
	139	2	4	
	140	6	0	
		29	11 (7.3)	2.6(4.0)
1300–1400..	141	4	0	
	119	6	2	
	45	8	1	
		18	3 (1.8)	6(10.2)
>1400.....	118	2	0	

[a] The numbers in parenthesis are the red stars without photometry corrected for possible foreground contamination.

The variation of the B/R ratio with distance (Fig. 32) from the center shows evidence for a gradient that is steep in the central region, the inner 1 kpc; but is nearly flat with a slight slope from 1 kpc out to 5 kpc from the center. Consequently there is little or no gradient in B/R in most of the spiral arm region or disk of M33. We think the high point between $r=500''$ and $600''$ is due to heavy dust affecting at least 6 of the 17 associations in this distance interval, and the high point at the $1300''-1400''$ interval is probably not significant since it has only three associations.

The upper part of Figure 32 also shows the variation of the log [O III]/Hβ ratio with distance from the center. Note that this figure is plotted so that the highest log [O III]/Hβ ratios are at the bottom. It was plotted this way to illustrate the similar shapes of the gradients of the two parameters, the B/R and log [O III]/Hβ ratios. The log [O III]/Hβ ratio was chosen for this comparison because of the large number of data points available in the literature for this line ratio (Searle 1971; Smith 1975).

The log [O III]/Hβ ratio is largest in the outermost parts of M33, although just as for the B/R ratio there is little variation from 1 to 5 kpc from the center. Most of the evidence for a gradient also comes from the innermost 1 kpc. Shields and Searle (1978) showed that variations in the [O III]/Hβ intensity ratio are not due primarily to chemical composition differences, but instead to a gradient in the temperature of the ionizing stars. In M33 then, there are presumably hotter stars ionizing the gas in the outer parts than near the center.

Figure 32 certainly suggests a correlation between the behavior of the B/R ratio and the [O III]/Hβ ratio. Although the [O III]/Hβ variations are due primarily to a temperature gradient in the ionizing radiation, it has been suggested (van den Bergh 1968) that variations in B/R are due to metallicity gradients across the disks of galaxies such that the metal abundances (and B/R) are lower in the outer parts. Presumably the luminosities of the red supergiants will be increased by a reduction in the opacities and the B/R ratio will be reduced by the presence of more luminous red stars, but Humphreys has found little or no evidence for variations in the red supergiant luminosities in different galaxies due to chemical composition differences including the SMC (Humphreys 1979*c*). Humphreys and Davidson (1979) suggested that although the B/R gradient is most likely a composition effect other factors certainly influence it, such as the luminosities of the stars used. They find that B/R ratios are much higher for the stars of highest luminosities probably because mass loss (stellar winds) play a much stronger role in the evolution of the most massive stars (>40 $\mathfrak{M}_\odot$), limiting their evolution to cooler temperatures and preventing the formation of high luminosity red supergiants.

Examination of the data for M33 shows that the high B/R ratios near the center are due to a lack of red stars in the innermost regions when compared to the other distance intervals. It is now generally believed that higher metallicities occur in galactic nuclei than in the disks or spiral arms. If this is the case in M33, could increased metallicity have reduced the numbers of red supergiants? If mass loss rates are higher or stellar winds greater where the metal abundance is larger then the evolution of supergiants with lower mass (20–40 $\mathfrak{M}_\odot$) might be affected in much the same way as the most massive stars and their red counterparts might be rarer. Models for massive star evolution (with mass loss) with metal abundances greater than solar are required to test this possibility.

d) The Associations Seen From a Distance

i) *The Intrinsic Size*

The intrinsic sizes of the association boundaries marked in Figure 2 can be fit by a Gaussian distribution of characteristic diameter ($\sigma \approx 200$ pc). The few largest have diameters of ~600 pc, but most are in the 100–300 pc range. The association diameters have been compared with associations in our galaxy and M31 by Humphreys (1979*d*). This comparison suggests that the size of what we call a young OB association apparently depends upon our spatial resolution.

Hence, if M33 were seen from the distance of the Virgo Cluster at 20 Mpc, the associations would appear as knots in the spiral arms of mean diameter $\sigma \approx 200$ pc and would subtend only ~2″ diameter. The largest with core diameters of ~600 pc would subtend 6″.

ii) *Luminosity*

The integrated apparent V luminosities of the six associations, calculated by summing the individual stars by $V_T = -2.5 \log \Sigma_i \text{ dex } (-0.4\ V_i)$, are given in Table 13 together with other parameters for these regions. The first five columns give the intrinsic properties, while the last two show the angular diameter and integrated apparent magnitude as seen from a distance of 20 mpc.

These properties make it almost certain that many objects identified by Hubble (1936) as *brightest stars* in galaxies are, in fact, *associations* and, of course, H II regions as well (see Humason, Mayall, and Sandage 1956, Appendix C). It remains to be seen how valuable such groupings will be for determining distances (Wray and de Vaucouleurs 1980). It is well known that M_V for the associations is a very steep function of absolute magnitude and especially of type of the parent galaxy, with much scatter. The single example that shows the difficulties inherent in using them as distance indicators is NGC 2841 (p. 14 of the Hubble Atlas) where *no* associations of this type are visible, yet the galaxy, of type Sab, is intrinsically bright.

VII. THE EVOLUTIONARY FATE OF M33

In this section we will discuss how our observations of the stellar content may pertain to the problem of the origin and maintenance of the spiral arms in M33 and the possible evolutionary history of M33 as an Sc spiral.

a) The Spiral Arm Problem

The mechanism by which the spiral features of galaxies arise and maintain themselves over periods of several galactic rotations is a problem for which there is still no entirely satisfactory explanation. The density-wave theory in Lin and Shu (1964, 1966) and their colleagues can account for some of the observed features of spiral galaxies especially in the well-defined tow-armed spirals, but many galaxies are multiarmed, and their material arms are difficult to form and maintain. With sufficiently accurate observations, magnitudes, colors, and ages, of the stellar population and adequate resolution for the distribution of the gas and dust in the same galaxies we may eventually be able to distinguish among the possible mechanisms for the origin and maintenance of spiral arms. For example, accurate CM diagrams would allow us to calculate the age of a spiral arm, both along and across the arm. The density-wave theory makes specific predictions that the youngest objects should be on the inner edge of the arms.

With the data in this paper we can make a beginning at this type of investigation, although more accurate magnitudes and colors and even spectra are needed for many more stars. Accurate CM diagrams will be eventually needed for most of the associations to fully understand stellar evolution in the spiral features of M33, and we anticipate that this information will be forthcoming in the next few years.

However, even with our limited data, we can obtain some information relevant to this program. In addition to the six associations with CM diagrams discussed in § VI, we can also estimate the ages for 42 of the remaining 137 associations using the first method described in § VI. For these 42 associations, magnitudes and colors

TABLE 13

PROPERTIES OF SIX ASSOCIATIONS

NUMBER	DIAMETER				AS SEEN FROM 20 MPC	
	Arcsec	Parsec[a]	V_T	M_{V_T}[a]	DIAMETER	V_T
10.....	85	350	15.1	−9.5	4″	22.0
12.....	80	330	14.6	−10.0	3″	21.5
17.....	85	350	15.0	−9.6	4″	21.9
127.....	125	510	14.4	−10.2	5″	21.3
131.....	150	620	14.3	−10.2	6″	21.3
137.....	130	530	14.3	−10.3	5″	21.2

[a]The assumed apparent modulus of M33 is $(m-M)_{AV} = 24.65$.

are available for enough stars to estimate the position of the main sequence turnoff and the age. With incomplete CM diagrams this method is not very accurate. Combined with an error of ~0.3 in the magnitudes we estimate that the turnoff point cannot be found to better than 0.5 mag, which leads to an error in the ages of at least 10^6 years. Nevertheless we find that all 48 associations are essentially the same age with a range of $4-6\times10^6$ years.

There is no evidence for an age gradient along either of the two major arms, I S and I N. We have also looked for differences in ages across these two arms, but the age differences, for example, between associations 17 (4.3×10^6 years) and 127 (4.9×10^6 years) and 77 (5.1×10^6 years) and 84 (4.7×10^6 years) are not significant when one considers the errors. Much more accurate dating will be necessary to check for possible age gradients. There is some evidence that the large associations in the outer spiral features such as 110, 112, 131, and 137 may be somewhat younger than the innermost spiral arms, but again more and better data are required to confirm this preliminary result.

i) *Requirements of the Density-Wave Theory*

In the density-wave theory we expect star formation along a continuous front as the gas encounters the wave and is shocked. The model predicts that the gas, dust, youngest stars, and H II regions will occur on the inside edge of the visible arm nearest the position of the presumed shock. Somewhat older stars and the stellar associations will be further from the shock toward the outer side of the arm.

In M33 the best evidence for the density-wave comes from the two innermost arms, especially arm I S. In arm I S we observe prominent dust lanes along the inner edge of the brightest part of the optical arm and a prominent string of small Stromgren spheres (Fig. 28). These features of the southern arm have been noted by others especially Dubout-Crillon (1977), Boulesteix *et al.* (1974) and Newton (1980). In his recent H I survey of M33 Newton finds a good correlation between the H I and the dust and H II regions along the inside edge of the arm. He also finds velocity perturbations in the H I along this inner spiral arm which agree with the predictions of the density-wave theory. Our data for the associations in this arm can also be interpreted as supporting the density-wave model. The associations are essentially the same age with a mean of 4.8×10^6 years and a range of $4.3-5.5\times10^6$ years. Although there is little evidence for a gradient across the arm, more accurate dating is required to check this prediction.

Because several structural features of arm I S agree with the density-wave model we might expect the other major arm, its northern counterpart, to be similar, but this is not the case. The distribution of the spiral tracers in arm I N is not nearly so regular. There is no well-defined string of H II regions and the prominent dust lanes for the most part lie on the outer side of the optical arm. Newton also finds poorer correlation between the optical arm and the H I features. On the basis of the density wave model we would expect the morphology of these two arms to be more alike. A simple interpretation in terms of the density-wave will not suffice for arm I N at this time. More information especially for detailed comparison of the stellar content with the H I and dust distribution in arm I N, is required before we can interpret its structure.

In their density-wave based modelling of M33, Roberts, Roberts and Shu (1975) placed the outer corotation point at 2.8 kpc from the center which corresponds almost exactly with the termination of our optical arms I S and I N. These authors admit that their best fit model for M33 will yield only weak shocks which would produce "massive" arms like I S and I N. However young stars, large OB associations and H II regions are prominent beyond the corotation point. Density-wave models for M33 do not account for the outer spiral features, arms II–V, which give M33 its filamentary and chaotic appearance on long exposure photographs. It is not that multiarm spirals are impossible in the density-wave theory, but that the arm spacing or the separation between inner and outer corotation becomes too small ($m=10$ for M33), although several modes may be present which could produce additional features. Apparently we should consider other mechanisms for producing the outer spiral features.

ii) *Other Theories of Spiral Structure*

The major problem of spiral structure is perhaps accounting for the multiarmed appearance of most spiral galaxies. The material arms, the pieces of spiral arms, which are especially common in the outer parts of many galaxies, are responsible for their multiarmed appearance. In a recent review Toomre (1977) has reemphasized the problem of material arms and their importance to the appearance of spiral galaxies. Their origin, regeneration, and maintenance over several galactic rotation periods have not been adequately explained.

Various mechanisms proposed include amplification of instabilities in the disk (Goldreich and Lynden-Bell 1965) and tidal instabilities from the passage of another galaxy, especially a companion (Toomre and Toomre 1972) which produces a major distortion in the outer disk or halo. Recently Mueller and Arnett (1976) and Gerola and Seiden (1978) have proposed models in which aggregates of young stars are produced by a chain reaction process of shock waves from supernovae. The star formation is thus self-propagating, and the appearance of spiral features due to differential rotation is self-maintaining over several rotations. In a

recent paper Elmegreen (1979) has shown how the density-wave model and the stochastic self-propagating model of Gerola and Seiden can act together to produce spiral features.

In M33 the OB associations and H II regions in the outer parts define only what appear to be pieces of spiral arms (material arms) that cannot be traced for very long distances. In outlining the outer spiral features, arms II–V, in M33 (§ V*b*) we found that it was not possible to simply connect the regions of current active star formation, but instead it was necessary to use long exposure photographs to reveal the spiral pattern (Fig. 24) caused by the enhancement in surface brightness by a fainter, but still relatively young stellar population. This observation of a somewhat older population revealing a spiral pattern that connects the youngest regions may eventually aid in defining the mechanisms of origin and maintenance of the material arms. In this regard, the warping of the M33 plane now observed in both the radio (Rogstad, Wright, and Lockhart 1976) and optical (SH) may play a role in both the origin and maintenance of the spiral features in the outer disk.

The spiral structure of M33 appears to be a combination of density-wave arms in the inner parts and more filamentary material arms in the outer parts.

b) The Evolution of M33 as an Sc Spiral

M. S. Roberts (1963) was the first to calculate the life time of spiral galaxies as population I star producers. His method was to divide the estimated present birth rates for stars into the measured total H I mass for various galaxy types to find how long the H I supply will last under the present consumption rates. His influential conclusion was that spirals of types Im, Sc, and Sb can continue to produce stars at their present rate for many Hubble times, and hence that such galaxies have not evolved appreciably along the Hubble sequence since shortly after their formation.

We now make an order of magnitude calculation of the same kind for M33 using the fact that the M33 associations are nearly the same age (10^7 years) and therefore that the statistics of star formation can be treated by considering star formation in particular generations with discrete ages.

Counts by Madore, van den Bergh, and Rogstad (1974) over the face of M33 on ultraviolet plates give $\sim$7000 stars brighter than $U=20.2$. If these are effectively A stars with $U-B=B-V=0$, then this limit corresponds to $V=20.2$ or $M_V\approx-4.5$. (If, on the other hand, $U-B\approx-1$, $B-V\approx0$, then $M_V\approx-3.5$. The consequences of this fainter count limit is that fewer total stars are being produced in M33 per generation by about a factor of 3 than for the brighter limit. We return to this point later.)

The crux of the problem is, then, to estimate the total number of stars formed in the present generation, knowing that 7000 stars have been formed brighter than $M_V=-4.5$. Clearly, this requires knowledge of the luminosity function for currently forming stars, and we now show that the question of whether M33 is a rapid or slow evolver depends solely on the steepness of the formation function (a problem for which no really satisfactory current solution exists).

The formation luminosity function (FLF) is certainly less steep than the traditional van Rhijn-Luyten $\phi(\mathfrak{M})$ in the solar neighborhood. Rather, the question is whether the Salpeter (1955) function applies in OB associations over all mass ranges (in particular for $\mathfrak{M}<\mathfrak{M}_\odot$), or whether only few faint stars form in the presence of the massive OB groups, for reasons put forward by Herbig (1962). The first suggestion that massive stars form independently from those with $\mathfrak{M}<\mathfrak{M}_\odot$ was made by M. S. Roberts (1958) from his star counts in young galactic clusters. The results were confirmed by van den Bergh and Sher (1960) and the implications have been recently discussed by many authors (cf. Smith, Biermann, and Mezger 1978; Silk 1977, etc.).

Although it is by no means clear that most of the low mass dwarfs in our galaxy were formed early in its history and hence that the FLF is discontinuous somewhere near $M_V\approx+4$ with the brighter part composed of younger stars formed in the O associations, there is evidence to support such a view. Note in particular the lack of faint dwarfs in the τ Canis Majoris cluster (see Johnson 1950, Fig. 1) and the varying ratio of luminosity functions in IC 1613 between the field and the young association (Sandage and Katem 1976, Fig. 3).

In the calculations that follow we adopt various absolute magnitude cutoffs, fainter than which no stars are assumed to form in the OB associations in M33. We then ask, given that 7000 young stars (of age 10^7 years) exist in M33 brighter than $M_V=-4.5$, how much mass is permanently tied up in stars per generation. Since all young stars will eventually evolve to collapsed objects of mass $\sim1\mathfrak{M}_\odot$, with the excess mass being returned to the interstellar medium, we need only count the FLF as it is normalized to 7000 stars in the absolute magnitude interval $M_V=-4.5$ to -5.5. This function is terminated at various fainter M_V values. When the termination was made fainter than $M_V\approx+5$, for which the mass of the stars is less than $\mathfrak{M}_\odot$, the appropriate mass was multiplied by the number of stars in the FLF in the calculation. The form of the initial luminosity function is taken from Sandage (1957, Table 1, final column).

The results are displayed in Table 14. Column (1) gives the absolute magnitude interval fainter than which no stars are assumed to form. Column (2) is the total mass bound up in stars, found by counting the FLF

TABLE 14

BIRTHRATES AND FUTURE EVOLUTIONARY TIMES FOR VARIOUS CUTOFFS OF THE IMF

Termination Interval (M_V) (1)	Mass Bound Up in Stars in This Generation ($\mathfrak{M}_\odot$) (2)	Rate of Mass Lockup[a] ($\mathfrak{M}_\odot$ year^{-1}) (3)	Time To Consume Remaining H I[b] (4)
−0.5–+0.5.....	4.8×10^5	0.05	4×10^{10}
+0.5–+1.5.....	8.0×10^5	0.08	2.5×10^{10}
+1.5–+2.5.....	1.3×10^6	0.13	1.5×10^{10}
+2.5–+3.5.....	2.1×10^6	0.21	9.5×10^9
+3.5–+4.5.....	3.4×10^6	0.34	5.9×10^9
+4.5–+5.5.....	5.9×10^6	0.59	3.4×10^9
+5.5–+6.5.....	8.6×10^6	0.86	2.3×10^9
+6.5–+7.5.....	1.0×10^7	1.0	2.0×10^9
+7.5–+8.5.....	1.2×10^7	1.2	1.7×10^9
+8.5–+9.5.....	1.4×10^7	1.4	1.4×10^9
+9.5–+10.5....	1.6×10^7	1.6	1.2×10^9
+10.5–+11.5...	1.8×10^7	1.8	1.1×10^9
+11.5–+12.5...	2.0×10^7	2.0	1.0×10^9
+12.5–+13.5...	2.1×10^7	2.1	1.0×10^9
+13.5–+14.5...	2.2×10^7	2.2	9×10^8
+14.5–+15.5...	2.3×10^7	2.3	9×10^8
+15.5–+16.5...	2.3×10^7	2.3	9×10^8

[a]Assumes that the present generation of OB associations has a characteristic age of 1.0×10^7 years.

[b]Based on present H I fuel supply of 2×10^9 $\mathfrak{M}_\odot$ and that the current rate of conversion into stellar masses (from column [3]) remains constant.

from its brightest end to the termination luminosity, normalized to 7000 stars brighter than $M_V=-4.5$, and where appropriate, multiplied by the stellar mass when $\mathfrak{M}<\mathfrak{M}_\odot$.

Column (3) is column (2) divided by 10^7 years (the assumed order of magnitude age of the current generation) and is the birth rate of the mass that is forever tied up into stars in units of solar masses per year. Column (4) is the remaining life-time of the 2×10^9 solar masses of H I in M33 (see M. S. Roberts 1969; Huchtmeier 1973) if it is consumed at the current rate of column (3). As mentioned earlier, these times should be increased by a factor of ~3 if the 7000 counts refer to $M_V=-3.5$ rather than -4.5. The conclusion from Table 14 is that if no stars fainter than $M_V\approx0$ are now forming in M33, then the galaxy can last for ~2 more Hubble times as an Sc, but if more and more stars are tied up on the fainter main sequence, this age decreases drastically to only $\sim10^9$ years. The conclusion is, of course, contingent on there being no replenishment of the H I field from the outside.

It is clear from these calculations that an answer to how fast galaxies can evolve as they use their present H I supply, depends on the shape the of formation luminosity function fainter than $M_V\approx0$. The determination of the appropriate FLF for young aggregates will undoubtedly be one of the major problems of the observational effort in the coming decade.

We would like to thank John Bedke of the Mount Wilson Observatory photographic laboratory for finding charts and reproductions during the many phases of this extended investigation. The line drawings and drafting for the many figures in this paper were prepared by William Porter and William Gabler at the University of Minnesota and by Nancy Newton at Mount Wilson. We are especially grateful for their skill in preparing the many difficult and tedious figures.

REFERENCES

Ambartsumian, V. A. 1947, *Stellar Evolution and Astrophysics* (Armenian Acad. of Sci.).
_____. 1949, *Soviet Astr.—A. J.*, **26**, 1.
_____. 1955, *Observatory*, **75**, 72.
Blaauw, A. 1964, *Ann. Rev. Astr. Ap.*, **2**, 213.
Boulesteix, J., Courtes, G., Laval, A., Monnet, G., and Petit, H. 1974, *Astr. Ap.*, **37**, 33.
Chiosi, C., Nasi, E., and Sreenivasan, S. R. 1978, *Astr. Ap.*, **63**, 103.
Code, A. D., Davis, J., Bless, R. C., and Brown, H. R. 1976, *Ap. J.*, **203**, 417.
Conti, P. S. 1978, *Ann. Rev. Astr. Ap.*, **16**, 371.
Courtes, G. 1977, in *Topics in Interstellar Matter*, ed. H. van Woerden (Dordrecht: Reidel) p. 209.

Danver, G. C. 1942, *Ann. Obs. Lund*, No. 10.
de Groot, H. 1925, *M.N.R.A.S.*, **85**, 535.
_____. 1926, *M.N.R.A.S.*, **86**, 146.
de Vaucouleurs, G. 1959, *Ap. J.*, **130**, 728.
Dixon, M. E. 1971, *Ap. J.*, **164**, 411.
Dubout-Crillon, R. 1977, *Astr. Ap.*, **56**, 293.
Elmegreen, B. G. 1979, *Ap. J.*, **231**, 372.
Gerola, H., and Seiden, P. E. 1978, *Ap. J.*, **223**, 129.
Goldreich, P., and Lynden-Bell, P. 1965, *M.N.R.A.S.*, **130**, 125.
Herbig, G. H. 1962, *Adv. Astr. Ap.* **1**, 47.
Hiltner, W. A. 1960, *Ap. J.*, **131**, 372.
Hodge, P. M. 1977, *Ap. J. Suppl.*, **33**, 69.
_____. 1978, *Ap. J. Suppl.* **37**, 145.
Hodge, P. M., and Lucke, P. B. 1970, *A. J.*, **75**, 933.
Holmberg, E. 1950, *Medd. Lund Astr. Obs.*, Ser. 2, No. 128.
Hubble, E. 1926, *Ap. J.*, **63**, 236.
_____. 1936, *Ap. J.*, **84**, 158.
Hubble, E. and Sandage, A. 1953, *Ap. J.*, **118**, 353.
Huchtmeier, W. 1973, *Astr. Ap.*, **22**, 91.
Humason, M. L., Mayall, N. U., and Sandage, A. 1956, *A. J.*, **61**, 97 (Appendix A).
Humphreys, R. M. 1978, *Ap. J. Suppl.*, **38**, 309 (Paper I).
_____. 1979*a*, *Ap. J. Suppl.*, **39**, 389 (Paper II).
_____. 1979*b*, *Ap. J.*, **234**, 854 (Paper IV).
_____. 1979*c*, *Ap. J.*, **231**, 384.
_____. 1979*d*, in *The Large-Scale Characteristics of the Galaxy*, ed. W. B. Burton, (Dordrecht: Reidel), p. 93.
_____. 1980*a*, *Ap. J.*, **238**, 65, (Paper V).
_____. 1980*b*, *Ap. J.*, in press (Paper VI).
Humphreys, R. M., and Davidson, K. 1979, *Ap. J.*, **232**, 409 (Paper III).
Hutchings, J. B. 1976, *Ap. J.*, **203**, 438.
Johnson, H. L. 1950, *Ap. J.*, **112**, 240.
Keeler, J. E. 1908, *Pub. Lick Obs.*, **8**, Plate 3 for M33.
Lin, C. C., and Shu, F. H. 1964, *Ap. J.*, **140**, 646.
_____. 1966, *Proc. Nat. Acad. Sci.*, **55**, 229.
Lucke, P. B., and Hodge, P. M. 1970, *A. J.*, **75**, 171.
Lundmark, K. 1921, *Pub. A. S. P.*, **33**, 324.
_____. 1925, *M. N. R. A. S.*, **85**, 890.
Madore, B. F. 1978, *Observatory*, **98**, 169.
Madore, B. F., van den Bergh, S., and Rogstad, D. H. 1974, *Ap. J.*, **191**, 317.
Morgan, W. W., Whitford, A. E., and Code, A. D. 1953, *Ap. J.*, **118**, 318.
Morton, D. C. 1967, *Ap. J.*, **147**, 1017.
_____. 1969, *Ap. J.*, **158**, 629.
Mueller, M. W., and Arnett, W. D. 1976, *Ap. J.*, **210**, 670.
Newton, K. 1980, *M. N. R. A. S.*, **190**, 689.
Racine, R., 1969, *A. J.*, **74**, 1073.
Reynolds, J. H. 1927*a*, *Observatory*, **50**, 185.
_____. 1927*b*, *Observatory*, **50**, 308.
Ritchey, G. 1910, *Ap. J.*, **32**, 26.
Roberts, I. 1899, in *Photographs of Stars, Star-Clusters, and Nebulae*, **2** (London: "Knowledge" Office, High Holborn).
Roberts, M. S. 1957, *Pub. A. S. P.*, **69**, 59.
_____. 1958, *Pub. A. S. P.*, **70**, 462.
_____. 1963, *Ann. Rev. Astr. Ap.*, **1**, 149.
_____. 1969, *A.J.*, **74**, 859.
Roberts, W. W. 1969, *Ap. J.*, **158**, 123.
_____. 1970*a*, in *IAU Symposium No.* 38, *The Spiral Structure of our Galaxy*, ed. W. Becker and G. Contopoulos (Dordrecht: Reidel) p. 415.
Roberts, W. W. 1970*b*, in *Galactic Astronomy*, Vol. **2**, ed. H. Chiu and A. Muriel (New York: Gordon and Breach), p. 201.
_____. 1977, in *Vistas in Astronomy*, Vol. **17**, ed. A. and P. Beer (Oxford: Pergamon Press), p. 914.
Roberts, W. W., and Burton, W. B. 1977, in Topics in Interstellar *Matter*, ed. H. van Woerden (Dordrecht: Reidel), p. 195.
Roberts, W. W., Roberts, M. S., and Shu, F. H. 1975, *Ap. J.*, **196**, 381.
Robertson, J. W. 1972, *Ap. J.* **177**, 473.
_____. 1974*a*, *Astr. Ap. Suppl.*, **15**, 261.
_____. 1974*b*, *Ap. J.*, **191**, 67.
Rogstad, D. H., Wright, M. C. H., and Lockhart, I. A. 1976, *Ap. J.*, **204**, 703.
Romano, G. 1978, *Astr. Ap.*, **67**, 291.
Salpeter, E. 1955, *Ap. J.*, **121**, 161.
Sandage, A. 1957, *Ap. J.*, **125**, 422.
_____. 1962, in *Problems of Extragalactic Research*, ed. G. C. McVittie (New York: MacMillan Co.), p. 359.
Sandage, A., and Humphreys, R. M. 1980, *Ap. J.* (*Letters*), **236** L1 (SH)
Sandage, A., and Johnson, H. L. 1974, *Ap. J.*, **191**, 63 (SJ).
Sandage, A., and Katem, B. 1976, *A. J.*, **81**, 743.
_____. 1977, unpublished.
Sandage, A., and Sersic, 1960, unpublished.
Sandage, A., and Tammann, G. A. 1974*a*, *Ap. J.* **190**, 525. (ST 1).
_____. 1974*b*, *Ap. J.*, **191**, 603 (ST 2).
Seares, F. H., Kapteyn, J. C., and van Rhijn, P. J. 1930, *Mount Wilson Catalogue of Photographic Magnitudes in Selected Areas 1–139*, (Washington, DC: Carnegie Institute), Publication No. 402.
Searle, L. 1971, *Ap. J.*, **168**, 327.
Shapley, H. 1919, *Pub. A.S.P.*, **31**, 265.
Sharpless, S. 1965, in *Stars and Stellar Systems*, Vol. **5**, *Galactic Structure*, ed. A. Blaauw and M. Schmidt (Chicago: University of Chicago Press), p. 131.
Shields, G. A., and Searle, L. 1978, *Ap. J.*, **222**, 821.
Silk, J. 1977, *Ap. J.*, **214**, 71.
Smith, H. E. 1975, *Ap. J.*, **199**, 591.
Smith, L. F., Biermann, P., and Mezger, P. G. 1978, *Astr. Ap.*, **66**, 65.
Snow, T. P., and Morton, D. C. 1976, *Ap. J. Suppl.*, **32**, 429.
Stothers, R. 1969, *Ap. J.*, **155**, 935.
_____. 1972, *Ap. J.*, **175**, 717.
Stothers, R., and Chin, C. W. 1969, *Ap. J.*, **158**, 1039.
_____. 1976, *Ap. J.*, **204**, 472.
Toomre, A. 1977, in *Ann. Rev. Astr. Ap.*, **15**, 437.
Toomre, A. and Toomre, J. 1972, *Ap. J.*, **178**, 623.
Walker, M. F. 1964, *A.J.*, **69**, 744.
Warner, P. J., Wright, M. C. H., and Baldwin, J. E. 1973, *M.N.R.A.S.*, **163**, 163.
Wray, J., and de Vaucouleurs, G. 1980, *A.J.*, **85**, 1.
Wright, M. C. H., Warner, P. J., and Baldwin, J. E. 1971, *M.N.R.A.S*, **155**, 337.
van den Bergh, S. 1964, *Ap. J. Suppl.* **9**, 65.
_____. 1968, *J.R.A.S. Canada*, **62**, No. 4.
van den Bergh, S., Herbst, E., and Kowal, C. T. 1975, *Ap. J. Suppl.*, **29**, 303.
van den Bergh, S., and Sher, D. 1960, *Pub. David Dunlap Obs.*, **2**, No. 7.

ROBERTA M. HUMPHREYS: Department of Astronomy, 116 Church Street S.E., University of Minnesota, Minneapolis, MN 55455

ALLAN SANDAGE: Mount Wilson and Las Campanas Observatories, 813 Santa Barbara Street, Pasadena, CA 91101